Research supported by the
National Science Foundation through
Grants ATM-9313716 and ATM-9618684
and a graduate fellowship from AMS/ITT.

MAY 1996 AND MAY 1997 LINEAR MESOSCALE CONVECTIVE SYSTEMS OF THE CENTRAL PLAINS: SYNOPTIC METEOROLOGY AND A REFLECTIVITY-BASED TAXONOMY

by

Matthew David Brown Parker

Richard H. Johnson, PI

Colorado State University

DEPARTMENT OF ATMOSPHERIC SCIENCE

PAPER NO. 675

MAY 1996 AND MAY 1997 LINEAR MESOSCALE CONVECTIVE SYSTEMS OF THE CENTRAL PLAINS: SYNOPTIC METEOROLOGY AND A REFLECTIVITY-BASED TAXONOMY

by

Matthew David Brown Parker

Department of Atmospheric Science
Colorado State University
Fort Collins, CO 80523

Spring 1999

Atmospheric Science Paper No. 675

ABSTRACT

MAY 1996 AND MAY 1997 LINEAR MESOSCALE CONVECTIVE SYSTEMS OF THE CENTRAL PLAINS: SYNOPTIC METEOROLOGY AND A REFLECTIVITY-BASED TAXONOMY

A survey of linear mesoscale convective systems (MCSs) occurring in the central United States during the months of May 1996 and May 1997 is presented. MCSs are identified and analyzed using 2-km national composite radar reflectivity data. Based upon the radar-observed characteristics of the 88 documented linear MCSs, a new taxonomy is proposed comprising convective lines with trailing (TS), leading (LS), and parallel (PS) stratiform rain. While the TS archetype is found to be the dominant mode of linear MCS organization (confirming the study by Houze et al. 1990), the LS and PS archetypes compose nearly 40% of the studied population. Synoptic meteorological features attending each class of linear MCS, as well as the population in general, are presented and analyzed. The proposed taxonomy is then evaluated using pre-storm rawinsonde and near-storm wind profiler observations, as well as National Centers for Environmental Prediction (NCEP) reanalyses. Finally, case studies exemplifying the two less-studied linear MCS archetypes are presented.

The MCSs in this study occurred mainly in a region of lower tropospheric warm advection in advance of an upper tropospheric short wave trough, much as found by Maddox (1983). The MCS population presented here exhibited a nocturnal maximum in occurrence, with a secondary maximum near sunrise such as that observed by Geerts (1998). All three

MCS classes were observed to move roughly along the 1000-500 hPa thickness contours and the 700-300 hPa wind shear vector in the mean, in accordance with the results of Merritt and Fritsch (1984). TS MCSs in this study persisted for nearly twice as long as LS and PS MCSs, and moved the most rapidly of the three classes. The environments of TS cases, on average, were supportive of stronger surface cold pools than the environments of PS and LS cases. The stratiform rainfall distributions associated with each class were consistent with the advection of hydrometeors by the mean middle and upper tropospheric winds.

The LS case study presented herein (from 18 May 1997) was able to survive surface inflow of rain-cooled air to its convective line by ingesting buoyant air from the rear, approximately 1 km above ground level. The PS case study presented herein (from 26 May 1996) occurred along a quasi-stationary outflow boundary in an environment with deep line-parallel winds.

Future investigation of the less-studied linear MCS archetypes is commended by this study. Such work is needed to improve the ability of forecasters to recognize the likelihood of different convective modes. As well, better understanding of the linear MCS classes presented here would increase the capacity of numerical models to simulate their resultant effects on the atmosphere.

Matthew David Brown Parker
Department of Atmospheric Science
Colorado State University
Fort Collins, Colorado 80523-1371
Spring 1999

ACKNOWLEDGEMENTS

The research reported here was supported by the National Science Foundation under grants ATM-9313716 and ATM-9618684, as well as a one year graduate fellowship from the American Meteorological Society and ITT Aerospace Communications Division.

National radar composite data were provided by the Global Hydrology Resource Center, satellite images by Purdue University, NCEP Reanalyses by the National Center for Atmospheric Research, and rawinsonde and wind profiler data by the National Climate Diagnostics Center.

I am indebted to P. Haertel for his insight into density currents, to B. Zajac for his help with the national radar data, to A. Kankiewicz for his explanation of radars and wind profilers, and to J. Knievel for his conversational contributions to this work. Dr. B. Geerts kindly provided several of his manuscripts concerning a topic not unlike my own. D. Van De Kamp and M. Barth of the Forecast Systems Laboratory answered many questions about the NOAA Profiler Network. My graduate committee, Profs. B. Bienkiewicz, R. Johnson, and S. Rutledge, invested much time and energy in reviewing this manuscript and evaluating my work. I am especially thankful to my advisor, Richard Johnson, who willingly allowed me to experiment, fail, and ultimately succeed on my *own* terms. I am also deeply indebted to the staff of the mesoscale research group: G. Cordova, R. Taft, and P. Ciesielski ably answered questions and solved problems throughout this study. Finally, I am thankful to my wife, Kerri, who both proofread this manuscript and unconditionally supported me during my long hours as this work came to its fruition. *SDG.*

CONTENTS

FIGURES

TABLES

Thither let us bend our thoughts, to learn
What creatures there inhabit, of what mould
Or substance, how endued, and what their power
And where their weakness...

—Milton,
Paradise Lost

Chapter 1

INTRODUCTION

Zipser (1982) first defined "mesoscale convective systems" (hereafter, MCSs) as, "cloud and precipitation systems, together with their associated circulation systems, which include a group of cumulonimbus clouds during most of the lifetime of the system." The ubiquity and duration of MCSs, in addition to their frequently attendant severe weather, have motivated many studies since this initial appellation. The present investigation represents a continuation of work on the problem of MCS organization and its relationship to the environment as well as a renewed attempt to construct a taxonomy of midlatitude convective systems.

A topic of particular interest to forecasters, meso-meteorologists, and numerical modelers is the relationship of convective modes to the environments in which they occur, a problem taken up once again in this study. Organized convective structures, movements, and lifetimes have been compared to the qualitative and quantitative charactertistics of the surrounding atmosphere in numerous case studies, the earliest of which include those by Newton (1950) and Pedgley (1962). As well, *populations* of MCSs have been periodically observed by field experiments, facilitating analysis of their attendant conditions (e.g. Barnes and Sieckman 1984 for the GARP Atlantic Tropical Experiment, or GATE; Alexander and Young 1992 for the Equatorial Mesoscale Experiment, or EMEX; and LeMone et al. 1998 for the Tropical Ocean Global Atmosphere- Coupled Ocean-Atmosphere Response Experiment, or TOGA-COARE). Attempts have also been made to construct MCS populations from *operational* datasets such as the National Weather Service (NWS) radars, and to

compare them with conventional observing platforms such as rawinsondes (e.g. Bluestein and Jain 1985– hereafter BJ85, Bluestein et al. 1987– hereafter BMJ87, Houze et al. 1990– hereafter HSD90, Augustine and Caracena 1994, Hashem and Biggerstaff 1998, and Corfidi 1998). Finally, the above observational studies have also been complemented by numerical modeling investigations of deep convection's sensitivity to environmental variations, among the first of which was performed by Orville (1968).

A specific sub-set of MCSs known as mesoscale convective complexes (MCCs, as defined by Maddox 1980) have received a great deal of additional attention (e.g. Maddox 1983, McAnelly and Cotton 1986, Laing and Fritsch, 1993a, 1993b, and 1997, and the lineage of annual summaries begun by Rodgers et al. 1983) due to their ease of identification from infrared satellite imagery. The full global coverage of satellite data makes them particularly useful in the assembly of a study population, and indeed MCC studies represent an important step in the road to understanding MCSs. However, satellite images depict only the tops of the cumulonimbi which compose MCSs. Images of cumulogenic anvil cirrus clouds are satisfactory for the diagnosis of MCCs, but reveal little, if any, of the actual organization and structure of the underlying convection. There exists a vast spectrum of linear and non-linear convective systems, many of which may generate similar cloud shields (as observed from satellite imagery) that satisfy the MCC criteria.

Radar data allow a detailed look at the arrangement *and* intensity of precipitation on very fine temporal and spatial scales. Using radar, MCSs can be identified based upon more physical criteria than anvil size. The linearity, arrangement of stratiform rain elements, and location of deep convection with respect to points of interest (e.g. surface observations, wind profilers, rawinsonde stations) can be assessed without the ambiguity presented to satellite platforms by an upper tropospheric cloud shield. Geerts (1998) pointed out that, "composite reflectivity imagery is... a unique but underutilized tool for research and nowcasting." National 2-km composite reflectivity data (cf. Section 3.2) were chosen for the present study as they permitted the examination of a relatively large horizontal region (such as

might expand previous single-radar studies, e.g. BJ85, BMJ87, and HSD90) while still affording the increased detail provided by radar.

No *true* national climatology of United States MCSs exists, probably due to the spatial and temporal limitations of conventional observing networks. As well, MCSs' high frequency and ubiquity make identification and bookkeeping quite time-consuming for long temporal and large spatial scales. Undaunted, however, I proceeded toward this goal. I began with the month of May 1996, investigating national radar composites and cataloguing MCSs within 17 climatic/geographic regions of the United States, trying to document relevant regional variations as well as long-term correlations between MCSs and their environments. I learned a great deal by observing this large population. I also gradually accepted that the time restrictions on my study would prohibit the actual generation of a U.S. climatology for MCSs. Importantly, however, the large volume of radar data I'd reviewed planted the seeds for a more focussed investigation.

HSD90 found that a majority of the mesoscale precipitating systems in Oklahoma during the spring months of 1977–1982 exhibited a "leading line trailing stratiform" precipitation structure. However, the initial investigation of May 1996 MCSs for the entire United States left me with a subjective impression: that in certain regions and synoptic regimes, modes of linear convection *other* than the oft-referenced leading-line trailing-stratiform archetype were common or even predominant. In particular, numerous cases were observed for which a large proportion of the stratiform rainfall appeared to exist in *advance* of a moving convective line. Yet a third mode existed in which stratiform rain appeared to move (in a storm-relative sense) parallel to an MCS's convective line. These observations, initially thought to be anomalous, motivated a more detailed analysis of MCSs in the central United States (due to the wind profiler network and high frequency of MCSs there).

At first, the arrangement of stratiform rain may appear to be a relatively less important problem in the purview of MCS studies. However, an accurate understanding of the conditions associated with various recurrent precipitation archetypes is an instrumen-

tal part of correct parameterization (in numerical models) and operational forecasting of MCSs. Convective storms circulate mass and redistribute momentum and entropy in the troposphere. Mapes (1993) pointed out that the heating profiles in stratiform and convective rain regions produce different effects in the surrounding atmosphere. LeMone and Moncrieff (1994) showed that *organized lines* of convection do so in different ways than isolated cumulonimbi, often transporting momentum up-gradient and *increasing* the vertical wind shear. If various *archetypes* of linear MCSs could also be shown to perform the above functions differently from one another, increasingly detailed convective parameterizations could be developed for numerical general circulation models. In addition, Doswell et al. (1996) pointed out the relevance of stratiform rain distribution to flash flooding associated with MCSs (cf. their Fig. 3). The operational forecaster, aware of likely characteristics for organized convection based upon environmental parameters, might more successfully forecast MCS severity, duration, areal coverage, movement, and potential to produce flash floods.

This study does not provide a completely conclusive result. It is, however, one step down a road of increasing awareness to different convective archetypes and their environmental conditions. Synoptic patterns and features for time periods of MCS activity and inactivity are discussed. Thereafter, a new taxonomy is presented in order to characterize the most common modes of linear MCS organization. The taxonomy is then supported by means of statistically significant differences between the linear MCS classes and in turn related to synoptic regimes attending each group. Several hypotheses regarding the physical differences between archetypes are also evaluated. Finally, case studies exemplifying the two less-studied linear MCS archetypes are presented. While the limited seasonal and spatial nature of the data used in this study preclude the development of a full climatology or a set of forecasting rules, the possible character of such end-products may be cautiously inferred from these initial results.

Chapter 2

BACKGROUND FOR THIS STUDY

2.1 Definitions

Before venturing into subsequent chapters, it will be helpful for the reader to have an initial grasp of the terminology utilized in this manuscript. Several of the terms glossed below will be more fully defined at a later point in the text. Their inclusion here was deemed useful, however, as a means of orientation prior to the literature review in Section 2.2.

2.1.1 General terminology

Numerous interpetations of Zipser's (1982) initial definition of MCSs have arisen in the past 16 years. In particular, radar meteorologists have imposed reflectivity-based criteria upon the definition to expedite and objectify the selection of cases and compilation of populations for study. A physically motivated, quantitative definition of MCS as it pertains to this investigation is presented in Section 3.1. For now, suffice it to say that MCSs are cloud systems, comprising amalgamated deep convective cells and wide-spread cumulogenic hydrometeors, that circulate air on temporal and spatial scales greater than an individual cumulonimbus.

Within this manuscript, MCSs are discussed using several descriptors, among which are *linear* and *non-linear*. Linear MCSs are considered to be those containing a *convective line*, by which is meant a contiguous or nearly contiguous *chain* of convective echoes (defined as those with reflectivity factors $\geq$ 40 dBZ, cf. Section 3.2.2), whether in a nearly straight or moderately concave pattern, that share a nearly common leading edge

and move approximately in tandem. Within the context of this study, large convecting systems with highly eccentric precipitation patterns but without convective lines were *not* considered linear MCSs (a departure from the nomenclature of Laing and Fritsch 1998). MCSs that attained the requisite size and duration for definition as an MCS but did not exhibit convective lines were called non-linear.

As well, this study makes use of the distinction between *warm sector* and *elevated* MCSs. These terms are meant to be mutually exclusive in this manuscript. Warm sector MCSs occur in the warm, moist, (typically) conditionally unstable airmass demarked by synoptic fronts, a region referred to as a warm sector in the seminal work of Bjerknes and Solberg (1922). By contrast, elevated MCSs are those which occur aloft of the cold air in advance of (typically, to the north of) a synoptic scale warm or stationary front, so-called because they exist and draw air from above a frontal inversion. The designation of an MCS as "warm sector" does *not* preclude the possibility of a buoyant air source aloft, but refers to the MCS's location with respect to synoptic features. Ultimately, for the purposes of this paper an elevated MCS could be more verbosely described as "non-warm sector". The motivation for this distinction is expanded upon in Section 3.1.

Within this manuscript, the scales of various meteorological phenomena are described according to the nomenclature proposed by Orlanski (1975). Since their introduction, these definitions have gradually become the *de facto* standard for mesoscale subclassification, and are therefore presented without a philosophical argument on their behalf. Phenomena ranging in horizontal extent from 2–20 km are said to occur on the *meso-*γ scale. Those with length scales between 20 and 200 km are called *meso-*β scale. Finally, phenomena ranging from 200-2000 km are here referred to as *meso-*α scale. Motions and entities larger than 2000 km are called by the broad moniker *synoptic.*

Finally, it is expedient to mention the commonly used term, *squall line.* BJ85 presented a lucid summation of the term's history and current application, pointing out that while the appellation *squall line* was initially reserved for *non-frontal* convecting lines with

wind shifts (cf. Huschke 1959), it has increasingly been applied to almost all types of thunderstorm lines. Indeed, Rotunno et al. (1988, hereafter RKW88) merely defined a squall line as, "...any line or narrow band of active thunderstorms." I have attempted to refrain from use of the term squall line altogether due to its vagaries. When it does appear in this manuscript, it is to emphasize the familiarity between the present study and those of the past that, in name or in substance, specifically treated "squall lines". For such cases, *I* have inferred the latter, more general meaning for squall lines used by BJ85 and RKW88.

2.1.2 Initial introduction of linear MCS archetypes

I have made every attempt to structure this manuscript in a logical and readable manner. However, there were instances in which it was appropriate, even necessary, to refer to the linear MCS archetypes in my taxonomy before their formal presentation. Therefore, in order to facilitate discussion prior to the full definitions given in Chapter 5, the three MCS classes within this study are here glossed in short. Should curiousity overcome the reader, he/she may chose to read Section 5.1 now in order to further enlighten the condensed definitions given here.

A well-known configuration for MCS precipitation is the leading-line trailing stratiform (hereafter in this manuscript, TS) model, defined by HSD90. Their definition was accepted *a priori*, in order to facilitate intercomparison as well as due to its prevalence in the literature. In short, TS MCSs exhibit a convective line with stratiform rain predominantly distributed opposite the direction of the line's motion (i.e. trailing it, cf. Fig. 2.1). By contrast, MCSs with leading stratiform rain, that is, precipitation predominantly distributed in the *same* direction as that of the convective line's motion, are called LS. Finally, MCSs whose stratiform rain is distributed neither ahead, nor behind the convective line, but rather in a band parallel to it, are called parallel stratiform (hereafter, PS) MCSs.

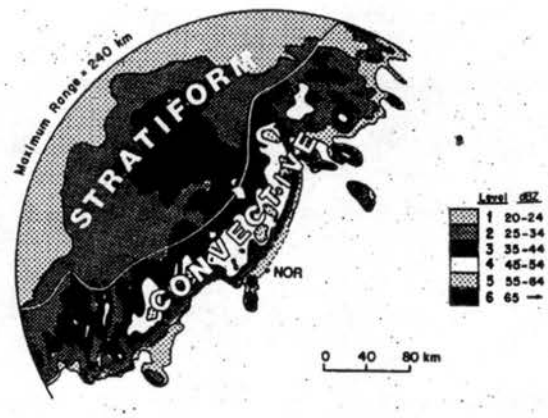

Figure 2.1: Example of a leading line trailing stratiform MCS's reflectivity from Houze et al (1990). Motion is toward the southeast (lower-right).

2.2 Review of previous work

2.2.1 MCS environments

A great deal is known about the general local conditions needed to support a cumulonimbus, specifically a lifting mechanism (or *trigger*) to raise parcels until positively buoyant in a conditionally unstable atmosphere. Numerous studies, regarding both midlatitude and tropical convection, have sought further correlations between specific parameters (e.g. critical values of state variables, computed indices, etc.) and convective modes, movements, and orientations. A sampling from the wealth of such studies is presented in Section 3.5 as motivation for the parameters investigated in the current study.

As well, the synoptic conditions associated with large regions of mid-latitude convective development have been documented and discussed for some time. Maddox and Doswell (1982) discovered that low level warm advection, rather than upper tropospheric vorticity advection, often accounted for the synoptic or mesoscale ascent observed during extended periods of intense convective storms. Maddox (1983) composited conditions for 10 *mesoscale*

convective complexes (or MCCs, a specific subset of MCS defined from infrared satellite imagery) and found that they often occurred ahead of weak middle tropospheric short wave troughs, predominantly in a region of lower tropospheric warm air advection (often associated with a *low-level jet*). Both Velasco and Fritsch (1987) and Augustine and Howard (1991, hereafter AH91) found that MCCs frequently occurred on the "periphery" of a long-wave middle tropospheric anticyclone. It was suggested by AH91 that their compositing technique merely failed to resolve the upstream short-waves analyzed by Maddox (1983). The predominant role of low-level thermal forcing for MCCs reported by Maddox (1983) was also confirmed by Velasco and Fritsch (1987), Cotton et al. (1989), and AH91. Augustine and Caracena (1994) emphasized the role of low-level jets and frontogenetic circulations in the development of nocturnal MCSs in a region similar to that of the present study. Notable compilations of MCCs, including the annual summaries presented by Maddox (1980,1981), Maddox et al. (1982), Rodgers et al. (1983, 1985), and Augustine and Howard (1988, 1991) also discussed the general synoptic regimes for periods of relatively frequent and infrequent MCC occurrence. While for MCCs, these results are nevertheless relevant indicators of the typical large-scale conditions attending large regions of deep convective clouds (i.e. MCSs in general).

The current investigation comprised 88 linear MCS cases from the month of May for two successive years, of which 54 uncorrupted (by bad data or other contamination) warm sector cases were investigated vis a vis environmental parameters. Differences between active and inactive periods (as defined in Section 4.2) for linear MCSs as well as between the synoptic regimes of May 1996 and May 1997 were investigated. As the latter period produced far more MCSs in the central Plains than the former, the differences between the time periods *also* to some degree indicate the sorts of environments that will or will not support long-lived convective systems.

Of additional interest were the studies performed by BJ85 and BMJ87. They found that a great deal of squall lines occurred near cold fronts, but that squall lines were gener-

ally distributed near many types of surface boundaries, including drylines and warm fronts. Further, some squall lines were found near the intersection of outflow boundaries. This confirmed work by Purdom (1986) emphasizing the importance of thermal boundary interactions in convective generation. This spectrum of linear surface triggers, as well as the predominance of cold frontal forcing, was confirmed by the present study of linear MCSs (Section 4.1.2).

2.2.2 Diurnal variation in MCS frequency

Wallace (1975) was the first to formally document the nocturnal maximum in convective storm occurrence over the central Plains. HSD90 found a nocturnal maximum in large "mesoscale precipitation systems" over Oklahoma. As well, numerous studies (e.g. Maddox 1980, McAnelly and Cotton 1986, Augustine and Howard 1988, and AH91) have noted that MCCs occur most often during the nighttime hours. All of the above studies have generally revealed that the frequent presence of a nocturnal southerly lower tropospheric wind maximum (the *low-level jet*) over the central Plains plays a significant role in this diurnal cycle due to its northward transport of buoyant air. The MCS population in the present study conformed to the previously discovered diurnal cycle in linear MCS frequency. A distinct nocturnal maximum was noted for TS cases. In addition, a secondary maximum near local sunrise was noted (particularly for LS cases), a signal also documented for MCSs in the southeastern United States by Geerts (1998). Gray and Jacobson (1977) discussed the nighttime strengthening of solenoidal overturning due to imbalances in radiational cooling of cloudy and clear areas, claiming that the "maximum accumulated nighttime radiational cooling effects should occur 1–2 h after sunrise". The mechanism proposed by Gray and Jacobson (1977) may indeed explain this less-frequently documented phenomenon. These results are presented and discussed in Section 4.3.

2.2.3 *MCS structure: evolution, circulations, and stratiform rain distribution*

Newton (1950) was the first to point out that long-lived convective lines comprise a system of continuously maturing and decaying thunderstorm cells, and suggested a mechanism for an ongoing, *multicellular* thunderstorm line related to the triggering of new cells by downdrafts. Since then, understanding of the evolution and dynamics of line convection has continuously increased, with more detailed observations, modeling studies, and increasingly refined conceptual models, such as that presented by Houze et al. (1989). Ludlam (1963) was the first to note that within mature thunderstorm lines, a mean updraft existed that was canted toward the storm's rear with height (notably, an observation of a TS line). Apart from lines composed of *supercells* (long-lived rotating storms first defined by Browning 1964), scientists have continued to find a multicellular structure within most linear deep convective bands. Recently, Fovell and Dailey (1995) found that various modes of modeled line convection, regardless of regeneration periodicity, fit a common observation that new convection in multicells appears near the leading edge of storm outflow and subsequently moves upward and rearward within the canted updraft flow described by Ludlam (1963). The result is a deposition of hydrometeors to the rear of the convective line (or, a TS structure).

Moncrieff (1992) showed with an idealized analytical model that this ascending front-to-rear flow (called the "jump updraft" in his work) *should* exist theoretically, as well as an "overturning" updraft directly above the leading edge of the surface outflow (Fig. 2.2a). Notably, Ludlam (1963, Fig. 2.2b) and Thorpe et al. (1982, Fig. 2.2c) also appeared to include both updraft types in their conceptual models of multicellular storms. Similar conceptual models were also adapted by RKW88 from studies by Zipser (1977) for GATE, Newton (1963) for the Thunderstorm Project, and Carbone (1982) for a California squall line (Fig. 2.3). The prominence of the front-to-rear, or jump, updraft in the recent literature has probably arisen from the numerous observations of TS systems presented both by HSD90 and a host of papers regarding TS MCSs from PRE-STORM. Fankhauser et al. (1992)

correctly noted that while early attention to squall lines was focussed on systems with leading anvil cloudiness and a significant overturning updraft (e.g. Newton and Newton 1959, Newton and Fankhauser 1964, and Newton 1966), the advent of *MCS* studies began increased attention to the front-to-rear movement of hydrometeors.

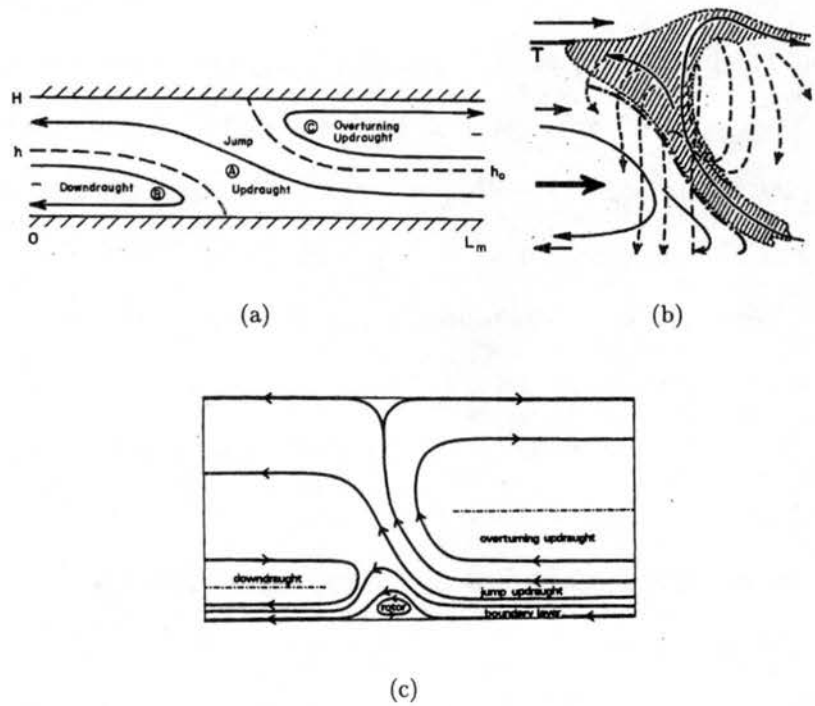

Figure 2.2: Conceptual models of convective lines depicting both jump and overturning updrafts: (a) from Moncrieff (1992); (b) from Ludlam (1963); (c) from Thorpe et al. (1982).

The common observation that decaying convective cells in a multicell line move rearward has been subject to many theoretical descriptions. Perhaps the most prominent of these was the "theory for long-lived squall lines" advanced by RKW88. This work represented a refinement of the numerical modeling effort of Thorpe et al. (1982), who hypothesized that the advance of an evaporatively-driven surface cold pool could be retarded by the presence of strong low-level shear, producing a quasi-steady state. RKW88 hypothesized that the solenoidal circulation at the leading edge of a surface cold pool would produce a nearly vertical jet of air if it exactly balanced the horizontal vorticity of the pre-gust

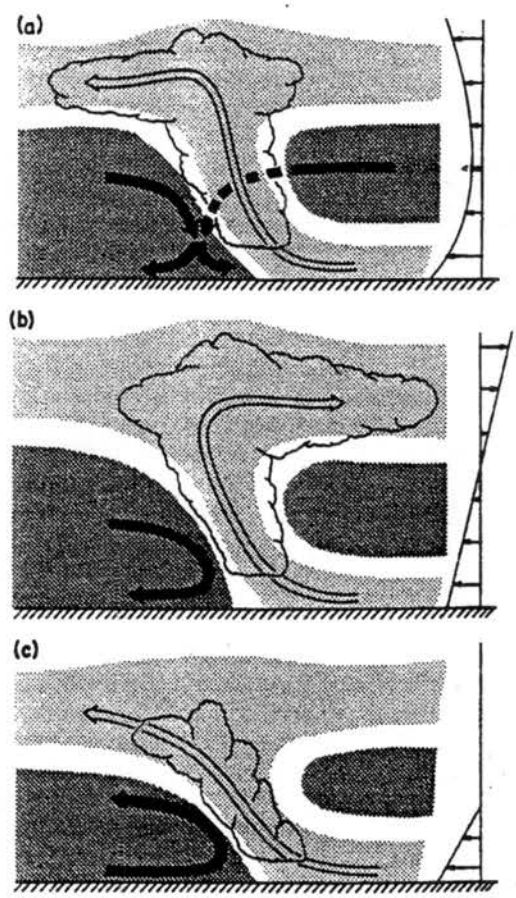

Figure 2.3: Conceptual models of convective lines adapted by Rotunno et al. (1988) from (a) Zipser (1977); (b) Newton (1963); (c) Carbone (1982). Vectors indicate sense of vertical wind profile, broad arrows indicate general draft structure.

front environment (cf. Fig. 2.4). They suggested that this would be an optimal state for strong, long-lived squall lines due to the maximization of vertical momentum in an updraft (Fig. 2.4d). Non-ideal solutions would produce canted updrafts. While criticisms have been levied against this hypothesis (e.g. by Lafore and Moncrieff 1989, who claimed that baroclinic generation of vorticity in stratiform rain regions must be considered), the so-called *RKW theory* continues to be an idea with which many case studies and models are compared (e.g. Fankhauser et al. 1992, Grady and Verlinde 1997).

Notably, long-lived cases exist which are not "ideal" according to RKW88. The commonly observed TS class of MCSs is known to be very long-lived, yet apparently represents

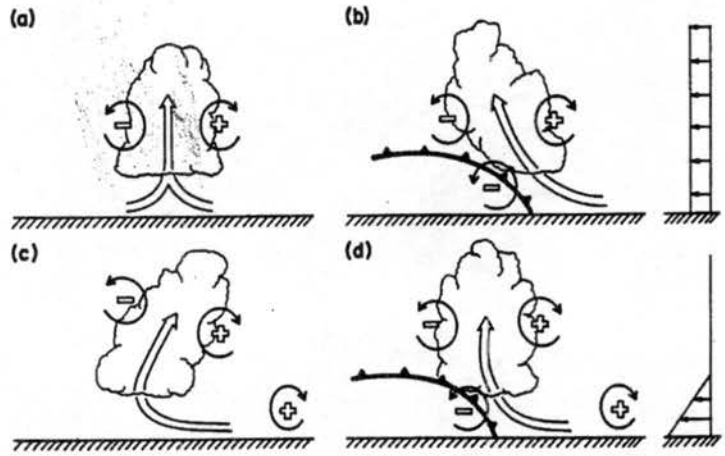

Figure 2.4: Schematic depicting the balance of cold pool circulation and shear for idealized scenarios in Rotunno et al. (1988): (a) no cold pool, no shear; (b) cold pool, no shear; (c) no cold pool, low-level shear; (d) cold pool with low-level shear. (d) is the *optimal state* suggested by Rotunno et al. (1988).

a "less than optimal shear" state (approximately that in Fig. 2.4b). In effect, however, it is this less-than-optimal low-level shear that promotes the rearward canting updrafts and provides the mechanism for gust front regeneration as discussed above and as modeled by Fovell and Ogura (1988). While RKW88 considered a long-lived "greater than optimal shear" solution (approximately that in Fig. 2.4c), in which inflow air passes through a rain curtain and slows in a convergent region, they claim that, "the overly strong shear depletes the cells of their convective vigor." An important observation of the present study, therefore, is the notably high reflectivities and visibly "active" appearance of many LS MCSs. Others (e.g. Grady and Verlinde 1997, see below) have also considered this problem, and have found that the applicability of the RKW88 theory is limited in a variety of different shear scenarios, and that the cold pool/low-level shear relationship may be less significant than the upper-level shear in determining the updraft tilt and structure for particular tropospheric wind profiles. This issue provided additional motivation for the present study, in which numerous *long-lived* linear MCSs existed in states that were far different from the RKW88 optimal state.

2.2.4 MCS taxonomies

Several noteworthy attempts at classifying MCSs have been advanced in the literature. Perhaps the first was undertaken by BJ85 and BMJ87, who presented a taxonomy based upon the organizational "pathway" along which convective systems developed. They found that common modes of squall line formation included broken line, back building, broken areal, and embedded areal (cf. Fig 2.5). While the methods of the present study are quite similar to those used by BJ85 and BMJ87, the *focus* of my work is a description of the arrangement of convective and stratiform elements in long-lived convection (rather than an investigation of formational modes). This distinction *is* non-trivial, as Loehrer and Johnson (1995) found that a TS precipitation archetype could arise from several evolutionary modes (Fig. 2.6). Therefore, while the present investigation is certainly descended of BJ85 and BMJ87, it seeks to answer a different question.

Another undertaking, quite similar to that of the present work, was presented by Blanchard (1990, hereafter B90). Radar data from the Preliminary Regional Experiment for STORM-central (PRE-STORM) were evaluated and a new taxonomy comprising 3 categories was presented. Over a period of 2 months, 25 cases were documented and assigned to the classifications of linear, occluding, or chaotic (Fig. 2.7). I did not attempt to incorporate B90's taxonomy into my own due to several philosophical disagreements with its premises. Firstly, B90 considered all non-linear systems to be "chaotic". While the present manuscript only treats linear modes of convection, a preliminary examination of *all* MCSs over the entire United States strongly supported the idea that there are probably non-linear yet well-organized (i.e. *not* chaotic) convective systems. Secondly, the difference between B90's examples for linear and occluding systems was vague. Indeed, Doswell (1990) pointed out several instances of possible overlap between the two categories. In addition, Loehrer and Johnson (1995) documented the evolution of long-lived symmetric lines (which would presumably be deemed "linear" by B90) toward an asymmetric pattern quite similar to that called "occluding" by B90 (cf. Figs. 2.6 and 2.7). Doswell (1990) further critiqued the

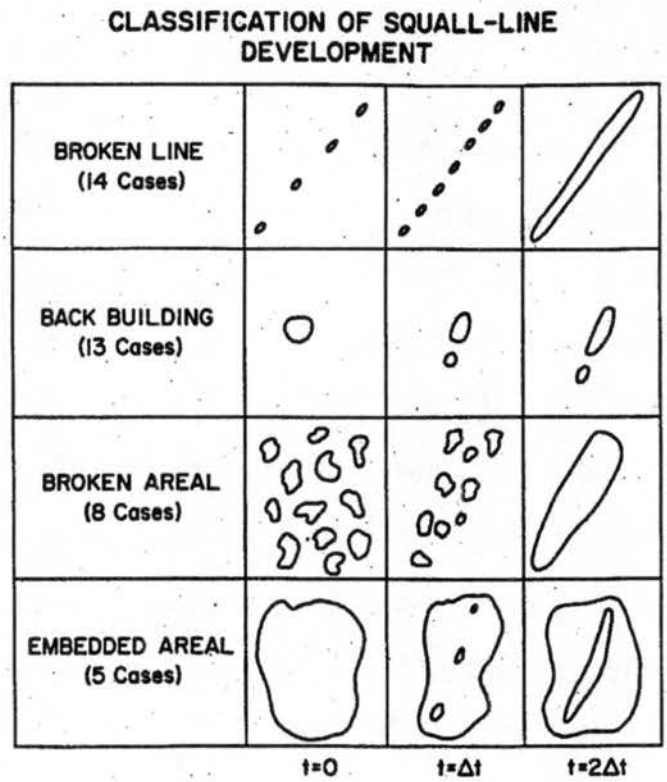

Figure 2.5: Idealized reflectivity depictions of squall line formation from Bluestein and Jain (1985)

use of the term "occluding", which had previously only been applied to baroclinic systems. Finally, the species of "linear" cases, while appropriately describing a part of the MCS population, is not sufficiently evocative to indicate the commonalities among *sub-groups* of linear MCSs.

Perhaps the present study most resembles the work of HSD90, who considered 63 "mesoscale precipitation systems" that were observed within the Norman, Oklahoma Weather Surveillance Radar (WSR)-57 range during the spring (April, May, and June) months of six successive years, discussing related environmental parameters in addition to associated severe weather events. Their objective was to evaluate the degree to which the population of observed precipitation systems (which were, for the most part, MCSs based upon the criteria in the present study) conformed to a "leading-line trailing-stratiform" (TS) struc-

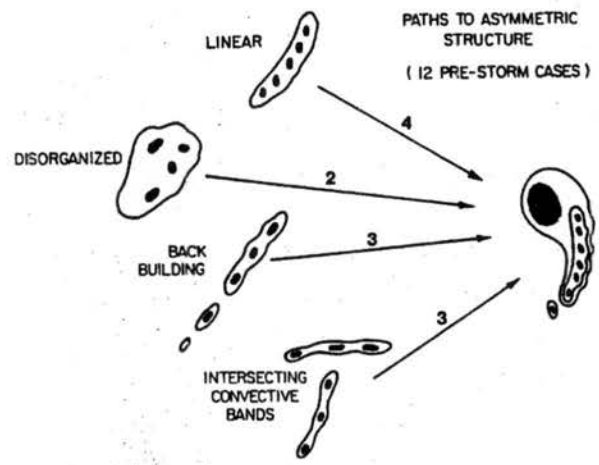

Figure 2.6: Schematic of paths to asymmetric reflectivity structure discussed by Loehrer and Johnson (1995), from an adaptation by Hilgendorf and Johnson (1998).

tural archetype such as that depicted in Fig. 2.1, as well as to determine the degree to which MCSs were "asymmmetric". Based upon the discussion of "classifiability" given by HSD90, it is believed that the 21 cases deemed "unclassifiable" by HSD90 were essentially non-linear, leaving 42 catalogued linear "mesoscale precipitation systems" whose recognition criteria were very similar to those I used for MCSs. Details of HSD90's results are discussed further in Section 2.2.5.

In a related effort, Schiesser et al. (1995, hereafter SHH95) documented the mesoscale structure of "severe precipitation systems" in Switzerland. In fact, SHH95 presented a figure *implying* a taxonomy similar to that presented in this study (cf. Fig. 2.8). Their "trailing" schematic is the well-known TS archetype, while their "ahead" schematic corresponds quite obviously to the LS archetype in the present study. The "none" schematic presented by SHH95 includes almost no stratiform rain, a condition (as discussed in Section 5.1) for *unclassifiability* in my work. It is possible, however, that the "none" schematic could correspond to PS MCSs for which the stratiform rain region was simply beyond the range of Switzerland's two weather radars. The issue is a bit confusing as their description of the "none" cases merely stipulates, "no significant stratiform rain either ahead of or behind

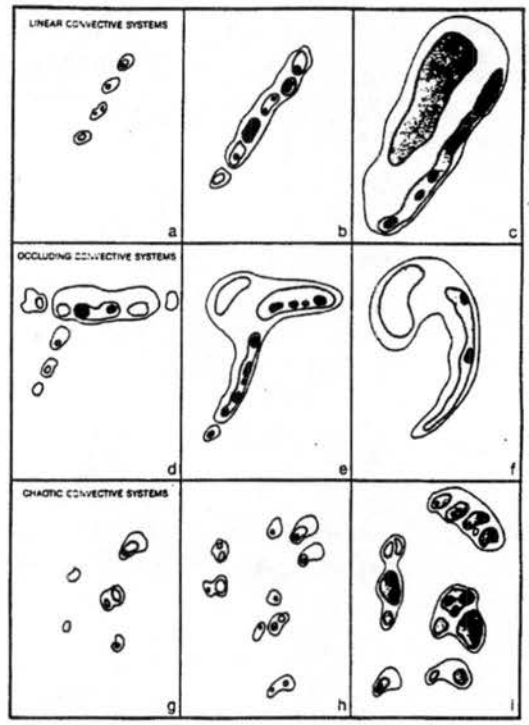

Figure 2.7: Schematic of reflectivity evolution for the three convective modes documented by Blanchard (1990) from PRE-STORM. (a-c): linear convective systems; (d-f): occluding convective systems; (g-i): chaotic convective systems.

the line." Therefore, it is unclear whether SHH95 considered parallel stratiform rain or not. Despite SHH95's recognition of these recurrent MCS precipitation patterns, they treated all non-TS precipitation systems (following the HSD90 criteria) as "unclassifiable".

Finally, Rickenbach and Rutledge (1998) discussed convection in TOGA-COARE and constructed a taxonomy to describe the scale and organization of the events considered. Convection was characterized based upon extent (MCS vs. sub-MCS) and linearity (linear vs. non-linear). While this taxonomy is appropriate for the segregation of an entire population of deep convective storms, the present study shall deal only with *sub-divisions* of what Rickenbach and Rutledge (1998) have deemed the "linear MCS" category.

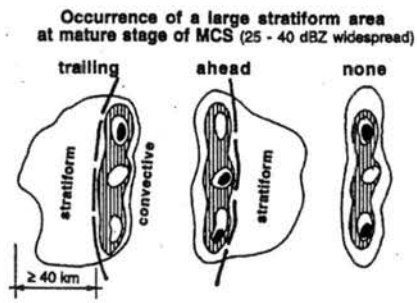

Figure 2.8: Schematic reflectivity drawings of the organization of Swiss mesoscale convective systems from Schiesser et al. (1995).

2.2.5 Why a new taxonomy?

Interestingly, of the 42 linear cases compared to the TS archetype by HSD90, 10 were deemed "weakly classifiable", indicating an overall negative score in 10 categories of TS "classifiability". An additional 18 of the 42 linear cases were called only "moderately classifiable" by HSD90. Therefore, 67% of the linear convective systems catalogued by HSD90 had several or many characteristics which were *inconsistent* with the TS archetype. The present work identified 2 *more* prominent archetypes for linear MCS organization. In my study, 38.6% of the total linear MCSs catalogued were described by these additional archetypes.

The classification of cases not conforming to the TS archetype is appropriate *if* sufficiently large sub-populations of MCSs resemble one another *more* than the TS (or any other) archetype. While a majority (51, or 58.0%) of the 88 cases that I considered conformed well to the TS archetype, 17 (19.3%) were most like the LS archetype and 17 (19.3%) most resembled the PS archetype. The notable advantage of the taxonomy presented in this manuscript is its drastic reduction of "weakly classifiable" linear cases, from 24% in HSD90 to 3% (called *unclassifiable*) in the present study. In addition, it provides appropriate nomenclature for the "unclassifiable" cases presented by SHH95.

It seems clear that nearly all taxonomies *should* include an "unclassifiable" category (which is meant to include examples not easily fitting some pre-conceived model)

to address unusual cases as well as significant variations from idealized archetypal structures. As Gould (1989) discussed and Doswell (1990) reiterated, trying to "shoehorn" *every* real-world example into a category not only dulls the classes' archetypal essence, but also trivializes the existence of "oddball" cases. This is particularly true for convective motions in a chaotic fluid such as the atmosphere. It is, however, viewed as an accomplishment that most MCSs catalogued during the presently studied period *were* deemed classifiable and were well-described by the nomenclature herein. Note that the taxonomy presented in this work is based solely on the radar charactertistics of MCSs, not on environmental or dynamical observations. The possibility of a related dynamical classification, perhaps similar to that presented here, is left open for future studies. While sub-divisions even beyond what are presented here are indeed possible, the designations I've suggested represent dominant modes (from a radar perspective) within a significant majority of the linear MCSs observed in this study.

The utility of a more detailed taxonomy is not merely philosophical, however. The initial survey of MCSs for the entire United States in May 1996 (undertaken during the evolutionary stages of this project) suggested that during certain time periods and for certain regions, the TS archetype may *not* be the dominant mode of organized long-lived convection. It is therefore important that MCS cases be compared not *only* to the TS model, but also to other (albeit less prominent) species of MCS. Only in this manner will forecasters learn whether non-TS models are applicable to given locations, periods, and conditions.

As a final note, it is important to emphasize that the previous taxonomies and the current work are *not* mutually exclusive. For sake of example an MCS might, quite fairly, be called "back-building" by BJ85/BMJ87, "linear" by B90, "moderately classifiable and asymmetric" (with respect to the TS model) by HSD90, and "PS" within the present study. This is not seen as a problem (no more so than an automobile being described as both "red" and "a convertible"). However, the strong correlations between certain environmental

variables, synoptic regimes, and the linear MCS classes presented in this study are, in this author's opinion, a compelling argument for adoption of the suggested nomenclature.

2.2.6 Paying attention to previously undifferentiated MCSs

Let the reader not be misled into believing that I have *discovered* new modes of convection. This manuscript, rather, represents a call for attention to sub-sets of MCSs which have been periodically observed but given little study. Remarkably, SHH95 (who used HSD90's TS criteria) found that for the 17 (of 43 total) "unclassifiable" (i.e. non-TS) Swiss line-structure MCSs, 12 had a structure described by their "none" schematic (some of which *I* believe may actually be PS MCSs), and 5 had a structure such as that called LS in the present study. Why then have non-TS MCSs been relatively overlooked? Firstly, it is believed that when scientists choose case studies, they select MCSs that are particularly large, strong, and long-lived, qualities which are most commonly associated with TS MCSs (cf. Section 5.2). In addition, however, HSD90's exhaustive study found the TS model to represent a majority of Oklahoma MCSs. Since that time, a great deal of work has been devoted to the description and explanation of smaller and smaller scales within these most common of linear MCSs, certainly a worthwhile effort. I merely suggest that the less-studied, non-TS modes of linear MCS *also* deserve continued attention.

This is certainly not to say that non-TS MCSs have never been investigated. Indeed, examples of quasi-LS MCSs have occasionally appeared as published case studies. Houze and Rappaport (1984) documented a squall line from GATE, during which precipitation appeared in advance of the convective line for a period of time (Fig. 2.9). However, the transience of the pre-line rain with respect to the entire lifetime of the squall line would compel me to place this case within the TS class in my study. Kessinger et al. (1987) presented a squall line case study with a strong overturning updraft and pre-line anvil cloud (Fig. 2.10). As the archetypes in the present study are defined by *base scan reflectivity*, however, the Kessinger et al. (1987) line would also be classified as TS herein. Fankhauser

et al. (1992) documented a squall line formed in strong shear that had a pre-line anvil and a small amount of leading stratiform rain (Fig. 2.11). Again, however, this case would not have been classified as LS based upon its low-level reflectivity. Indeed, Fankhauser et al. (1992) stated that the majority of precipitation associated with the squall line fell to the rear of the updraft. Notably, Fankhauser et al. (1992) discovered several supercellular characteristics within their studied squall line. Weisman et al. (1988) suggested that lines of supercells could be long-lived and exhibit a leading anvil, a possibility which had to be considered in this study. Grady and Verlinde (1997) documented a squall line that *met* the objective criteria for LS in the present study (cf. Fig. 2.12). They attributed the forward leaning updraft and leading stratiform rain to the strong upper tropospheric shear far above the surface cold pool. Finally, while sharing some characteristics with PS cases, the MCS studied by Nachamkin (1998) also exhibited a lobe of leading stratiform rain (not shown) such that this author considers it an LS example. As only two previous case-studies meeting the definition of LS are known to the author, it is believed that the LS examples represented herein are extreme members within a spectrum of MCSs exhibiting leading anvil clouds, thus making their prominent representation in this study even more noteworthy. Before moving on, it is additionally emphasized that while quasi-LS MCSs have been periodically studied *individually*, almost no attention has heretofore been given to them *as a group*.

Even less has apparently been published regarding the so-called PS cases in this manuscript. Reasons for this are unclear. It may be that since the majority of MCS case studies and populations have focussed on a relatively small area (i.e. within a radar's range), that very rarely have *both* the convective line and parallel stratiform region been captured within the observed domain. As well, many of the hypotheses about circulations near the convective lines of TS MCSs involve hydrometeor microphysics within the nearby stratiform rain region (e.g. Gallus and Johnson 1995). Perhaps PS cases were in part ignored due to their apparent lack of relevance to such specific problems. In any case, the author *was* able to locate several possible examples of PS reflectivity structures within the radar examples

given by HSD90, presented here in Figure 2.13. As will be emphasized later, however, the entire *evolution* of an MCS must be considered in classification, not merely an instantaneous snapshot. Notably, the three quasi-PS examples fell within HSD90's "moderately" and "weakly classifiable" grades and were therefore not considered *archetypally* TS (by HSD90).

Grady and Verlinde (1997) and Nachamkin (1998) pointed out the marked differences between individual linear convective systems and the TS conceptual model. The existence of the TS model *is* beneficial to the extent that it explains the dynamics of quasi-TS MCSs, which *do* appear to constitute a majority of convective systems. This should not preclude investigation into the dynamics and structure of other frequently observed archetypes, however. While the present study has only approached the relatively less-investigated LS and PS classes from a horizontal reflectivity and general environmental standpoint, it will hopefully spur into action additional, more dynamical studies of LS and PS MCSs. The ideal end products of this strain are conceptual models that represent all *three* archetypes of linear MCS, thereby describing almost the entirety of the linear MCS population, not simply its most frequent class.

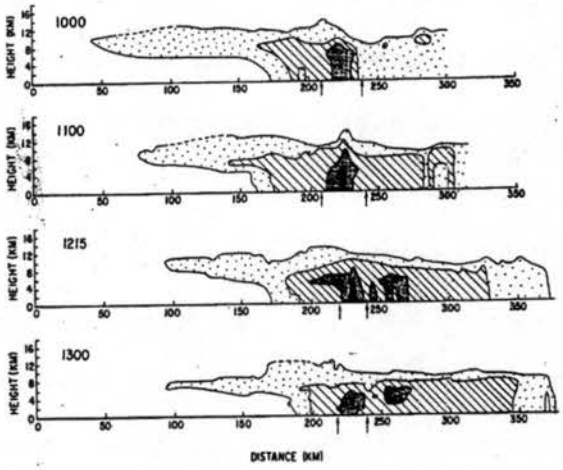

Figure 2.9: Sample of the evolution of vertical reflectivity structure in the squall system from Houze and Rappaport (1984). Cross sections are along the direction of propagation, with motion from right to left. Shading thresholds are for the minimum detectable echo, 24, 34, and 44 dBZ.

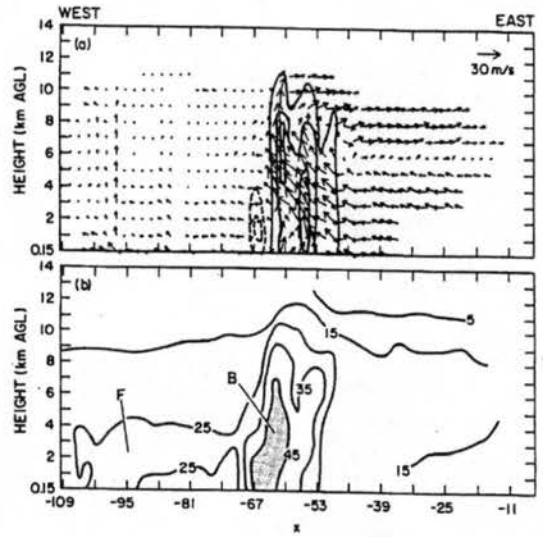

Figure 2.10: East-west vertical cross section through squall line case presented by Kessinger et al. (1987). (a) line-relative winds along the cross section and (b) reflectivity (dbZ_e).

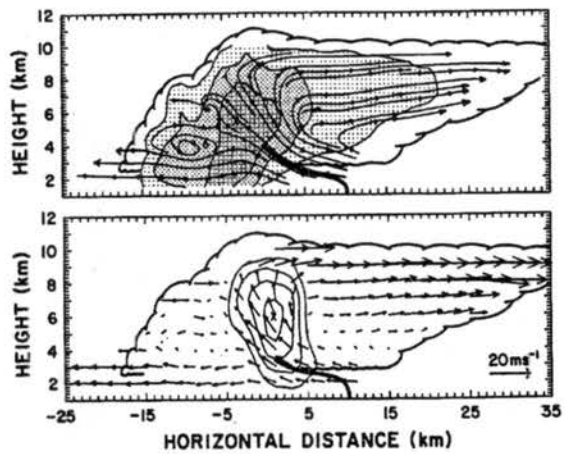

Figure 2.11: Vertical cross section through squall line presented by Fankhauser et al. (1992). (a) streamlines and radar reflectivity (shading thresholds of 5, 20, and 35 dBZ); (b) air motion vectors and vertical velocity contours at 2 m s^{-1} increments. Cloud boundary indicated, along with forward boundary of cold pool (heavy line).

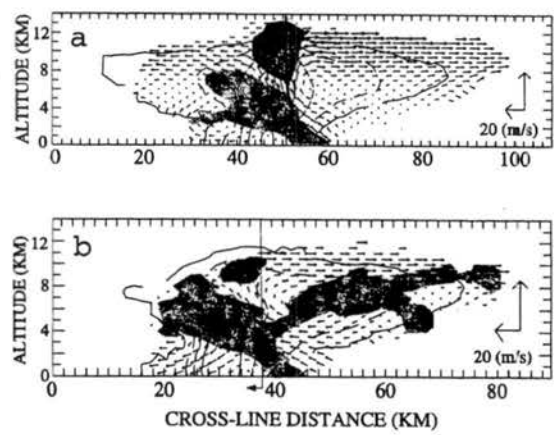

Figure 2.12: Along-line averaged cross sections at two times for squall line from Grady and Verlinde (1997). Reflectivity contours are in 10-dBZ increments beginning with 10 dBZ. Vectors depict line-relative flow. Light shading indicates convergence, dark shading indicates divergence.

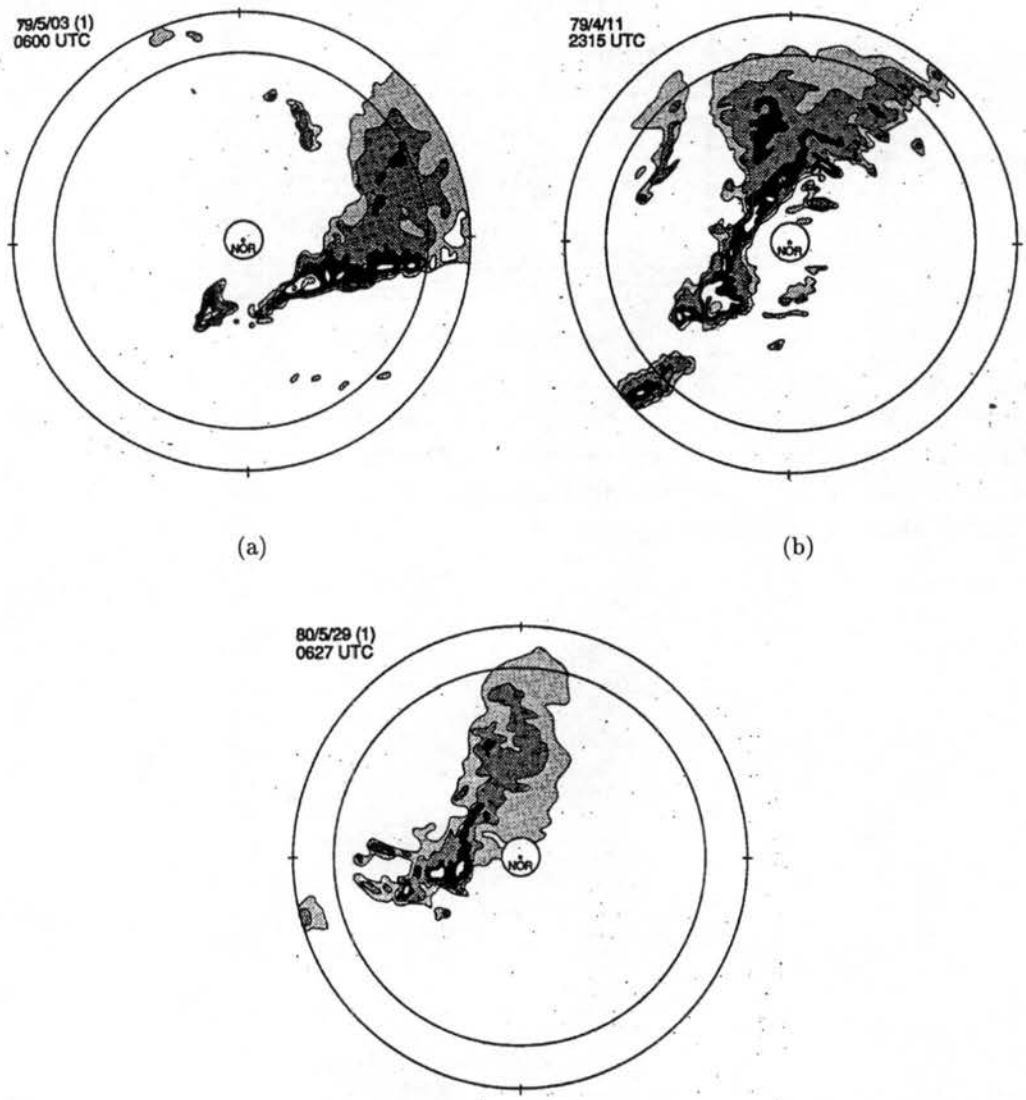

(a) (b)

(c)

Figure 2.13: Examples of radar-observed MCSs from Houze et al. (1990) which might be classified as PS cases in this study. Shading thresholds are (approximately) 20, 25, 35, 45, and 55 dBZ.

Chapter 3

DATA UTILIZED AND METHODS OF ANALYSIS

3.1 Choice of cases

The spatial domain for this study generally included the Great Plains of the United States, from about 31° to 45° N and 89° to 106° W, a region known both for its frequent convective weather and its operational array of wind profilers (the NOAA Profiler Network, or NPN; cf. Section 3.4). Linear MCSs from the months of May 1996 and May 1997 were catalogued and analyzed. The month of May was chosen for its widespread convective activity within the NPN. In addition, the month of May represents a period of transition between the strong baroclinic forcing of early spring and the weaker, more barotropic forcing of the summer months. In this respect, the cases selected should comprise a broad spectrum of convective modes and forcing types. Two years were selected in order to alleviate to some extent any annual bias in the data as well as to ensure that a sufficient number of cases were present to allow for high confidence in the statistical results of this survey. The inclusion of additional years and months was not possible due to the limited time available.

In order to undertake a study of mesoscale convective systems, it is necessary to determine what shall be considered an MCS. I wished to consider phenomena for which the Coriolis acceleration is *not* negligible (i.e. *is* of the same order as other terms in the Navier-Stokes equations). This acceleration is given by:

$$\left(\frac{Du}{Dt}\right) = fv, \tag{3.1}$$

wherein u and v are the eastward and northward components of the horizontal velocity and

f is the Coriolis parameter. By non-dimensionalizing:

$$\frac{U}{T}\left(\frac{Du^*}{Dt^*}\right) = fU(v^*) \tag{3.2}$$

(where U and T are scaling factors and starred quantities are non-dimensional), the appropriate time scale is easily shown to be f^{-1}, which is identical to that chosen by Emanuel (1986). Using a typical midlatitude value for f of 10^{-4} s^{-1} yielded an MCS time scale (τ) of approximately 3 hours. The length scale for this study was defined to be $L = U\tau^{-1}$ (where U is a velocity scale). Using an average advective speed (U) of 10 m s^{-1} yielded a MCS length scale of 100 km, identical to that suggested by Houze (1993). Only those groups of convective echoes with extents greater than 100 km and durations greater than 3 hours were included in my study.

Several cases were omitted from the study due to the quality of data available for investigation. Of the 88 cases initially catalogued from the investigation of radar data (cf. Section 3.2), 2 were omitted due to the absence of a rawinsonde observation that reasonably represented their environment (cf. Section 3.3). Additionally, 2 cases were omitted from the study due to obvious contamination of the available rawinsonde data by the presence of precipitation. One case, which appeared to represent the airmass within which an MCS occurred, was omitted due to a lack of conditional instability. It is possible that modulation of the sounding occurred at a later time, such as Trier and Parsons (1993) found in a case study. It is also possible that this case belongs to the class discussed by Colman (1990), wherein symmetric instability may be responsible for the dominant mode of overturning. In either case, the treatment of such soundings is beyond the scope of this investigation.

Finally, all cases which were "elevated" (those which occurred on the cold side of a synoptic scale front) were omitted from the study. I deemed MCSs to be elevated if *1)* they were located on the cold side of a front, *as analyzed by the National Centers for Environmental Prediction (cf. Section 3.6.1)*, or *2)* a strong frontal inversion existed in a nearby sounding (cf. Section 3.3). These cases were discarded due to their lack of surface-based convective available potential energy (a problem treated by Colman 1990)

as well as the ambiguity of density current dynamics and inflow layer location for MCSs far above the surface. While the (discarded) elevated cases composed 31% of the total MCSs documented by this study, their omission facilitated a more detailed look at "warm-sector" convective systems, which are more amenable to investigation with the conventional operational datasets I used. Certainly, future work on elevated cases is called for given their large representation in this survey. For the time being, the reader is referred to Colman (1990) for an overview of such cases. Statistics on the cases omitted (for any reason) from this study and a brief discussion of their ramifications are given in Appendix A.

3.2 National radar base scan summaries

3.2.1 Dataset information

In order to identify and characterize the convective systems in this study, national radar composite summaries (initially produced by Weather Services International, WSI) were obtained from an archive maintained by the Global Hydrology Resource Center (GHRC). Such composites are generated from the radar reflectivity factor (in dBZ) for base scans (0.5° elevation) from the currently operational National Weather Service radars in the continental United States. The radar data have a pixel resolution of 2 km x 2 km and comprise 16 levels of reflectivity factor in 5 dBZ increments (beginning with 0-5 dBZ). The composite reflectivities represent the largest *instantaneous* reflectivity measurement for a point at each compositing time. If a location is within the unambiguous range of more than one radar, the radar recording the maximum value is utilized. The composites are produced every 15 minutes in this manner by WSI.

The national radar summaries were chosen for their reasonable temporal and spatial resolution along with their ability to provide a general overview of regional radar returns. Individual convective elements could not be resolved in the 2 km x 2 km, 15 minute data. The focus of this study, however, was the meso-β scale organization and evolution of large, persistent convective systems, which were well-depicted by the composite data. As the

position, movement, and horizontal extent of MCSs often preclude complete sampling by one radar site, the use of composited data provided an advantageous depiction of storms in their entirety. Since the temporal resolution of the national composite data was insufficient for the observation of transient convective elements, the evolution of MCSs on a cellular scale was not treated by this study. A discussion of the reflectivity scale used for radar images in this manuscript is given in Appendix B.

3.2.2 Radar analysis methodology

The 2-km national radar summaries were investigated with a four step process. First, the 15 minute summaries were animated and observed for the entire study domain, approximately from 31° – 45° N and 89° – 106° W. From this initial step, persistent linear convective systems were noted for further investigation. Next, a 6° x 6° domain was constructed for each case noted in step 1. Within this domain, the 15 minute radar images were again animated, providing a detailed sense of the structural formation and evolution of each convective system throughout its entire lifetime. Any cases which failed to meet the criteria for duration and length discussed in Section 3.1 were excluded from the study at this time. Three "snapshots" of interest were then selected from the lifetime of an MCS for comparison with NOAA Profiler Network wind observations. These selected times roughly divided an MCS lifespan into quarters, much as was done by Hilgendorf and Johnson (1998), giving a broad distribution of observations throughout the MCS lifetimes.

Once the radar snapshots were selected, an MCS's location, orientation, and distribution of stratiform rain were noted. Location was defined as the centroid of an ellipse encompassing the MCS, as suggested by Hilgendorf and Johnson (1998). Orientation was measured as the mean azimuthal angle of *1)* a tangent to the convective line at its centerpoint and *2)* a line connecting the two endpoints of the convective line.

According to Houghton (1968), the primary difference between convective and stratiform hydrometeors is the magnitude of the in-cloud vertical motions *during hydrometeor*

growth. Accordingly, several authors (e.g. Steiner et al. 1995) have attempted to partition precipitation into convective and stratiform components by using gradients in the reflectivity field in addition to the value of the reflectivity factor itself. These complicated schemes, however, do not drastically change the resultant partitioning (S. Rutledge, personal communication). In this study, convective echoes were simply defined as those with reflectivity factors greater than 40 dBZ. Stratiform echoes were defined as those with reflectivity factors from 20 dBZ – 40 dBZ. Echoes less than 20 dBZ were not considered during the measurement. These definitions correspond to the criteria used by Geerts (1998), who discovered that slight modifications to the thresholds (i.e. 15 dBZ vs. 20 dBZ for the minimum stratiform echo) had little effect on MCS recognition or partitioning.

The distribution of stratiform rain was evaluated at a point equidistant from the ends of the convective line and centered (front-to-rear) within the convective line itself. The extent of both pre-line and post-line (with respect to MCS movement) stratiform echoes were measured with a ruler. The ratio between the forward measurement (f) and the rearward measurement (r) was a part of the classification process detailed in Section 5.1.

Finally, thirty minute (3 image) animations were constructed for the half hour bracketing the above times of interest in order to calculate system motion vectors. The system motion vector was defined as the change in the location of the center of the leading edge of the convective line with time. No attempt was made to document or measure the movement of individual convective cells due to the limited temporal and spatial resolution of the national radar summaries.

3.3 National Weather Service rawinsonde observations

Rawinsonde measurements of the atmosphere are taken twice daily, at 0000 and 1200 UTC, from irregularly located stations (cf. Table 3.1 and Figure 3.1) in the United States by the National Weather Service (NWS). The characteristics of such measurements were detailed by Golden et al. (1986). One radiosonde observation (raob) was selected for each

Table 3.1: Location of NWS rawinsonde stations utilized in this study.

Identifier	Location
LCH	Lake Charles, Louisiana
MAF	Midland, Texas
JAN	Jackson, Mississippi
SHV	Shreveport, Louisiana
FWD	Fort Worth, Texas
LZK	Little Rock, Arkansas
AMA	Amarillo, Texas
OUN	Norman, Oklahoma
SGF	Springfield, Missouri
DDC	Dodge City, Kansas
TOP	Topeka, Kansas
DNR	Denver, Colorado
LBF	North Platte, Nebraska
OAX	Valley, Nebraska
DVN	Davenport, Iowa
UNR	Rapid City, South Dakota
MPX	Chanhassen, Minnesota
ABR	Aberdeen, South Dakota
BIS	Bismarck, North Dakota

MCS case in order to depict the environment within which the studied convective systems occurred. The data utilized for this study were retrieved from an archive maintained at the National Climatic Data Center (NCDC). These data included pressure, height, wind speed, wind direction, dry bulb temperature, and relative humidity. There were approximately 80 vertical levels per sounding report.

Elliott and Gaffen (1991) discussed several shortcomings of the NWS rawinsonde measurements and pointed out that upper-air data are taken "largely for weather forecasting purposes, not to determine climatology." Nevertheless, the paucity of alternative data sources as well as the prevalent use of NWS rawinsonde data in studies similar to my own (e.g. BJ85, BMJ87, HSD90) suggests that these data are desirable and efficacious for studies of MCS environments despite their drawbacks. Schwartz and Doswell (1991) recommended increased attention to quality control of NWS rawinsonde data, particularly for research applications. Accordingly, careful visual review of the data utilized in this study was undertaken. As no quality control information was included in the NCDC dataset,

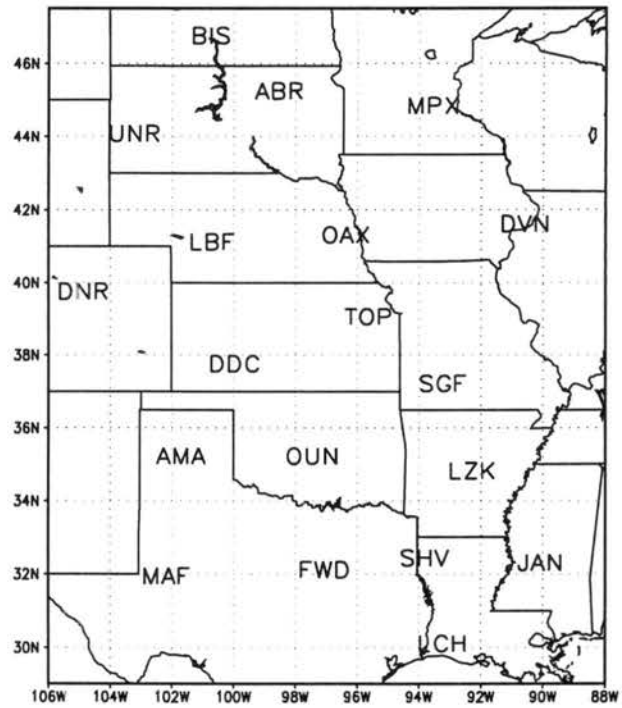

Figure 3.1: National Weather Service rawinsonde stations located in or near the studied domain. Station locations are shown by three letter identifiers.

the rawinsonde data used in this study were accepted as within the "noise level" of the radiosonde instruments. The omission of cases due to contamination is further discussed in Section 3.1.

In many recent studies (e.g. Bluestein and Parks 1983, BJ85, BMJ87, Rasmussen and Straka 1998), an interpolation of rawinsonde soundings toward a near-storm environment was attempted. Such an endeavor results in a sounding which, to the degree of accuracy afforded by linear interpolation, better represents the environment at a point of interest. Similarly, Brooks et al. (1994) suggested the use of numerical models to modify (depict the evolution of) operational raobs. In the present study, however, soundings were not interpolated toward a point location's environment. Instead, an individual sounding believed to best represent the airmass within which a convective system occurred was chosen and utilized without modifications, much as was done by Rasmussen and Wilhelmson (1983) and HSD90. The motivation for this was three-fold: firstly, close proximity soundings are

not so essential for MCS cases (as compared to supercell cases) due to their large horizontal extent and distance traversed (i.e. "swept-out area"), secondly, interpolated soundings may not be immediately or easily available to the operational forecaster (for whom these results are in part intended), and thirdly, use of soundings prior to an MCS's approach ensured that the deep convection in no way altered or contaminated the utilized raob. Soundings were investigated to ensure continuity with the large scale environment (through intercomparison with nearby raobs and NCEP Reanalyses) as was suggested by Bluestein and Parks (1983). Following HSD90, a sounding was only considered to represent the *first* MCS to traverse a region. Subsequent convective systems (prior to another sounding time) were not considered due to the high probability that convection significantly altered the environment.

3.4 The NOAA Profiler Network

The representation of a convective environment is challenging given the twice-per-day frequency and large horizontal separation (approximately 400 km) of rawinsonde observations. In order to more fully characterize the wind field near MCSs, wind profiler data were utilized. The domain for this study was chosen to coincide with an array of 404 Mhz wind profilers, the National Oceanic and Atmospheric Administration (NOAA) Profiler Network (NPN). Data from the NPN were retrieved for this study from an archive maintained by the Data Support Section (DSS) at the National Center for Atmospheric Research (NCAR). The locations of the wind profilers used in this study are listed in Table 3.2 and shown graphically in Figure 3.2.

The manner of observation for NPN wind profilers was detailed by Weber et al. (1993), and the NOAA data processing algorithms were detailed by Barth et al. (1994). Profiler measurements are taken in 6 minute cycles, utilizing three antennas and two power levels, at gates from 500-m to 16250-m AGL at 250-m intervals. The six-minute observations are then averaged into hourly winds. In addition, surface winds are recorded for each profiler site using conventional surface observation instruments. Hourly winds were combined with

Table 3.2: Location of NOAA Profiler Network wind profilers utilized in this study.

Identifier	Location
AZC	Aztec, New Mexico
BLM	Bloomfield, Missouri
BLR	Blue River, Wisconsin
CNW	Conway, Missouri
DQU	Dequeen, Arkansas
FBY	Fairbury, Nebraska
GDA	Grenada, Colorado
HBR	Hillsboro, Kansas
HKL	Haskell, Oklahoma
HVL	Haviland, Kansas
JTN	Jayton, Texas
LMN	Lamont, Oklahoma
LTH	Lathrop, Missouri
MBW	Medicine Bow, Wyoming
MRR	Merriman, Nebraska
NDS	Neodosha, Kansas
NLG	Neligh, Nebraska
PAT	Palestine, Texas
PLT	Platteville, Colorado
PRC	Purcell, Oklahoma
RWD	McCook, Nebraska
SLA	Slater, Iowa
VCI	Vici, Oklahoma
WDL	Wood Lake, Minnesota
WNC	Winchester, Illinois
WSM	White Sands Missile Range, New Mexico

corresponding surface observations to render the wind profiles used in this study.

The processing and quality control information provided by NOAA was accepted *a priori*. NOAA applies a continuity check to the 6-minute NPN data (as discussed by Barth et al. 1994) prior to hourly averaging. Data which do not pass the continuity check are excluded from the hourly averages, effectively removing outlying points prior to the averaging. In addition, NOAA quality control checks are performed for the hourly winds. I discarded those hourly data which failed any portion of the quality checks (for either the u or v wind component). I visually inspected hourly winds which passed NOAA quality control checks for vertical and temporal continuity. Questionable data were compared to neighboring profiler sites, rawinsonde observations, and NCEP reanalyses to ensure their

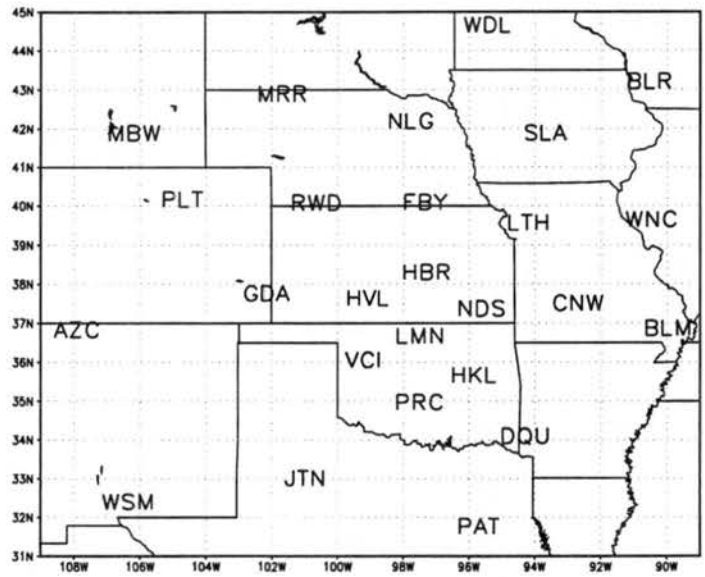

Figure 3.2: The central United States NOAA Profiler Network. Profiler locations are shown by three letter identifiers.

consistency. Data that I subjectively deemed to be inconsistent with other sources were removed from the study.

Wilczak et al. (1995) first pointed out the widespread contamination of wind profiler data by flying birds during periods of migration across the central Great Plains. This posed a potential problem to my study of May MCSs: Wilczak et al. (1995) found 64% of station days during the month of May 1993 to be contaminated. Since such contamination may not be evident in continuity checks (as the nature of the contamination is relatively continuous), an objective quality control check is desireable. The spectral character of contamination by migratory birds has been well-established (e.g. Wilczak et al. 1995 and Arrit et al. 1997) and has been used to develop detection algorithms for the NPN (e.g. Miller et al. 1997). The criteria currently used by NOAA to flag winds contaminated by migratory birds are shown in Table 3.3, as given by M. Barth (personal communication). These thresholds represent an improvement over those presented by Miller et al. (1997), with a critical success ratio of 45% (as defined by Miller et al. 1997), a probability of detection of 65%, and a false alarm ratio of 40% when compared to rawinsonde data. The high false alarm

Table 3.3: Criteria used by the NOAA Profiler Network objective bird contamination check for springtime migrations. The check is applied to hourly values for winds, velocity variance (σ^2), and vertical velocity.

Parameter	Contamination Threshold
time of year	Feb. 15 – June 15
time of day	0200 – 1200 UTC
height	$\leq$ 4500 m MSL
wind direction	90 ° – 270 ° azimuth
mean σ^2 for North and East beams	$\geq$ 1.7 m^2 s^{-2}
vertical velocity	$\leq$ 1.5 m s^{-1}

ratio for bird contamination algorithms is probably due to the existence of observations with appropriate winds (compared to rawinsonde observations) *despite* the presence of migratory birds (Miller et al. 1997). I tested the hourly profiler winds for this study with the NOAA bird contamination check given in Table 3.3. Cases which failed the contamination test were compared to regional rawinsonde observations and NCEP reanalyses (due to the high false alarm ratio discussed above as well as the possibility, discussed by Arrit et al. 1997, that low level jets may themselves be associated with high velocity variances). Neighboring profilers were not used for comparison, as the nature of contamination by migratory birds is frequently ubiquitous in the central Great Plains during periods of migration. I discarded hourly winds that were flagged by the contamination check and found to be unrepresentative of the consensus wind field.

3.5 Parameters derived from rawinsonde and wind profiler data

3.5.1 Rawinsonde parameters

Numerous thermodynamic and kinematic parameters were derived from the rawinsonde data in order to characterize the environment within which the observed squall line case studies occurred. Thermodynamic variables were chosen or developed to predict the conditional instability of the convective environment as well as the possible density current character of any convective lines, while kinematic variables were chosen or developed to describe the advective and propagational character of a convective line and its associated

stratiform rain. Additionally, several parameters were chosen to characterize the likelihood of rotating convective storms in the MCSs' environments.

Thermodynamic variables

The convective available potential energy (CAPE) for a non-entraining parcel was calculated using a finite summation over every layer of a rawinsonde observation to approximate the integral form:

$$CAPE \equiv g \int_{z_{LFC}}^{z_{EL}} \frac{\theta_{v_{par}(z)} - \overline{\theta_v}(z)}{\overline{\theta_v}(z)} dz, \tag{3.3}$$

wherein z_{LFC} is the geopotential height of the level of free convection (LFC, the level at which a lifted parcel becomes positively buoyant), z_{EL} is the geopotential height of the equilibrium level (EL, the level at which a parcel ascending by buoyancy forces becomes neutrally buoyant), $\overline{\theta_v}$ is the environmental virtual potential temperature, and $\theta_{v_{par}}$ is the virtual potential temperature of the ascending parcel of air. Liquid water was neglected in the virtual temperature and virtual potential temperature calculations, such that:

$$\theta_v = T_v \left(\frac{p_0}{p}\right)^{R_d/c_{pd}} = T \frac{1 + r/\epsilon}{1 + r} \left(\frac{p_0}{p}\right)^{R_d/c_{pd}}, \tag{3.4}$$

wherein r is the water vapor mixing ratio, ϵ is the ratio R_d/R_v, and p_0 is defined by custom as 1000 hPa.

Two possible scenarios for an ascending parcel's $\theta_{v_{par}}$ in Equation 3.3 were considered: the lifting (by whatever means) of a mean mixed layer parcel (MLCAPE) and the ascent of a near-surface parcel by convecting (TCCAPE). For the lifting case a parcel with the average mixing ratio, $\overline{r}_{ML}$, and potential temperature, $\overline{\theta}_{ML}$, of the surface-based mixed layer was raised adiabatically to its lifting condensation level (LCL), then pseudo-adiabatically through the remainder of the sounding. The mixed-layer depth for the computations presented here was chosen to be 1000 meters. For the convecting case a convective temperature, T_c, was computed. The T_c was defined so that $\theta(T_c, p_{sfc}) = \theta_{env}$ for the isobaric level at which the environment's saturation water vapor mixing ratio equals $\overline{r}_{ML}$ in a sounding.

In the absence of a lifting mechanism, the T_c must be achieved in order for surface-based convective clouds to occur. The level at which a convecting surface parcel in a well-mixed layer first saturates is the convecting condensation level (CCL). In order to compute $\theta_{v_{par}}$ for the convecting case, a parcel with initial $T = T_c$ and $r = \overline{r}_{ML}$ was raised adiabatically to the CCL, then pseudo-adiabatically through the remainder of the sounding. In addition, the *pickCAPE* was considered, a parameter developed here to alleviate to some extent the bias introduced by relatively stable 1200 UTC soundings. The *pickCAPE* simply equals the $MLCAPE$ in 0000 UTC soundings and the $TCCAPE$ in 1200 UTC soundings, such that the parameter "anticipates" diurnal heating of the 1200 UTC sounding.

For the lifted parcel, convective inhibition (CIN, the minimum amount of additional energy needed for a mixed-layer based parcel to be positively buoyant at some level) was calculated using a finite summation to approximate the integral form:

$$CIN \equiv g \int_{z_{sfc}}^{z_{LFC}} \frac{\theta_{v_{par}}(z) - \overline{\theta_v}(z)}{\overline{\theta_v}(z)} dz, \tag{3.5}$$

where z_{sfc} is the geopotential height of the surface and $\theta_{v_{par}}$ is computed using the mixed layer lifting method described above. In addition, the lifted index ($LI = \overline{T}(500hPa) - T_{par}(500hPa)$) of the lifted parcel was computed.

The equivalent potential temperature, θ_e, was computed using the empirical equation recommended by Bolton (1980). The wet-bulb temperature, T_w, and wet-bulb potential temperature, θ_w, corresponding to the calculated θ_e were retrieved iteratively. In order to determine potential cold pool strength, the sounding level with the lowest θ_w was identified since a saturated, unentraining downdraft from this level would produce the coldest possible surface temperature perturbation. When behaving as a simple density current, the speed at which a surface cold pool expands can be written as (following Simpson 1987):

$$|\mathbf{c}_{cp}| = \sqrt{2gh\frac{T_v'}{\overline{T_v}}}, \tag{3.6}$$

where h is the depth of the cold pool and $T_v' = T_{v_{cp}} - \overline{T_v}$ (only density variations due to temperature and water vapor content have been considered). Once the surface temperature

for a saturated downdraft from the level of $\theta_{w_{min}}$ was retrieved, its virtual temperature was calculated for comparison to that of the environment. This value shall be called the saturated downdraft virtual temperature, $T_{v_{sd}}$. An alternative downdraft scenario was also considered, in which a parcel undergoes saturated descent to the indicated cloud base height (should clouds form; this is the LCL) followed by adiabatic (unsaturated) descent to the surface. This formulation is intended to approximate the conditions for dry microbursts. The virtual temperature retrieved for such a downdraft shall be called the dry downdraft virtual temperature, $T_{v_{dd}}$. Since diurnal heating and the presence of deep convection can modify the environment, two additional environmental scenarios were also considered (in addition to the simple computation of T_v): the virtual temperature of the surface environment should T_c be acheived, $T_{v_{Tc}}$, and the virtual temperature of the surface environment should it be cooled to its T_w (e.g. by evaporation of falling precipitation), $T_{v_{Tw}}$. These five virtual temperatures can be used in Equation 3.6 to depict idealized downdraft scenarios for deep convective storms. If the depth of a cold pool is known, 6 possible cold pool speeds can be retrieved from the above idealized downdraft and environmental scenarios. While not considered from the standpoint of a surface temperature perturbation, the height at which $T_w = 0°C$, HWBZ, was also calculated. As sublimation and melting may provide additional cooling for downdraft air (in some cases, as much as 0.8 that by evaporation according to Atlas et al. 1969), this parameter may have some additional effect on downdraft strength.

It was suggested by Foster (1958) that characteristics of gust fronts (particularly the maximum observed wind speeds) may be well correlated with the kinetic energy realized by downdrafts within thunderstorms. Accordingly, the downdraft convective available potential energy (DCAPE) was calculated from the rawinsonde data for comparison to squall line motion speeds. A finite summation was used to approximate the integral form:

$$DCAPE \equiv g \int_{z_{sfc}}^{z_{\theta_{w_{min}}}} \frac{\overline{\theta_v}(z) - \theta_{v_{par}}(z)}{\overline{\theta_v}(z)} dz, \tag{3.7}$$

where $\theta_{v_{par}}$ is determined for an unentraining saturated descent to the surface from the level of $\theta_{w_{min}}$, following the suggestion of Emanuel (1994). Since descending downdrafts *do*

entrain environmental air, those which begin at higher altitudes are likely to be more diluted when reaching the surface. Gilmore and Wicker (1998) argued that the parcel DCAPEs of such downdrafts should be weighted less than those which originate nearer the surface and advocated the use of a 0-6 km density weighted DCAPE. This parameter was computed for comparison to the above DCAPE calculation using a finite summation to approximate the integral form:

$$DCAPE_{\rho} \equiv \frac{g}{\overline{\rho}} \int_{0m}^{6000m} \frac{\overline{\theta_v}(z) - \theta_v(z)}{\overline{\theta_v}(z)} \rho(z) dz, \tag{3.8}$$

where $\overline{\rho}$ is the average density in the layer.

Since the effects of entrainment may be essential to the accurate parameterization of downdraft strength, three additional environmental variables were computed in order to characterize the humidity of the environment: the precipitable water, PW, the mean relative humidity in the layer below $z(\theta_{w_{min}})$ (through which the principally considered downdraft would descend), RH_d, and the mean relative humidity of the entire troposphere (below 200 hPa), RH_t. It was further noted by Gilmore and Wicker (1998) that the environmental wind shear should effect the entrainment rate of parcels. In the present study, no attempt was made to modify the downdraft-related variables to account for this effect. The thermodynamic parameters discussed above are summarized in Table 3.4.

Kinematic variables

Since some component of MCS motion may be advective, mean winds from several layers of relevance were considered. In addition, many studies (e.g. Davies and Johns 1993) have found that particular types of organized convective storms propagate in a (climatologically) consistent manner with respect to environmental winds. The mean winds between 0 and 6 km above ground level (AGL), $\overline{\mathbf{V}}_{0-6}$, were computed, as this layer was the basis for a climatology of supercells assembled by Davies and Johns (1993). The mean winds between 3 and 10 km AGL, $\overline{\mathbf{V}}_{3-10}$, were also considered in order to facilitate comparison with the results of HSD90. The mean winds between 5 and 8 km AGL, $\overline{\mathbf{V}}_{5-8}$, were computed since

Table 3.4: Summary of all thermodynamic and kinematic parameters computed for the study ("available potential energy" denoted as APE). R: rawinsonde data, WP: wind profiler data.

Computed variable	Source	Symbol
mixed layer convective APE (J/kg)	R	MLCAPE
convective temperature convective APE (J/kg)	R	TCCAPE
convective inhibition (J/kg)	R	CIN
pressure of lifting condensation level (hPa)	R	LCL
pressure of level of free convection (hPa)	R	LFC
convective temperature (K)	R	T_c
pressure of convective condensation level (hPa)	R	CCL
parcel lifted index (K)	R	LI
minimum wet-bulb potential temperature (K)	R	$\theta_{w_{min}}$
height (AGL) of $\theta_{w_{min}}$ (m)	R	$z(\theta_{w_{min}})$
saturated downdraft virtual temperature (K)	R	$T_{v_{sd}}$
dry downdraft virtual temperature (K)	R	$T_{v_{dd}}$
surface virtual temperature (K)	R,WP	T_v
wet-bulb surface virtual temperature (K)	R,WP	$T_{v_{Tw}}$
convective surface virtual temperature (K)	R	$T_{v_{Tc}}$
height (AGL) of wet-bulb $0°C$ temperature (m)	R	HWBZ
downdraft convective APE (J/kg)	R	DCAPE
density-weighted DCAPE (J/kg)	R	$DCAPE_\rho$
precipitable water (In.)	R	PW
mean relative humidity below $z(\theta_{w_{min}})$ (%)	R	RH_d
mean relative humidity of troposphere (%)	R	RH_t
0-6 km mean winds (m/s)	R,WP	$\overline{\mathbf{V}}_{0-6}$
3-10 km mean winds (m/s)	R,WP	$\overline{\mathbf{V}}_{3-10}$
5-8 km mean winds (m/s)	R,WP	$\overline{\mathbf{V}}_{5-8}$
9-10 km mean winds (m/s)	R,WP	$\overline{\mathbf{V}}_{9-10}$
0-1 km wind shear vector (m/s)	R,WP	$\mathbf{V}_{z_{0-1}}$
0-3 km wind shear vector (m/s)	R,WP	$\mathbf{V}_{z_{0-3}}$
2-7 km wind shear vector (m/s)	R,WP	$\mathbf{V}_{z_{2-7}}$
0-10 km wind shear vector (m/s)	R,WP	$\mathbf{V}_{z_{0-10}}$
environmental helicity (J/kg)	R,WP	HEL
storm-relative helicity (J/kg)	WP	SRH
bulk Richardson number	R	BRN
bulk Richardson number shear	R	S_{BRN}

several studies (e.g. BJ85) have found a steering level near 6 or 7 km AGL on average for squall lines. The mean winds between 3 and 10 km AGL were generally quite similar to those between 5 and 8 km AGL. Finally, advective effects aloft may be important to anvil dispersion and consequently the location of stratiform precipitation. The mean winds from 9 to 10 km AGL, $\overline{\mathbf{V}}_{9-10}$, were therefore computed following the suggestion of Rasmussen and Straka (1998).

In addition, wind shear was computed for layers of interest. The theory for long-lived squall lines advanced by RKW88 requires the ingestion of air with horizontal vorticity associated with low-level wind shear. Therefore, the vertical shear of the low-level wind $\mathbf{V}_{z_{0-1}}$ was computed from the surface to 1000m, a layer believed to approximate the depth of typical storm inflow. Since the orientation of this shear vector with respect to the line is significant to the theory of RKW88, the component of the shear vector perpendicular to the line was also computed. A possible explanation for the location of stratiform rainfall near a convective system involves the tilting of the latent heat source aloft (as suggested by Nachamkin 1998). The 0 to 10 km shear, $\mathbf{V}_{z_{0-10}}$ was computed as a proxy for the difference in horizontal momentum between inflow air and the environmental air near the level of anvil detrainment from a convective storm.

Additionally, Alexander and Young (1992) and LeMone et al. (1998) discovered correlations between certain shear vectors and the orientation of tropical convective lines. The predictability of orientation is significant to the problem of stratiform rain arrangement in light of the ideas advanced by RKW88 and Nachamkin (1998). Alexander and Young (1992) found that the orientation of shear-perpendicular lines was well correlated to the orientation of the 950 to 700 hPa shear vector (when strong) in the tropics, while LeMone et al. (1998) improved this correlation by using the wind shear between 1000 and 800 hPa. I have considered these parameters, in part, to extend such correlations to midlatitude MCSs (since this issue has been shown by LeMone and Moncrieff 1994 to be important to the parameterization of momentum transports in general circulation models). The wind shear

$\mathbf{V}_{z_{0-3}}$ was computed between the surface and 3000 m for the present cases (the parameter was evaluated in height space in order to maintain the depth of the layer over different terrain elevations). Alexander and Young (1992) also found that shear-parallel lines were highly correlated to the vector wind shear between 800 and 400 hPa (when low-level shear was minimal) in the tropics. This parameter was evaluated in height space for the rawinsonde data between 2000 and 7000 m AGL ($\mathbf{V}_{z_{2-7}}$).

Finally, helicity and the bulk Richardson number were considered. Both parameters have proven useful in the descrimination of environments which will support rotating versus non-rotating convection. Helicity can be shown to be minus twice the (signed) area swept out by a hodograph (Davies-Jones et al. 1990), which from simple geometric considerations is given by:

$$HEL = -R^2\alpha, \tag{3.9}$$

where R is the average layer magnitude of the velocity vector in m/s and α is the total (layer) signed angle swept out in radians. The layer considered for the present calculations was 0 - 3000 m, which was chosen by Droegemeier et al. (1993) for the evaluation of supercell environments. The bulk Richardson number is a non-dimensional parameter which Weisman and Klemp (1982) found to be a good discriminator of ordinary, multicell, and supercell convective regimes, given by:

$$BRN = \frac{CAPE}{\frac{1}{2}(u_s^2 + v_s^2)}, \tag{3.10}$$

where $\mathbf{U}_s \equiv < u_s\,\hat{i}, v_s\,\hat{j} >$ is the vector difference between the density weighted 0-6 km mean wind and the density weighted 0-500 m mean wind. In the present study, the BRN was calculated from the rawinsonde data using the mixed-layer CAPE. As an additional shear parameter, the denominator of Equation 3.10 shall be called the bulk Richardson number shear, S_{BRN}. The kinematic parameters discussed above are summarized in Table 3.4.

3.5.2 Wind profiler parameters

Wind profiler sites record surface temperature and dew-point temperature. Therefore, the surface virtual temperature and wet-bulb surface virtual temperature were computed. No other thermodynamic parameters were calculated from the wind profiler data due to the lack of thermodynamic information above the surface. Instead, kinematic fields were computed for the near-storm environment using the high vertical and temporal resolution afforded by the wind profiler network. All of the kinematic parameters discussed in Section 3.5.1 were evaluated with the wind profiler data. In addition, the proximity of the wind profiler observations to the MCSs of interest permitted the incorporation of storm motion data. Line-relative winds were computed for the layers of interest discussed in Section 3.5.1 using the formula:

$$\mathbf{V}_{sr} = \mathbf{V}_{env} - \mathbf{c}, \tag{3.11}$$

wherein $\mathbf{V} \equiv < u\hat{i}, v\hat{j} >$ and $\mathbf{c}$ is the MCS motion vector (computed as explained in Section 3.2). The parameters computed for the wind profiler data are also summarized in Table 3.4.

3.6 Diagnosis of synoptic features

In order to describe the synoptic meteorlogy associated with the MCSs in this study, National Centers for Environmental Prediction (NCEP) surface analyses and gridded reanalyses, as well as National Weather Service (NWS) METAR surface observations, were used.

3.6.1 Surface data

The NCEP surface charts were investigated for the presence of cold, warm, and stationary fronts, drylines, surface pressure troughs, outflow boundaries, and "triple points". The determination and placement of these surface features by NCEP were accepted without reinterpretation for this study. In cases of missing NCEP analysis charts, subjective analysis

of surface features was performed. The number of missing charts for which subjective analyses were performed is 5, or about 4% of the total number of surface charts investigated. The positions of surface features were recorded at 12 hour intervals throughout the entire study period. Convective systems were deemed to be "associated" with a surface synoptic feature if more than half of their track coincided with the position of an NCEP-analyzed feature. For the case studies performed (Chapter 6), surface observations were retrieved from a METAR archive at NCAR and superposed upon regional reflectivity images. While not feasible for larger spatial and longer temporal scales, this approach provided an intimate look at the wind field near the intensively studied MCSs.

3.6.2 NCEP Reanalysis grids

NCEP reanalysis data were obtained in gridded form from the Data Support Section (DSS) at the National Center for Atmospheric Research (NCAR). A full description of the reanalysis data was given by Kalnay et al. (1996). The reanalysis grids utilized for this study comprised height, wind, temperature, and humidity data at mandatory levels throughout the troposphere and stratosphere. The NCEP data were utilized to diagnose the presence of low-level wind maxima (low level jets), upper level wind maxima (upper tropospheric jets), and midtropospheric shortwave troughs and ridges (including vorticity maxima and minima). The existence of low-level jets was determined from the wind fields at 925 hPa and 850 hPa. No minimum wind speed requirement was imposed upon the definition of a low-level jet. For consistency with previous work on low-level jets, low-level wind maxima were required to have a predominantly southerly component in order to be considered. MCSs coincident with the maxima themselves were deemed to be related to the "core" of the low-level jet. Those coincident with the northern extent of the low-level wind maxima (and velocity gradient found there) were deemed to be related to the "terminus" of the low-level jet. Nachamkin (1998) pointed out the presence of a meso-γ scale low-level jet near an MCS in Colorado and linked it to the existence and evolution of the convective

system. The coarse (2.5° × 2.5°) resolution of the NCEP reanalysis grids did not allow for the observation of such features in my study (unless by serendipitous colocation with a NPN site).

In addition to the initial diagnosis of attendant synoptic features, the NCEP reanalyses were also used to derive mean fields for the MCS archetypes discussed in Chapter 5. Data from NCEP reanalysis times that coincided with an MCS's occurrence in the study domain were compiled on two scales, as follows. Each MCS's position was interpolated to the nearest NCEP reanalysis grid point. The first interpolation grid extended 5° in each dimension from the MCS centroid, in order to illustrate the near-MCS state of the troposphere. The second interpolation grid extended 12.5° to the north, east, and south of an MCS centroid and 22.5° to its west; it was intended to illustrate the general synoptic regime attending MCS cases and to provide data comparable to those at an operational forecaster's disposal.

3.7 Statistical methods

As discussed in Chapter 5, three dominant modes of organized, long-lived convective storms were identified. The utility of such classification (for the forecaster and numerical modeler) lies in the predictability of the individual archetypes from pre-storm soundings and wind profiles. Accordingly, a rigorous statistical investigation of the data describing LS, PS, and TS environments in this study was undertaken.

3.7.1 Analysis of variance (ANOVA)

In order to determine the significance of the variance between several groups of data (in this case, between the LS, PS, and TS archetypes), an analysis of variance (ANOVA) was performed. The initial investigation for each variable, designed to reveal whether the three groups of data were *significantly* different, incorporated a *one-way analysis of variance* and an *F-test*. Qualitatively, these techniques compare the variance of data within a group

(archetype) to the variance between all groups (archetypes). Several assumptions must be made in order to carry out ANOVA procedures (Siegel and Morgan 1996):

1. Each group of data is normally distributed.
2. The variabilities within each group are approximately constant.
3. The data were obtained by random sampling (i.e. the observations are independent of one another).

The validity of the first assumption was checked using an approximation to Lilliefors' test for normality, following Dallal and Wilkinson (1986), within the spreadsheet data analysis package. For very small sample sizes (in this study, the LS and PS archetypes), the objective normality test could not reliably exclude non-normal distributions. Therefore, histograms were also constructed to ensure that no extreme outliers were present. The validity of the second assumption was checked using Bartlett's test (cf. Walpole and Myers 1989) as implemented by the spreadsheet analysis package (an objective check comparing the in-group variances for hypothetical equally sized samples). If either of the first two assumptions were not well-met by the data, a transformation (e.g. square root or logarithmic) was sought in order to create a more normally distributed and equally varied set of groups. If data could not be suitably transformed so that variances were approximately equal, one group's standard deviation (SD) was allowed to be up to twice as large as another, following Siegel and Morgan (1996). Variables with greater differences in variance were not subjected to ANOVA tests. The third assumption governs the random sub-sampling of a large population. This assumption was not violated in the present study, as the cases utilized represent the entirety of the linear, non-elevated MCS population during the investigated period (May 1996 and 1997). Although it is believed that variables which are highly correlated to different archetypes in this study may also have significance for larger MCS populations (in other months, years, and regions), any such conclusions are speculatory without further investigation, since assumption 3 is not valid for such a situation (i.e. the May data are not

a random sample of *all* MCSs).

The ANOVA provides information in the form of a *between groups mean square* and a *within groups mean square*. The former is expressed as:

$$between\ groups\ mean\ square = \frac{\Sigma[n_i \times (X_i - \overline{X})^2]}{k-1}, \tag{3.12}$$

where n is the number of samples in group i, X is the mean data value for group i, $\overline{X}$ is the grand mean (of all groups), and k is the number of groups. The latter is expressed as:

$$within\ groups\ mean\ square = \frac{\Sigma[(n_i - 1) \times S_i^2]}{[\Sigma n_i] - k}, \tag{3.13}$$

where n and k retain their meaning from Equation 3.12 and S is the standard deviation of group i. From these values, the *F-statistic* can be calculated simply as:

$$F = \frac{between\ groups\ mean\ square}{within\ groups\ mean\ square}. \tag{3.14}$$

The F-statistic measures how variable the group means are as compared to the overall randomness of the entire population (Siegel and Morgan 1996). This value is then compared to a critical value (from a statistics table), F_{crit}, which represents the minimum value of F for a particular level of confidence that the observed variability between the groups is non-random. A confidence level of 95% was chosen for this study, a typical choice for statistical work (Siegel and Morgan 1996). In order to be 95% certain that the differences between groups (archetypes) are significant, the computed F for the data groups must be greater than F_{crit} for the appropriate number of samples and data groups at the 5% significance level. If this condition is met, the *null hypothesis* (that the data groups are *not* significantly different) can be rejected with the confidence that there is only a 5% chance that the differences are due to random variability. Note that for a completely random assignment of MCSs to archetypes, about 5% of the investigated variables will *still* be statistically significant. A worthwhile test, therefore, is whether the actual population exceeds that value!

The analysis software used for this study permitted an even more valuable application of ANOVA tests. The level of confidence at which $F = F_{crit}$ (for the appropriate

number of degrees of freedom) was also computed by the statistical analysis routines. This provided additional information: not only was it possible to reject the null hypothesis for a specified level of confidence (i.e. 95%), it was also possible to determine the greatest level of confidence (lowest level of significance) at which the null hypothesis could be rejected. This value, $p \times 100\%$, was utilized to represent the statistical probability that the differences between mean data values for the studied archetypes could be due to random variability alone. The p-statistic can be used to answer several questions: *1)* If we assume that we have an *independent* sample, how likely is it that random variability could produce our result? In other words, how often would we be wrong if we inferred a relationship in the larger population based upon our result? *2)* How likely is it that our result is due to bad data and/or variability in the instruments and collection methods? *3)* How likely are we to get our result if we assigned cases to groups (archetypes) *randomly*? Question one is an important question, but cannot be satisfactorily answered since the assumption of independent samples is not justified (as discussed above). Question two is meaningful in that there are acknowledged shortcomings to the operational raob and wind profiler measurements. Question three is perhaps the most significant to this study, however. In effect, the p-statistic answers the question: "How much meaning did our taxonomy have?" If the p-statistic is relatively low, it is very unlikely that the magnitude of the differences between groups would occur if our taxonomy had no physical basis. However, if the p-statistic has a relatively large value, it is quite possible (even probable) that between-group differences of a similar magnitude would occur if we assigned cases to archetypes based upon the roll of a die.

Chapter 4

THE SYNOPTIC ENVIRONMENT OF MESOSCALE CONVECTIVE SYSTEMS DURING THE STUDY PERIODS

A great deal has been known about the general environments within which convective storms form, organize, and persist since the numerous studies of Newton (1950, 1963, 1966). In addition to local fields, as retrieved by rawinsondes, aircraft, and remote sensors, it is useful to know the synoptic features with which MCSs are frequently associated. Case studies of MCSs often describe the instantaneous large-scale conditions prior to or coincident with convective episodes. However, additional insight can be gained by averaging tropospheric variables over *longer* periods of time. To this end, I composited the daily 0000 UTC NCEP reanalysis fields in order to generally characterize the synoptic situations for May 1996 and May 1997. In addition, I compared *active* periods (those exhibiting MCSs) to *inactive* periods (those not exhibiting MCSs) during my study.

4.1 Interannual variations in synoptic meteorology and MCSs

That MCS populations depend upon the general synoptic scale flow is not surprising. May 1996 produced 33 MCSs in the study domain, of which 17 were elevated (cf. Appendix A. Table A.1). By contrast, May 1997 produced 55 MCSs, of which only 10 were elevated. Additionally, a large percentage of May 1996 cases were TS, while May 1997 exhibited a lower percentage of TS and higher percentage of PS cases (Table 4.1). The fraction of total MCSs with LS was relatively constant from year to year. These distributions suggest that particular archetypes (as well as elevated MCSs) may be more frequent (with

Table 4.1: Distribution of MCS archetypes by year. The righthand column represents the percentage of an archetype's total cases occurring within the time period given by the left-hand column.

time period	MCS type	# of cases	% of year's cases	% of type's cases
May 1996	unclass.	2	6%	67%
	LS	6	18%	35%
	PS	2	6%	12%
	TS	23	70%	45%
	total	33	100%	38%
May 1997	unclass.	1	2%	33%
	LS	11	20%	65%
	PS	15	27%	88%
	TS	28	51%	55%
	total	55	100%	62%

respect to the total MCS population) during certain regimes rather than equally represented as a fraction of the total number of cases in any period.

4.1.1 Differences in synoptic meteorology

The month of May 1996 exhibited, in the mean, an upper tropospheric ridge (in the geopotential height field) over the central United States (Fig. 4.1a). Due to the persistent strong ridge, only a few weak short wave troughs traversed the central Plains. Slightly upstream of the long wave ridge in the May 1996 mean was a southwestern U.S. short wave trough, largely due to a strong short wave that entered the western United States near the end of the month. In contrast, May 1997 exhibited an upper tropospheric ridge over the western United States (Fig. 4.2a). Nine short wave troughs aloft (5 of which were fairly strong) rounded the long wave ridge axis and crossed the central Plains from northwest to southeast in May 1997.

As shown by NCEP reanalysis difference fields, May 1997 exhibited slightly more negative vorticity advection (NVA) across the study region at 500 hPa than May 1996 (Fig. 4.3c). This was probably related to the more western location of the upper level ridge during the period. Although shortwave troughs frequently traversed the domain,

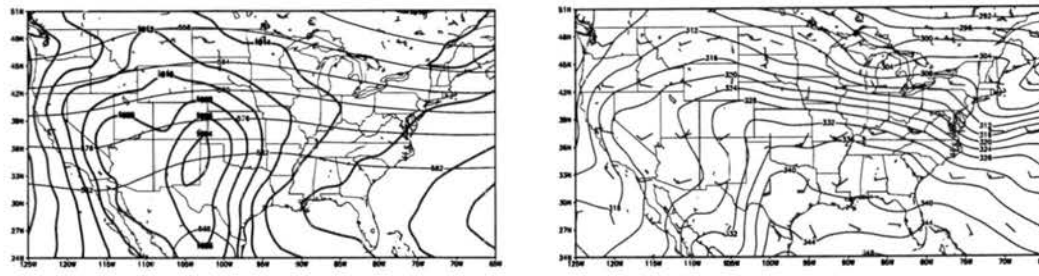

(a) (b)

Figure 4.1: NCEP Reanalysis mean fields for May 1996. (a) Surface pressure reduced to mean sea level (hPa: heavy contours) and 500 hPa geopotential height (dam: light contours). (b) Surface equivalent potential temperature (K: contours) and 850 hPa wind barbs. barb=5 m s^{-1}, half barb=2.5 m s^{-1}. Studied region extends from 31° – 45°N and 89° – 106°W.

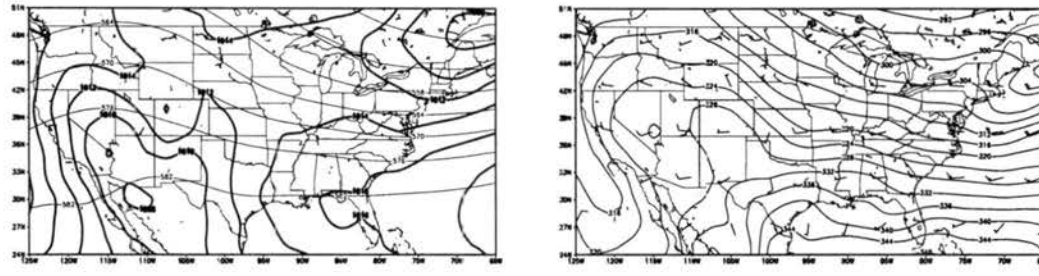

(a) (b)

Figure 4.2: Same as Fig. 4.1 but for May 1997.

their relatively rapid movement and variable tracks produced a smaller mean signal than the background pattern itself. While large elsewhere, the interannual changes in upper tropospheric winds were relatively small over most of the central Plains (Fig. 4.3d). As a result, the 700–300 hPa wind shear vectors exhibited little or no change between the periods over most of the studied region (Fig. 4.3a). The apparent superposition of a cyclonic gyre (upon the mean May 1996 pattern) over the central United States during May 1997 (Fig. 4.3 a,d) resulted from the mean westward shift in the upper level ridge from May 1996.

Beneath the high-amplitude long wave ridge over the central U.S. in May 1996 a warm, moist subtropical airmass was entrenched, as evident in the mean surface θ_e (Fig. 4.1b). For a large part of the month, a stationary front extended from west to east across the Plains. A lee surface pressure trough also persisted through much of May 1996, often with a closed low near the Texas/Oklahoma Panhandles, a feature evident in the monthly mean (Fig. 4.1a). As well, synoptic scale vertical motions caused by vorticity advection near (four) traversing short wave troughs enhanced surface cyclogenesis along the High Plains during May 1996, after which surface lows moved south-eastward across the central U.S., briefly assuming cold and warm fronts (as in the classic wave cyclone depicted by Bjerknes and Solberg 1922). However, as the short wave troughs aloft weakened the surface cyclones diminished in intensity and the fronts tended to stall. As a result, the signal of a persistent baroclinic zone exists over the northern Plains in the May 1996 mean surface equivalent potential temperature (θ_e) field (Fig 4.1b). In contrast, May 1997 saw 9 fully-formed wave cyclones traverse the Central Plains. The period for disturbances was much shorter for May 1997 than May 1996: typically 3 days. Therefore, warm moist airmasses were never long entrenched over the study region; linear frontal boundaries frequently entered the domain and displaced the subtropical air. The mean MSLP field was relatively diffuse in comparison to May 1996, exhibiting no strong surface low signal near the study region due to frequently traversing cyclones (Fig. 4.2a). The values of θ_e over the studied region were generally lower than in May 1996, reflecting the lack of persistent northward penetration by subtropical

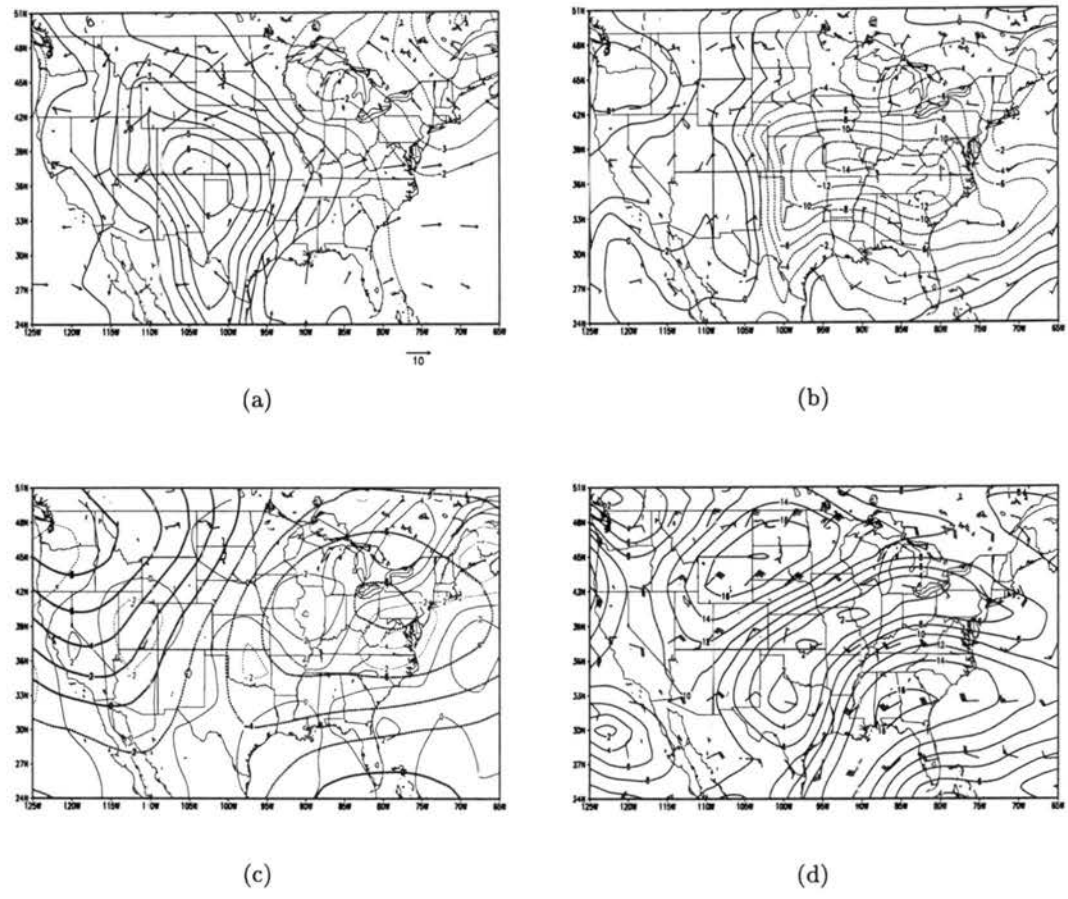

Figure 4.3: NCEP Reanalysis mean difference fields: May 1997 - May 1996. (a) Surface pressure reduced to mean sea level (hPa: contours) and 700–300 hPa wind shear vectors (m s^{-1}). (b) Surface equivalent potential temperature (K: contours) and 850 hPa wind barbs. (c) 500 hPa geopotential height (dam: heavy contours) and vorticity advection ($\times 10^{-10}$ s^{-2}: thin contours). (d) 250 hPa wind speed (m s^{-1}: contours) and wind barbs. Wind barb = 5 m s^{-1}, half barb = 2.5 m s^{-1}. Studied region extends from 31° – 45°N and 89° – 106°W.

airmasses (Figs. 4.2b and 4.3b).

4.1.2 Ramifications to linear MCS population

The relative scarcity of *linear, warm-sector* MCSs in May 1996 was probably related to the lack of strong linear triggers. The importance of such lifting mechanisms is evident in the data for this study: 60 of the 61 documented warm-sector (i.e. not elevated) cases occurred near some linear synoptic boundary (Table 4.2). The persistent stationary front

Table 4.2: Distribution of synoptic features related to the 88 studied cases. *Boundary intersection* MCSs occurred at or near the colocation of two features (B–F). Therefore, A+B+C+D+E+F+N–*int.* = 88. Percentages do not equal 100% due to rounding.

code	synoptic feature	# cases	% cases
A	elevated (non-warm sector)	27	31%
B	cold front	24	27%
C	warm or stationary front	20	23%
D	surface pressure trough	17	19%
E	dry line	8	9%
F	outflow boundary	8	9%
N	no NMC analyzed feature	1	6%
int.	boundary intersections	17	19%
G	low-level jet core	30	34%
H	low-level jet terminus	24	27%
X	no low-level jet feature present	34	39%

that lay across the region in May 1996 instead suggested an environment similar to that of clustered MCCs, as described by Laing and Fritsch 1998. Additionally, the high frequency of elevated MCSs was probably related to the interaction of this prevalent stationary front with the frequently attendant low-level southerly jet. The signal of this jet is unmistakable in the May 1996 monthly mean (Fig. 4.1b) and is expected given the general flow regime: a well-established Bermuda high to the east with (on average) High Plains low pressure to the west. Low-level jets were present less often during May 1997, as evidenced by the weaker southerly monthly mean wind (Fig. 4.2b). This was consistent with the weaker zonal pressure gradient in the May 1997 monthly mean (Fig. 4.2a). The presence of lower tropospheric wind maxima over the Great Plains was significant to the linear MCSs in this study: 61% of the catalogued cases were related either to its core or terminus (Table 4.2).

It is evident from their total displacements (Fig. 4.4) that the MCSs of May 1996 were generally longer-lived and traversed greater distances than did those of May 1997, which additionally exhibited more southeastward mean displacement vectors due to the persistent upper level northwesterly flow. In part, the 1996 path lengths may have resulted from the relatively higher θ_e (and therefore conditional instability, all things being equal)

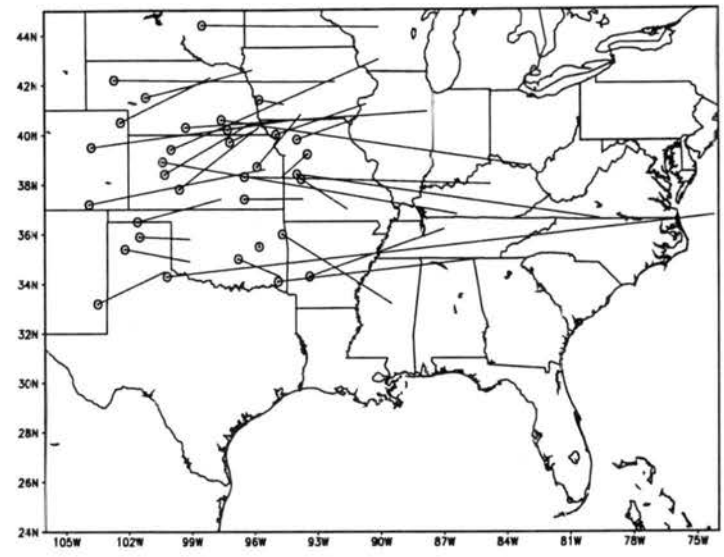

(a) May 1996

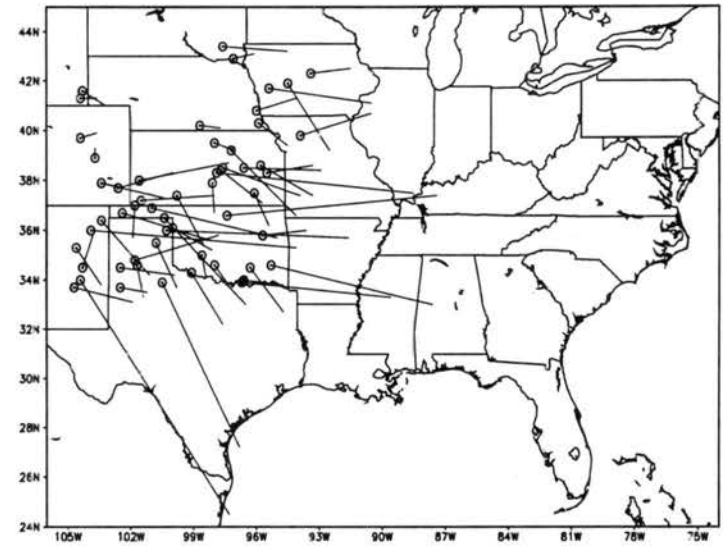

(b) May 1997

Figure 4.4: MCS genesis points and total displacements for (a) May 1996 and (b) May 1997.

of the surface subtropical airmass that was well-entrenched across the region for a large percentage of the month. In contrast, a relatively narrow axis of high θ_e extended from Texas into Colorado in May 1997. Further, the long west to east span of the stationary

front prevailing during May 1996 provided a persistent boundary along which MCSs could propagate. Additionally, a low-level jet, which could provide buoyant air to nocturnal convective storms, was often present in May 1996.

Finally, attention is turned to the unequal distribution of PS and TS cases in May 1996 and May 1997 (Table 4.1). The data suggest that linear MCS class distributions are not a simple fraction of the total number of cases (38% of the total MCSs occurred in May 1996, compared to 45% of the total TS cases and only 12% of the total PS cases during that period), but may depend upon other factors such as synoptic regime. As will be discussed in Sections 5.2.5 and 6.2.2, PS cases in this study often exhibited strong, deep tropospheric winds parallel to the linear boundaries on which they formed. Perhaps the relative lack of linear boundaries traversing the studied region during May 1996 provided for fewer occasions of favorable upper tropospheric wind–surface boundary relation.

4.2 Comparison of active and inactive periods

In order to compare episodes of linear MCS prevalence to episodes of their absence, means were constructed for periods deemed to be *active* and *inactive*. A period was defined as active if it *1)* averaged at least one MCS per day during the span and *2)* appeared as a discrete mode on a frequency versus date histogram. Based upon this partitioning, 85 of the 88 cases occurred during active periods.

The prevalant idea that MCS activity increases in the presence of an approaching short wave trough and/or classic wave cyclone (Kane et al. 1987 presented a summary for 74 MCCs, of which a majority occured in "synoptic" or "frontal" regimes) is borne out by the May 1996 and May 1997 data. During active periods, mean MSLPs were lower across the entire study domain (Fig. 4.5a). This result is consistent with surface cyclones traversing the region during periods of activity. The strongest signal in the active-inactive MSLP difference, however, is the tendency for a low pressure center in southwestern Kansas during active regimes. This can be attributed, to a large extent, to the bias introduced by

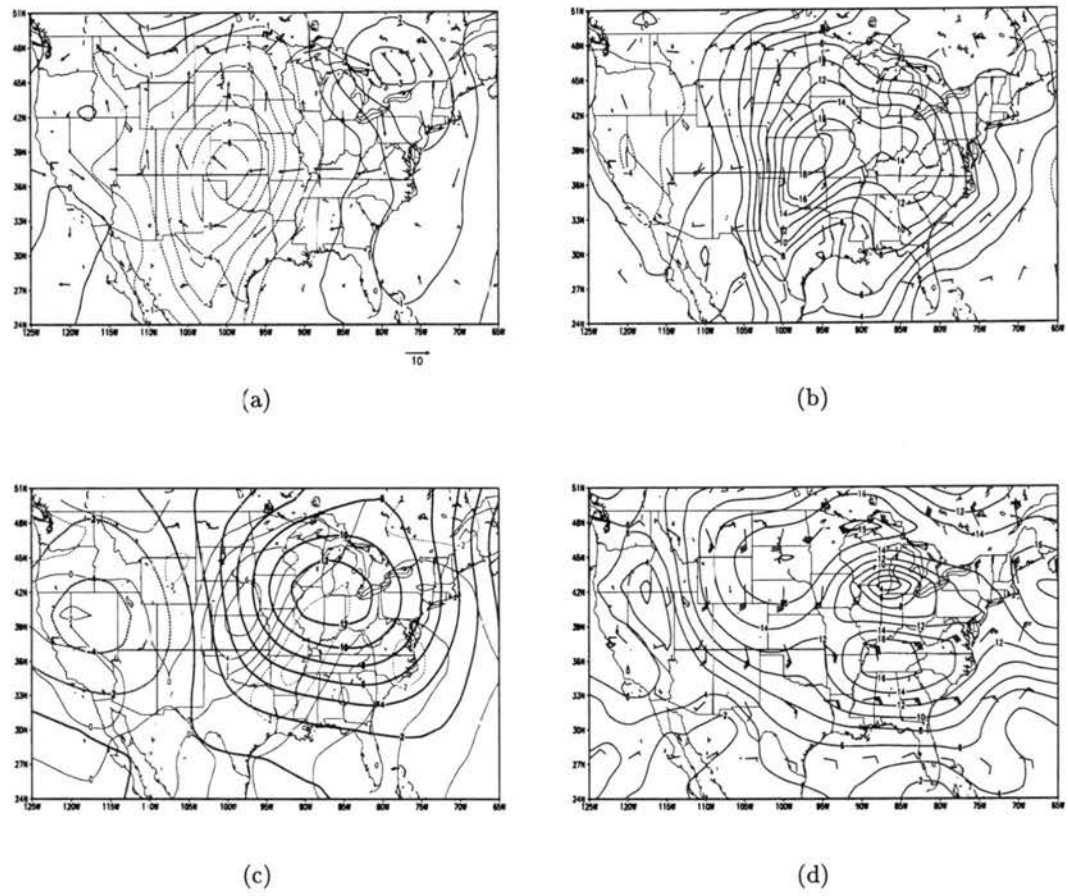

(a) (b)

(c) (d)

Figure 4.5: Same as Figure 4.3 except for difference: active - inactive periods.

the persistence of the High Plains low pressure feature during May 1996. As the mean fields are straight averages, persistent features can overwhelm transient features in the long term signal. In addition, however, the west to east (northwest to southeast) tracks of the cyclones which traversed the study domain originated mainly in the High Plains, a tendency that probably strengthened the mean perturbation in southwestern Kansas.

The mean surface cyclone appeared to be well-related to enhanced troughiness aloft in the western United States (Fig. 4.5c). The magnitude of the geopotential height difference does not, however, suggest a long-wave trough but rather reflects approaching shortwaves from a variety of latitudes and directions into the western United States. In association with the enhanced western troughiness, stronger positive vorticity advection (PVA) occurred

over the study domain during active periods (Fig. 4.5c), providing quasi-geostrophic lifting (assuming that PVA in the lower troposphere was exceeded by that in the middle and upper troposphere). The strengthened ridge over the central and eastern U.S. during active periods was consistent with a warm airmass in place over the Plains and Midwest during the MCS episodes. During active regimes, a tongue of high θ_e air extended into the central Plains from south-central Texas (Fig. 4.5b), probably in association with a low-level jet, which was on average stronger during active periods (at 850 hPa: Fig. 4.5b). In fact, on average during active periods general southerly flow existed at low-levels across the southern 2/3 of the study domain, which climatologically suggests the northward flow of warm, moist, increasingly buoyant air from the Gulf of Mexico region. Maddox and Doswell (1982) found that low-level thermal advection was a better predictor of many MCSs than upper tropospheric vorticity advection. While low-level warm advection may be more widely applicable, and particularly important during *summer* MCS episodes, the signals of *both* warm advection and PVA during the active MCS periods in my study were unmistakable.

At 250 hPa, a strong anticyclonic gyre was apparently superposed upon the eastern United States and a weaker cyclonic gyre upon the western United States during active periods (Fig. 4.5d), consistent with an enhanced western trough/eastern ridge pattern similar to that described at 500 hPa. The active periods of May 1996 and 1997 exhibited weaker westerly wind shear than did the inactive periods (Fig. 4.5a: easterly vectors in the difference field correspond to a decrease in westerly wind shear). Thorpe et al. (1982) found in numerical simulations that quasi-steady convective lines were most favored in environments with little or no middle and upper tropospheric shear. It is not clear whether the result from my study is immediately relatable to the findings of Thorpe et al. (1982): it may be that other tropospheric contributors to linear MCSs were more significant than the vertical wind shear during the study period. In order to attribute the difference in MCS activity to the mid-level shear *alone* (more to the point of the conclusion of Thorpe et al. 1982), a more controlled environment than the atmosphere would be necessary.

4.3 Diurnal cycle in MCS frequency

Nocturnal maxima have been established for thunderstorms (Wallace 1975), MCCs (Maddox 1980), and linear MCSs (Hilgendorf 1996) in the central Plains. In the present study, this nocturnal maximum was confirmed for 54 linear warm sector MCSs. As discussed in Section 3.2.2, each MCS lifetime was divided into fourths roughly corresponding to the scheme presented by Hilgendorf and Johnson (1998). At each of the three divisions, the MCS's radar characteristics were assessed and catalogued. Presented in Fig. 4.6 is a histogram of the linear MCS classes' 3-hour running mean diurnal distribution using the *central* (second of three) observation time for each MCS.

The dominant signal in the total curve for linear MCSs (Fig. 4.6) is centered at 0300 UTC (2200 CDT). This maximum agrees well with the finding of HSD90 that mesoscale precipitation systems with, "extremely large stratiform areas" were maximized between 0300 and 0900 UTC. Hilgendorf and Johnson (1998) pointed out that an MCS's maximum areal extent typically occurs later than the mid-point in its lifetime. As the times represented in the histogram are approximate *midpoints* in MCS lifetimes, the nocturnal maximum may therefore have been slightly displaced toward an earlier hour than that observed by HSD90, who used the time of "maximum stratiform echo".

A majority of TS cases occurred between 0100 and 0700 UTC (Fig. 4.6), with a smaller mode in PS cases (between 2300 and 0500 UTC) and LS cases (between 2200 and 0500 UTC). In addition, a secondary mode existed near local sunrise ($\approx$ 1100 UTC). While this secondary maximum was relatively small for TS MCSs (with respect to the amplitude of the archetype's curve), it appeared to be *the dominant mode* for LS MCSs. Geerts (1998) noted a similar maximum in MCSs of the southeastern United States. It may be that Geerts (1998) and I, by utilizing regional radar data, have uncovered a secondary maximum that was unapparent from the satellite imagery used in previous studies. The reasons for this near-sunrise mode are not fully understood at this time, and are left for future study. One hypothesis, advanced by Gray and Jacobson (1977) for tropical deep cumulus

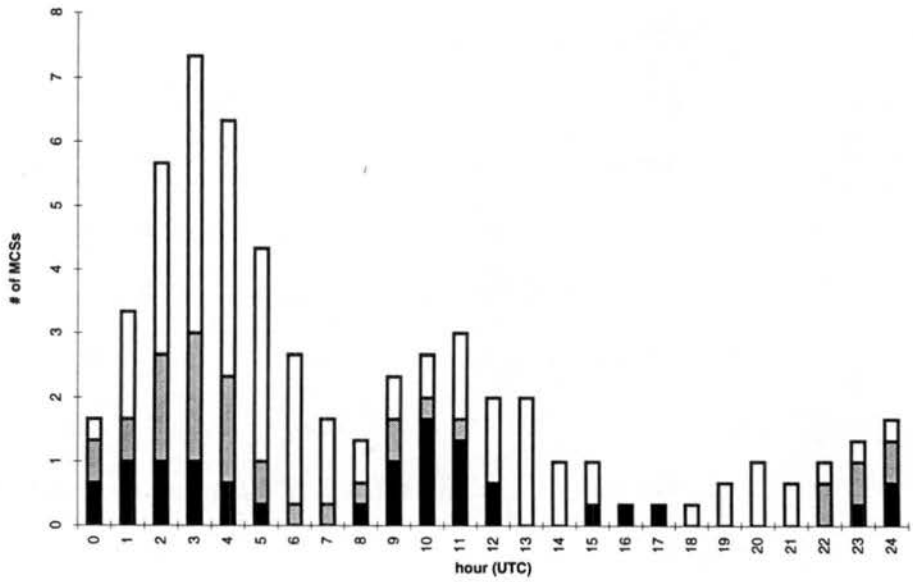

Figure 4.6: Histogram of linear MCS distributions (values are 3-hour running means). Black area: LS cases. Grey area: PS cases. White area: TS cases. Times are UTC. Central daylight savings time = UTC - 0500.

clouds, relates enhanced near-sunrise upward motions to solenoidal circulations forced by the difference in nocturnal radiational cooling between cloudy and clear areas. Indeed, they may have anticipated the present result: "morning convection maxima should be detectable along coastal regions, in humid land areas and during autumn and winter when the surface heating cycle is suppressed". More investigation of this near-sunrise maximum is clearly warranted.

Chapter 5

THREE CLASSES OF LINEAR MESOSCALE CONVECTIVE SYSTEMS: RADAR REFLECTIVITY AND PHYSICAL CHARACTERISTICS

When linear mesoscale convective systems are discussed, a common frame of reference (e.g. Geerts 1998) is the well-known *leading line-trailing stratiform (hereafter, TS)* model, as apparently first documented by Newton (1950) and as formally defined and compared to a group of MCSs by HSD90. However, an initial survey of May 1996 MCSs over the entire United States revealed, in addition to the prominent TS mode, numerous linear convective systems with a region of stratiform rain *in advance of* the convective line (which will be referred to as *leading stratiform*, or LS). Two known case studies of such systems have been reported (Grady and Verlinde 1997, Nachamkin 1998), but they have generally received little attention. The central Plains were therefore investigated in greater detail for modes of linear MCSs and their associated thermodynamic and kinematic environments. In the course of the investigation, a third class of linear convective systems was noted: those whose associated stratiform rain appeared to move (in a storm-relative sense) parallel to the line itself, yielding relatively little stratiform rain immediately leading or trailing the convective line (which will be referred to as *parallel stratiform*, or PS).

5.1 The archetypes defined

By *archetypes* I mean the ideal examples to which MCSs are compared for the purposes of classification. Idealized life cycles of the three archetypes from the present taxon-

omy are depicted in Fig. 5.1. Each will be discussed in detail momentarily. A case with many similarities to a particular archetype would be included in that *class* of the taxonomy. Several basic assumptions are implicit in the taxonomy presented here. Firstly, as has been emphasized, only *linear* MCSs (as defined in Chapter 2) were catalogued and described in this study. The following taxonomy makes no attempt to describe or account for non-linear MCSs. The author hastens to add that the term *unclassifiable* should *not* be uniformly applied to such non-linear cases (as was done by HSD90). The task of classifying non-linear MCSs is yet a *distinct* task from that which I've undertaken. Having excluded them from the present study, however, I leave the matter for others. Secondly, all of the cases classified herein (and on which the definitions are based) met the criteria used to define an MCS (cf. Section 3.1). Several previous studies (e.g. BJ85 and BMJ87) have discussed the characteristics of "squall lines". While the linear MCSs considered in the present study would probably be called squall lines (based upon the common usage of the term) by most meteorologists, not all squall lines would meet the more stringent length and duration criteria defining MCSs in this study. Thirdly, all the MCSs in this study were observed using national radar composites. Accordingly, the taxonomy presented here is based solely upon the meso-β scale radar reflectivity structures of the documented MCSs, *not* upon their dynamics, velocity fields, or otherwise observable properties.

5.1.1 Trailing stratiform

The TS convective archetype has been described by HSD90 (Fig. 5.2) and in the present study (Fig. 5.1a) I have not deviated from the definition they presented. The pertinent aspects of the definition advanced by HSD90 include: a convective line, "convex toward the leading edge," with "a series of intense reflectivity cells solidly connected by echo of more moderate intensity." The line has a "very strong reflectivity gradient at [the] leading edge (i.e. gradient much stronger at [the] leading edge than [the] back edge of the convective region)," and a trailing stratiform region of "large size (over 10^4 km^2)." In general, TS MCSs

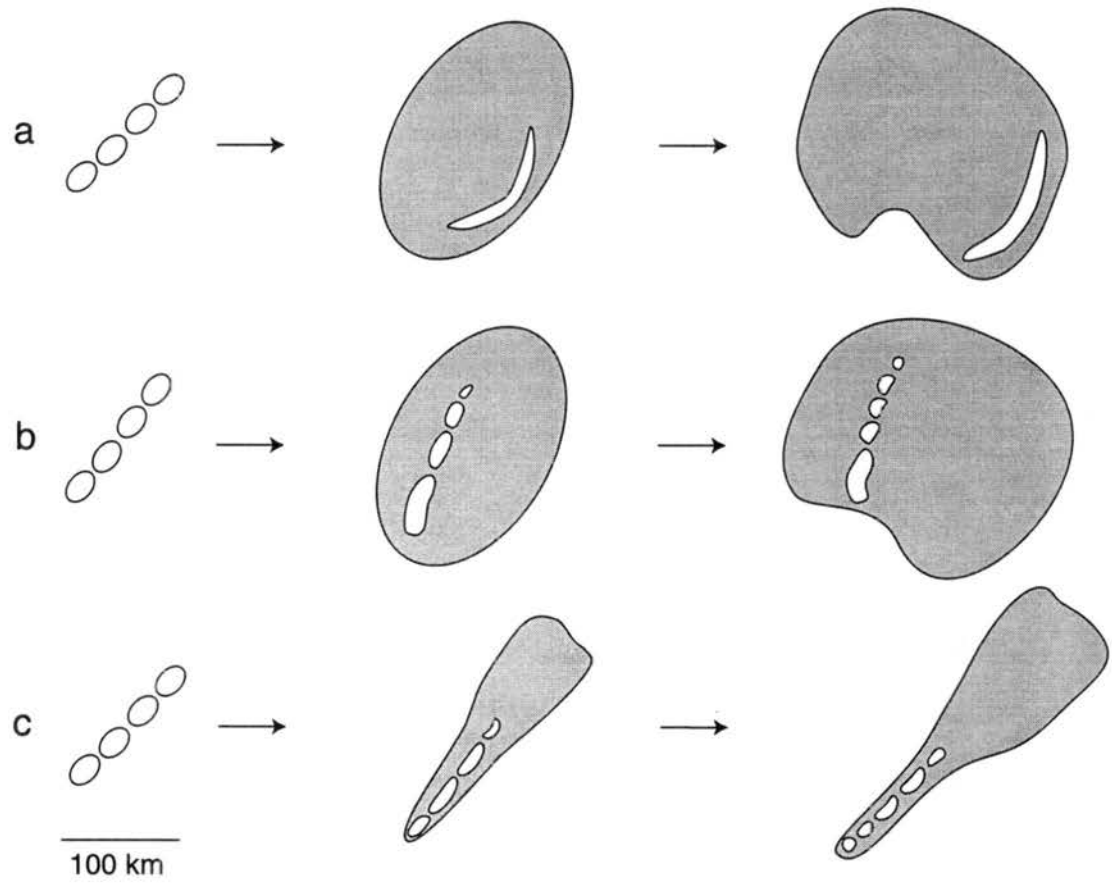

Figure 5.1: Schematic of idealized life cycles for three linear MCS archetypes: (a) leading line trailing stratiform (TS), (b) convective line with leading stratiform (LS), (c) convective line with parallel stratiform (PS).

move at speeds, "> 10 m s^{-1} in a direction normal to the line orientation," and exhibit a "secondary maximum of reflectivity" (often including a *bright band* due to the higher reflectivities of melting hydrometeors) in the stratiform rain region, "separated from the convective line by a narrow channel of lower reflectivity" commonly known as the transition zone. It is relevant to note that the TS archetype depicted by HSD90 exhibited very little leading stratiform rain. Cases exemplifying the TS archetype from the current study are shown in Fig. 5.3.

5.1.2 Leading stratiform

Linear MCSs whose stratiform rain is predominantly located in advance of the convective line (i.e. in the area toward which the MCS propagates) are defined as *convective lines with leading stratiform rain (or simply LS, Fig. 5.1b).* In the extreme, members of this archetype corresponded to a reversal of archetypal TS cases, with a convective line *preceded* by a transition zone and secondary swath of stratiform rain exhibiting a bright band (Fig. 5.4a). More frequently, the LS members exhibited moderate regions of stratiform rain without transition zones and secondary bands (as in Fig. 5.4b). On numerous occasions, the radar reflectivity pattern of convective lines in LS cases was distinctly cellular rather than homogeneous (Fig. 5.4c). Many LS MCSs were less pristine than the preceding examples and included *some* trailing stratiform rain as well (Fig. 5.4d).

The tendency of an MCS to generate predominantly pre-line rain was a criterion for LS classification even if TS rain was present. Cases with both pre-line and post-line rain obviously represented a transition between the two extreme archetypes. These were classified as LS based upon their greater qualitative similarity to the LS extreme than the TS extreme. Firstly, it is clear that for cases with stratiform rain both in advance of and trailing a convective line, the definition advanced by HSD90 for TS cases is not met (the pre-line reflectivity gradient is not significantly different from the post-line). As well, the cold pool dynamics associated with archetypal TS cases (cf. Houze et al 1989) suggest the

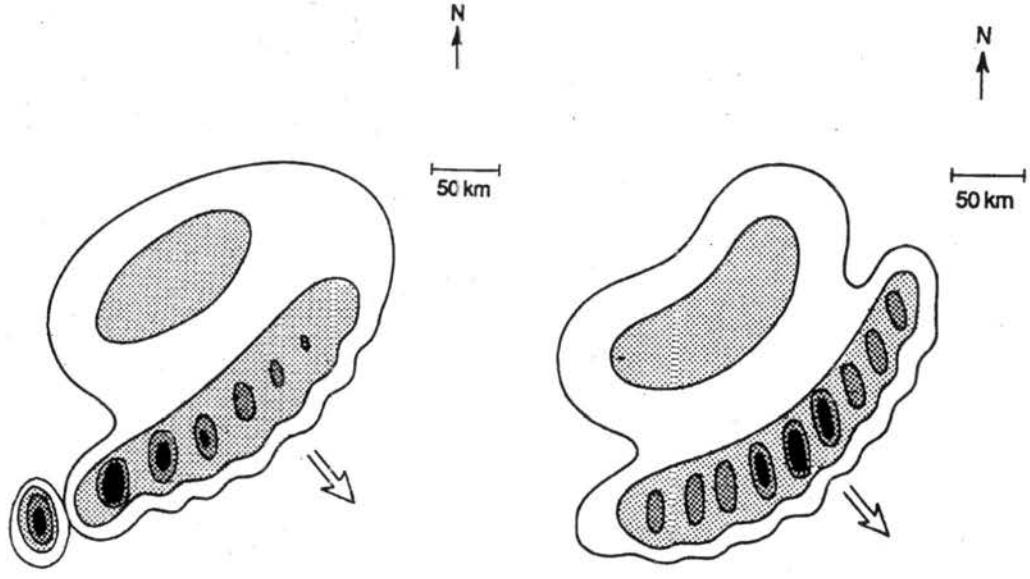

(a) (b)

Figure 5.2: Radar reflectivity archetypes for leading-line trailing-stratiform (TS in this manuscript) MCSs as depicted by Houze et al. (1990): (a) asymmetric TS archetype and (b) symmetric TS archetype.

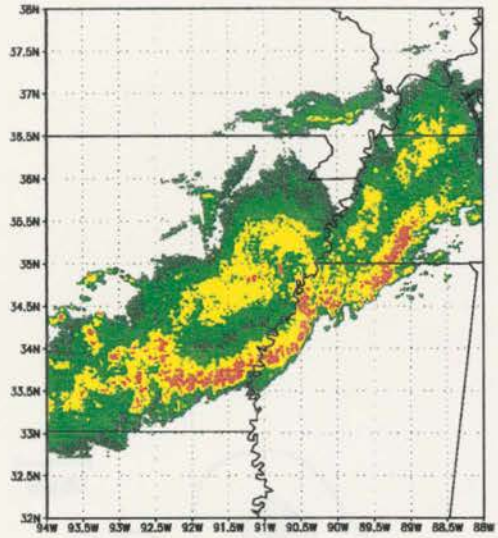

(a) 11 May 1996: 0800 UTC

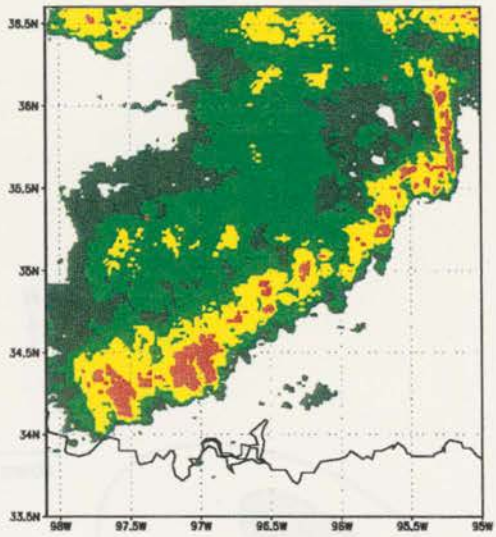

(b) 8 May 1997: 0700 UTC

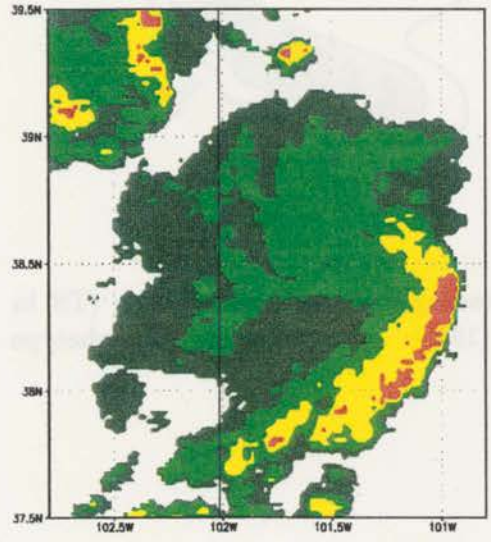

(c) 23 May 1997: 0200 UTC

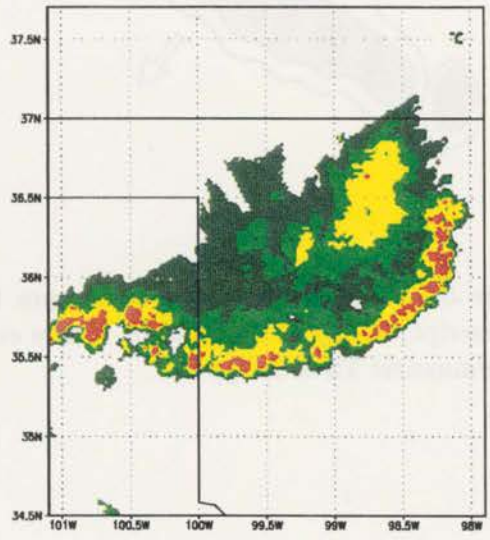

(d) 24 May 1997: 0200 UTC

Figure 5.3: Radar reflectivity: examples for trailing stratiform (TS) archetype.

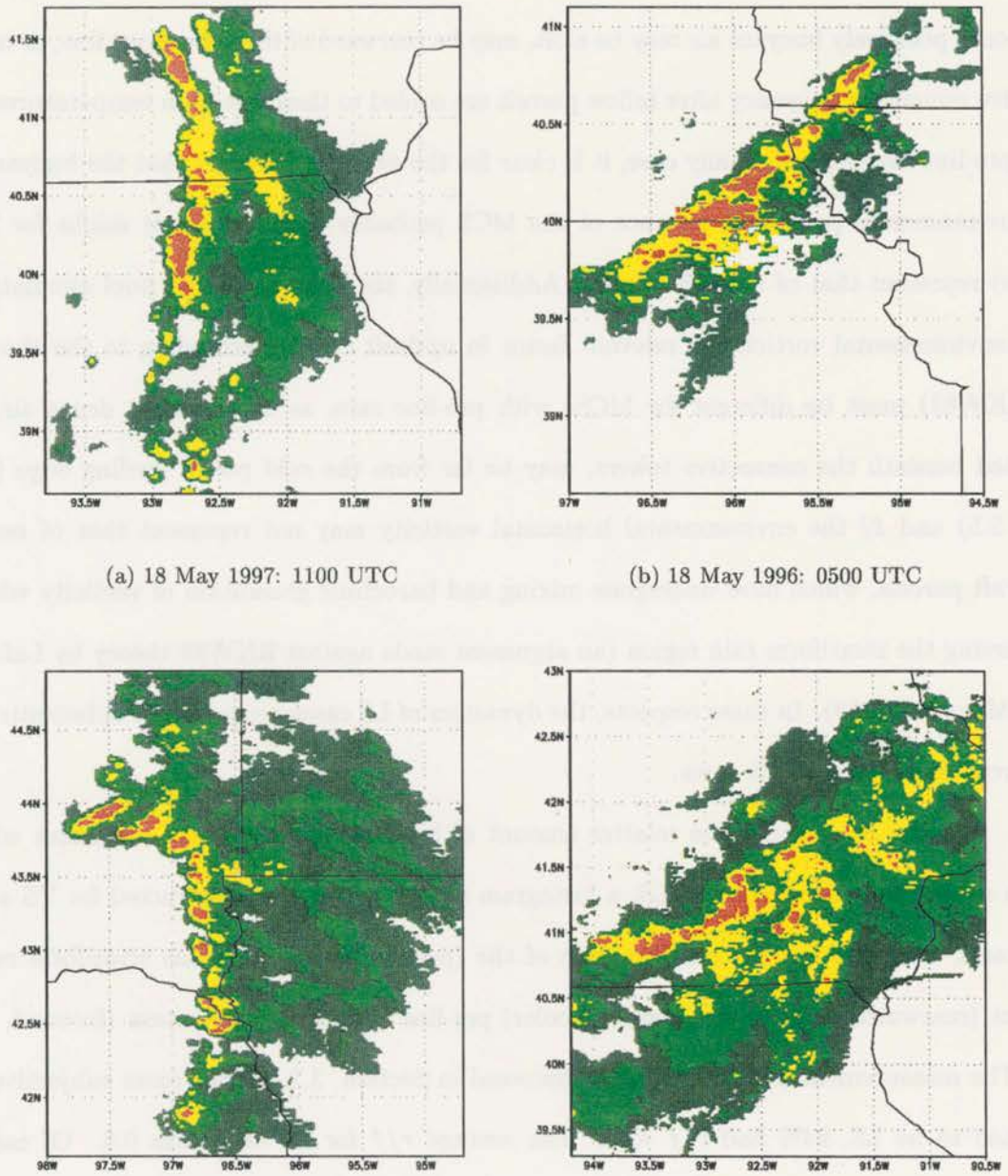

(a) 18 May 1997: 1100 UTC

(b) 18 May 1996: 0500 UTC

(c) 7 May 1997: 1100 UTC

(d) 8 May 1997: 0100 UTC

Figure 5.4: Radar reflectivity: examples for leading stratiform (LS) archetype.

convergence of very buoyant air at the gust front. In the LS extreme, the *leading edge* of the convective line encounters low-level air that has already been altered by evaporational cooling of pre-line rain, suggesting a decrease in inflow buoyancy. As later discussed, the source of positively buoyant air may be aloft, may be rearward of the convective line, or may involve remaining buoyancy after inflow parcels are cooled to their wet-bulb temperatures in the pre-line rain region. In any case, it is clear for the extreme LS cases that the buoyancy of environmental parcels in advance of the MCS probably does not (as it might for TS cases) represent that of updraft parcels. Additionally, the balance of cold pool circulation and environmental vorticity (a relevant factor in updraft canting according to the theory of RKW88) must be different for MCSs with pre-line rain, as *1)* the most dense air, if located beneath the convective towers, may be far from the cold pool's leading edge (cf. Fig. 5.5) and *2)* the environmental horizontal vorticity may not represent that of near-updraft parcels, which have undergone mixing and baroclinic generation of vorticity while traversing the stratiform rain region (an argument made against RKW88 theory by Lafore and Moncrieff 1989). In these respects, the dynamics of LS cases are probably substantially different from those of TS cases.

In order to quantify the relative amount of leading stratiform rain consistent with cases subjectively deemed to be LS, a histogram of r/f values was constructed for TS and LS cases, where r/f is the unitless ratio of the (perpendicular) post-line stratiform rain extent (rearward, or r) to the (perpendicular) pre-line stratiform rain extent (forward, or f). The measurement of these values is discussed in Section 3.2. Of the cases subjectively deemed to be LS, 94% had $r/f < 2$. The average r/f for LS cases was 0.8. Of cases subjectively deemed to be TS, 94% had $r/f \geq 2$. The average r/f for TS cases was 4.3. Accordingly, a subjective classification of MCSs might be objectively evaluated using a threshold of $r/f = 2$. Ultimately, however, the investigator must evaluate the *full evolution* of the linear MCSs (preferably by animation) rather than apply a simple numerical rule to one radar image or to a lifetime mean.

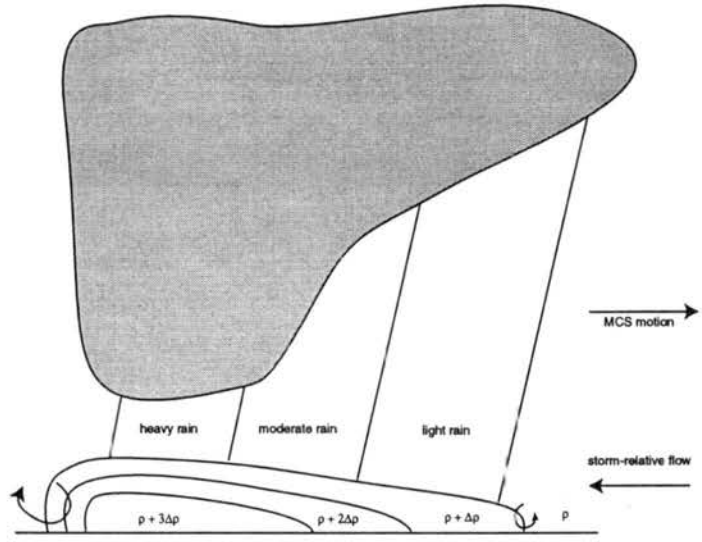

Figure 5.5: Schematic for possible LS cold pool scenario. Cold pool has been idealized as a dense, stratified outflow. Sense of circulation at cold pool edges is indicated.

5.1.3 Parallel stratiform

A linear MCS was deemed to have *a convective line with parallel stratiform (CLPS, or simply PS)* if most or all of the stratiform rain region associated with the convective line moved parallel to the line itself (in a storm-relative framework) and to the left of the line's motion vector throughout its life cycle (Fig. 5.1c; examples in Fig. 5.6). Very little stratiform rain surrounded the convective lines of PS cases. More formally, the reflectivity gradient was relatively large on *both* sides of the convective line; the region of high reflectivity cores was locally accompanied by little else. The stratiform rain regions' movement (as determined from animations) in PS cases generally deviated less than 30° from the convective lines' (azimuthal) orientation. In many cases, weaker convective echoes or dying convective cells were observed in the stratiform rain region moving parallel to the convective line (Fig. 5.6 a,b,c). Such observations are consistent with a line backbuilding to its right (with respect to MCS motion), whose decaying cells exist in a region of increasingly stratiform rain. It must be pointed out, however, that both LS and TS cases also exhibited back-building. As well, some PS cases exhibited little or no backbuilding behavior (Fig. 5.6d), and instead behaved as persistent entities whose stratiform rain happened to move parallel to the line itself.

5.1.4 Hybrid and unclassifiable cases

Naturally, a concern for any taxonomy is the handling of cases which do not completely conform to the archetypes presented. The investigator had to make choices: in the broad spectrum of MCS structures, should slightly non-conforming events be called *unclassifiable* or be put into classes with which they are moderately similar? I decided in favor of the latter. Much as HSD90 evaluated the similarity of MCSs to (only) the LLTS archetype, I chose to subjectively evaluate the similarity of each MCS to all three archetypes. If an MCS bore much greater likeness to any one of the three archetypes, it was classified as such. To facilitate classification of hybrids (those cases with more ambiguous combinations

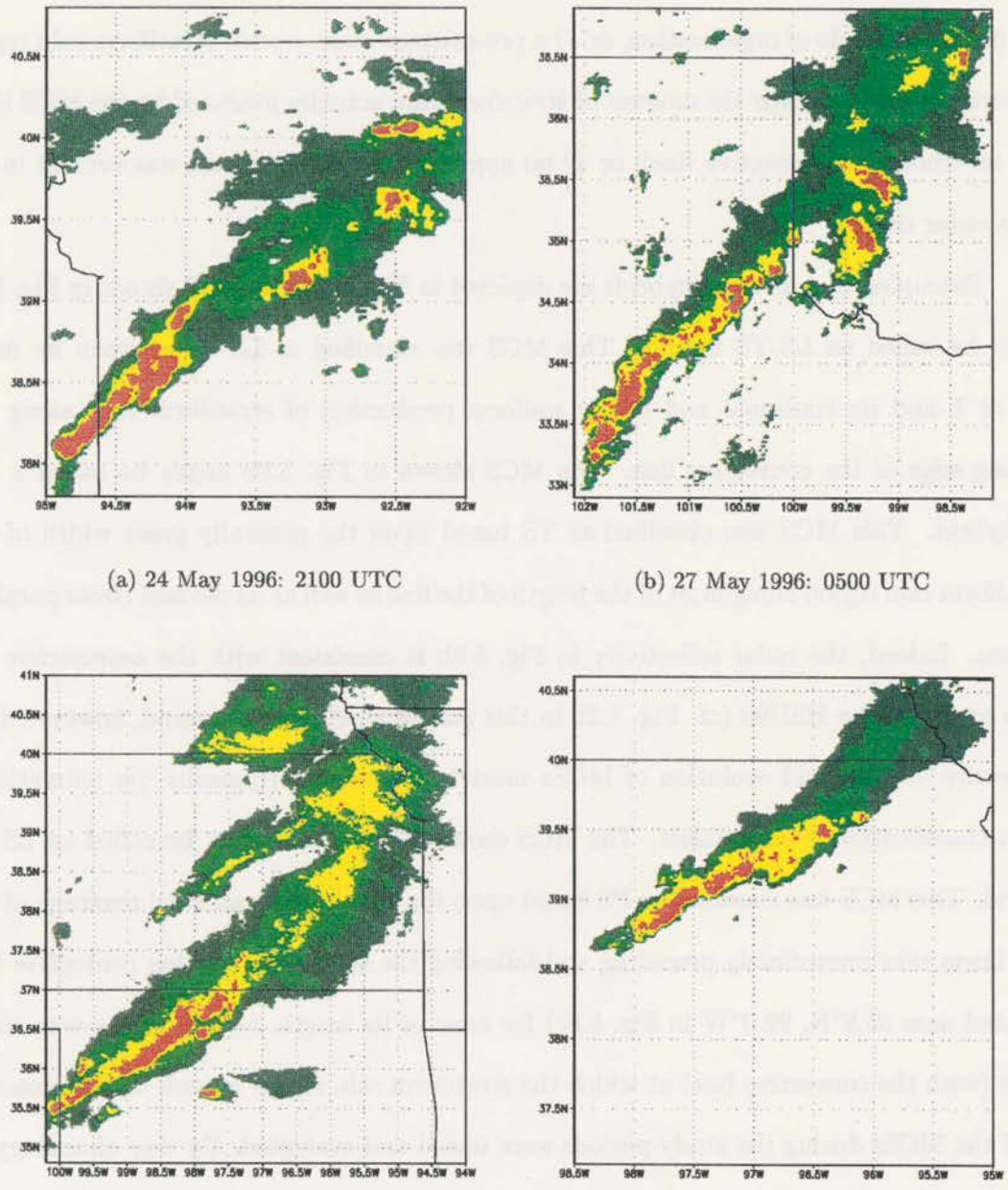

(a) 24 May 1996: 2100 UTC

(b) 27 May 1996: 0500 UTC

(c) 2 May 1997: 0400 UTC

(d) 26 May 1996: 1000 UTC

Figure 5.6: Radar reflectivity: examples for parallel stratiform (PS) archetype.

of archetypal qualities), a decision tree was developed and followed (Fig. 5.7). Cases from the radar study were *only* deemed "unclassifiable" if: *1)* they bore no resemblence to any of the three archetypes presented above, or *2)* they evolved among archetypes with no clear and dominant mode of organization, or *3)* a pre-existent meso-α scale stratiform rain region obscured or made unclear the amount of stratiform rain actually *produced* by the MCS itself (i.e. an embedded convective line), or *4)* no appreciable stratiform rain was evident in the 2-km radar data.

Examples of archetypal hybrids are depicted in Fig. 5.8. The MCS shown in Fig. 5.8a might be called an LS-TS hybrid. This MCS was classified as LS based upon its mean $r/f \approx 1$ and its continual and nearly uniform production of stratiform rain along the leading edge of the convective line. The MCS shown in Fig. 5.8b might be called a PS-TS hybrid. This MCS was classified as TS based upon the generally great width of the stratiform rain region along most of the length of the line as well as its deviant (from parallel) motion. Indeed, the radar reflectivity in Fig. 5.8b is consistent with the *asymmetric* TS cases presented by HSD90 (cf. Fig. 5.2b in this manuscript). Keep in mind, however, that the entire lifetime and evolution of MCSs must be considered (typically via animations) when classification is undertaken. The MCS shown in Fig. 5.8c might be called an LS-PS hybrid. This MCS was classified as PS based upon the relatively small areal coverage of the stratiform rain *immediately* preceding and following the southward moving convective line (located near 35.8°N, 99.0°W in Fig. 5.8c) for most of its length, as well as the very small angle (with the convective line) at which the stratiform rain region moved. In like manner, all of the MCSs during the study periods were tested and evaluated. By way of analogy to HSD90, it is believed that all of the classified cases were either "strongly" (i.e. exemplifying the archetype) or "moderately" (i.e. resembling the chosen archetype notably more than the other archetypes) classifiable, though these designations (here) are subjective. The existence of relatively few unclassifiable cases suggests that within the spectrum of linear MCSs, observable similarities to one of the three presented archetypes are common.

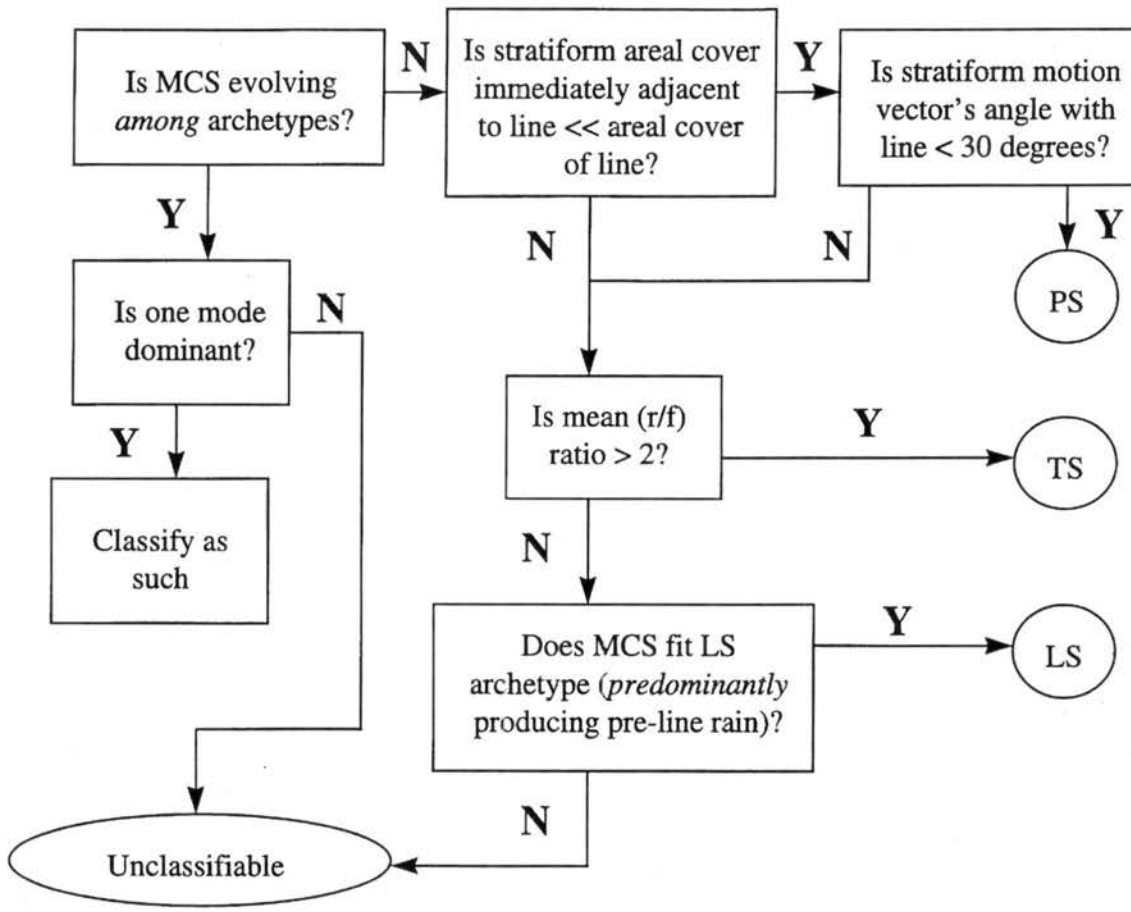

Figure 5.7: Decision tree for classifying hybrid cases.

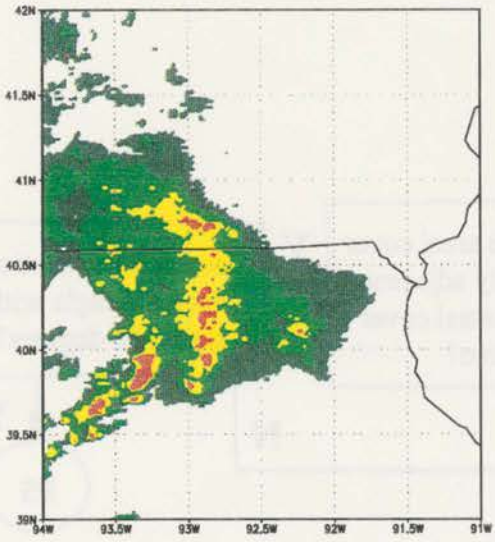

(a) 25 May 1996: 1900 UTC

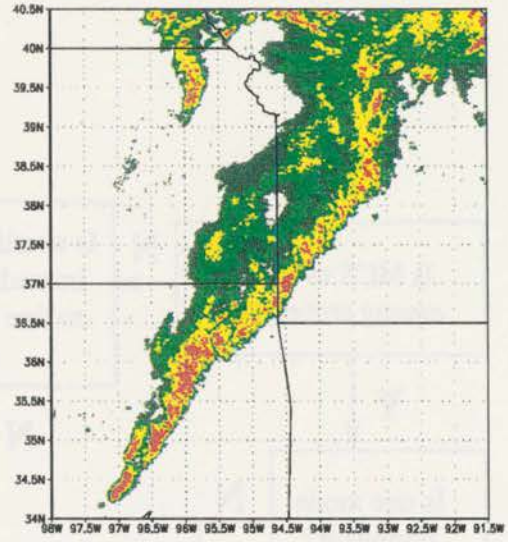

(b) 27 May 1996: 0500 UTC

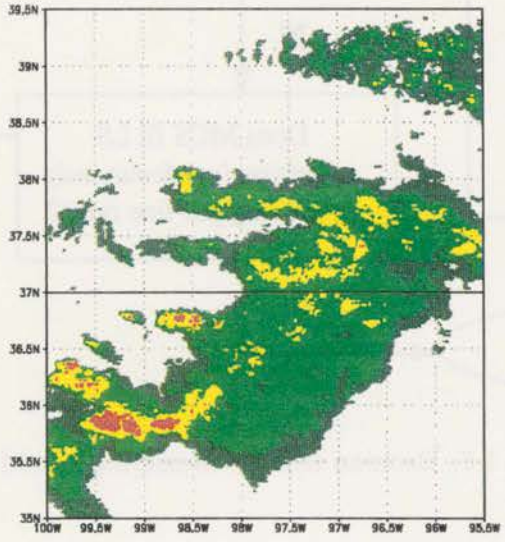

(c) 30 May 1997: 0300 UTC

Figure 5.8: Radar reflectivity: examples of archetypal hybrids.

5.1.5 *Evolution among archetypes*

As may be expected, linear MCSs can and do frequently evolve among archetypes between their initiation and decay. As detailed above, the cases in this study, when evolving, were classified based upon their *prominent* organizational modes. The quantitative distribution of such evolution for the studied MCSs is depicted in Figure 5.9. Not surprisingly (given the *total* MCS distribution), nearly half of all linear MCSs initially possessed TS characteristics. Relatively few MCSs which began as TS evolved into the other modes. Conversely, 30% of all cases that began as LS evolved to TS, and 58% of all cases that began as PS evolved to TS. In addition, though not documented as LS in their initial phase, many "unevolving" TS cases exhibited *some* pre-line rain in their earliest stages. These results may account for the large number of TS cases documented by HSD90: a great deal of linear MCSs appear to have TS characteristics at some point in their lifetimes, even if their initial organization is distinctly non-TS. It may be that, in time, MCSs tend to accelerate forward, such that TS rain is favored in their later stages. The reader should expect, however, that not every case which evolved toward TS was classified as TS; this decision was based upon the prominent mode of organization *throughout* an MCSs' lifetime (cf. Table 5.1). Notably, few MCS evolved *toward* the PS archetype. Perhaps the unique juxtaposition of boundaries and upper-level winds often observed for PS cases (cf. Sections 5.2 and 6.2) is not readily produced during convective events and must exist beforehand if PS organization is to occur.

5.1.6 *Overview of linear MCS archetypes' radar-observed properties*

The general differences between the three linear MCS archetypes are noteworthy. In the study domain during May 1996 and May 1997, LS and PS cases (both overall *and* in warm sectors) *each* composed approximately 20% of the total linear MCS population (Table 5.2). TS cases on average met the MCS length and reflectivity criteria for nearly twice as long as LS and PS cases. As well, their movements were the swiftest of the three classes. These two observations translate into a third, that TS cases traversed far greater

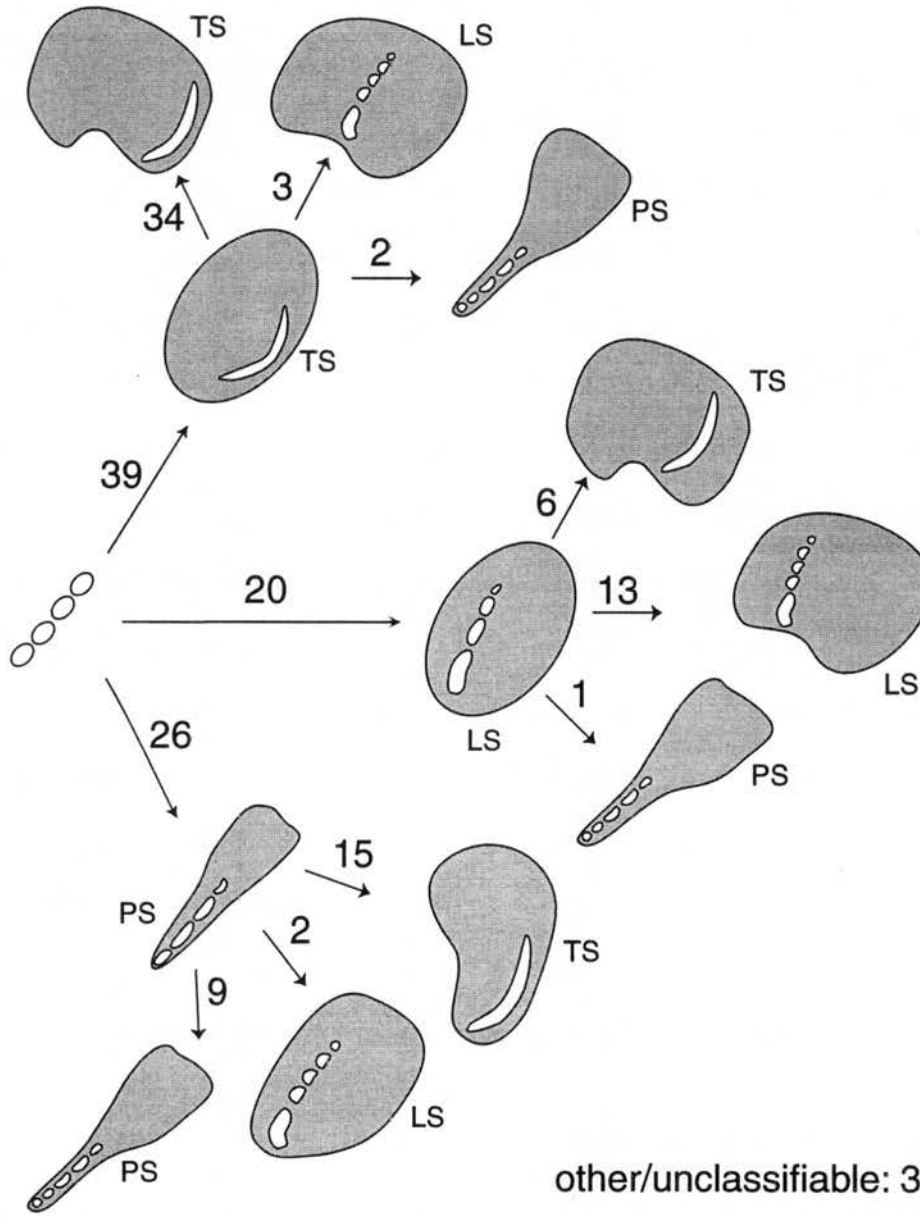

Figure 5.9: Schematic depicting evolution pathways of MCSs in this study. Phase one denotes initial organization, phase two denotes final organization, total number of cases following each step is indicated. For details on classification, cf. Table 5.1.

distances than other members of the linear MCS spectrum. The total area affected by storms during a convective episode is an important forecast problem (both operationally and in numerical models), in addition to the issues raised in Chapter 1. Accordingly, the synoptic and regional environments (such as a forecaster might consider) of the three linear MCS classes will be described.

5.2 Physical description of linear MCS archetypes and their environments

As previously stated, the archetype definitions and subsequent classification work were based solely on the radar-observed characteristics of the studied MCSs. Having laid out a description of the radar reflectivity signatures associated with the various archetypes, I shall now describe the relevant differences between the local and large-scale environments of these groups of MCSs and attempt to distill from these differences some meaningful physical descriptions of the three modes of linear MCSs. While *all* the MCSs in the study were classified, the mean fields presented in this section represent *only* the *warm-sector* MCSs not omitted for the reasons described in Section 3.1. The means depicted in this section include 33 TS MCSs, 12 LS MCSs, and 14 PS MCSs.

NCEP reanalyses were used to construct mean fields surrounding the MCSs in this study (cf. Section 3.6.2). For each case, a $5° \times 5°$ grid was produced to characterize the local fields, while a $35° \times 25°$ grid was produced to characterize the synoptic environment near and upstream of the MCS. The latitude and longitude of each mean grid are relative to the MCS location. While the NCEP reanalyses provided a convenient gridded dataset for averaging on larger scales, it was also important to consider the degree to which actual atmospheric measurements from rawinsondes and wind profilers were correlated with the three linear MCS archetypes in this study. The advantages of these data include their fine vertical resolution, their freedom from model input, and their occasionally very close proximity (temporally and spatially) to the studied MCSs.

Table 5.1: Distribution of evolution pathways for linear MCSs in this study. Within each pathway, the distribution of final classifications by archetype is indicated. Starred identifiers denote cases which did *not* evolve. Three MCSs were not classifiable using this scheme.

evolution pathway	# of occurrences	# classified as LS	# classified as PS	# classified as TS
LS*	13	13	0	0
LS → PS	1	1	0	0
LS → TS	6	1	0	5
PS*	9	0	9	0
PS → LS	2	1	1	0
PS → TS	15	0	6	9
TS*	34	0	0	34
TS → LS	3	1	0	2
TS → PS	2	0	1	1

Table 5.2: Summary of fundamental information for trailing stratiform, leading stratiform, and parallel stratiform classes of linear MCS. Indicated duration is the length of time that MCS criteria were met. Mean duration, speed, and heading were not calculated for unclassifiabe cases.

	TS	LS	PS	unclass.
total # cases (88)	51	17	17	3
# warm sector cases (61)	33	12	14	2
May 1996 warm sector cases (16)	10	4	1	1
May 1997 warm sector cases (45)	23	8	13	1
mean duration (hours)	12.1	6.8	6.4	n/a
mean speed (m s^{-1})	13.0	7.3	10.9	n/a
mean heading (azimuth)	276	294	289	n/a

5.2.1 *Synoptic meteorology attending the linear MCS classes*

The mean 500 hPa flow was fairly zonal for all three MCS classes, with wind maxima generally north of the MCS locations and associated negative vorticity near and south of the convective systems (Fig. 5.10a, 5.11a, 5.12a), a situation rougly corresponding to the longwave 500 hPa ridge associated with 10 MCCs investigated by Maddox (1983). The location of 500 hPa vorticity troughs varied from class to class. LS cases exhibited a mean vorticity trough coincident with the MCS itself, with PVA to its east and NVA to its west. In contrast, both the PS and TS classes exhibited mean vorticity troughs (stronger for the TS cases) to the west of the MCS, which was in a region of 500 hPa PVA. As well, all three MCS classes were, on average, located in the right entrance region of upper tropospheric jet streaks (Fig. 5.10b, 5.11b, 5.12b), a region frequently associated with upper-level divergence and upward motion as described by Uccellini and Johnson (1979). For each MCS class, surface convergence occurred in the MCS region (Fig. 5.13). These broad mean zones of convergence were quasi-linear and extended from southwest to northeast, orientations consistent with the frequently northeast to southwest orientation of the studied MCSs (Fig. 5.14).

5.2.2 *MCS classes' duration and associated conditional instability*

As noted in Table 5.2, a mean TS MCS lasted nearly twice as long as LS and PS MCSs. The airmass into which a TS case propagated was, on average, more unstable than that of either an LS or PS case (Fig. 5.13). The rawinsonde mean fields (Table 5.3) corresponded well to the NCEP reanalysis instability (LI) fields. The MLCAPE, pick CAPE, LCL, CCL, and LI were all consistent with the notion that the TS cases occurred in airmasses with the most instability, while PS cases occurred in airmasses with the least. This, along with relatively constant convergence at the *leading* edge of cold outflow probably explains a great deal of the TS MCSs' long durations (although this is, interestingly, *not* an optimal state as described by RKW88 due to its rearward-canted updrafts). By contrast, the relatively

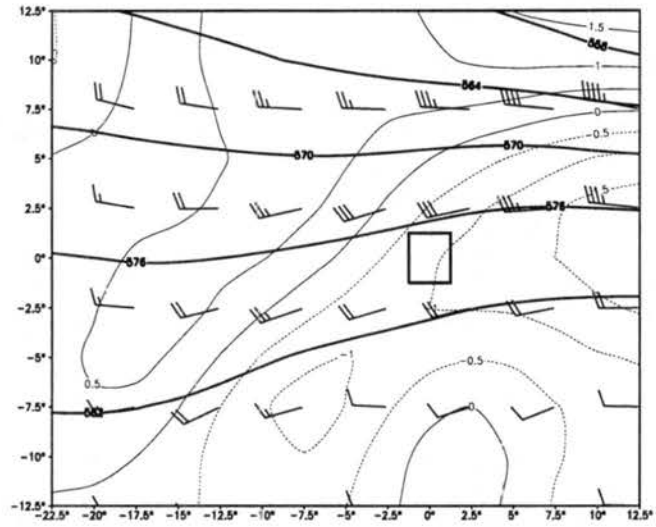

(a)

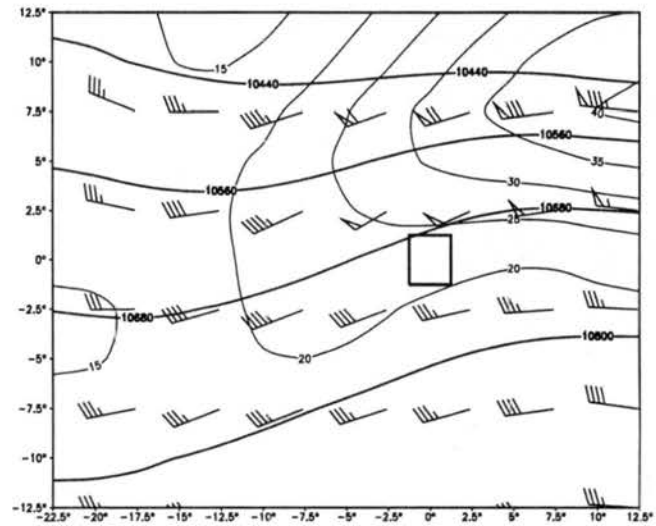

(b)

Figure 5.10: NCEP Reanalysis mean large scale fields for trailing stratiform (TS) archetype. (a) 500 hPa relative vorticity ($\times 10^{-5}$ s^{-1}: thin contours), geopotential height (dam: thick contours), and ground-relative wind barbs. (b) 250 hPa geopotential height (m: thick contours), wind speeds (m s^{-1}: thin contours) and ground-relative wind barbs. barb = 5 m s^{-1}, half barb = 2.5 m s^{-1}. Mean MCS location is denoted by heavy rectangle centered at 0°N, 0°W.

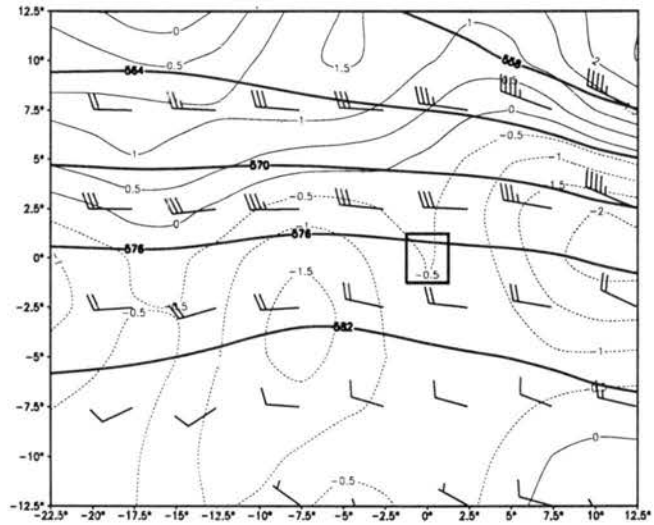

(a)

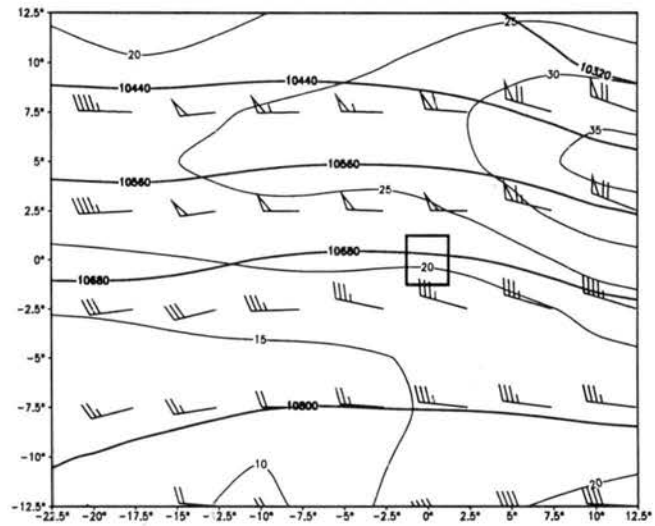

(b)

Figure 5.11: Same as Fig. 5.10 except for leading stratiform (LS) archetype.

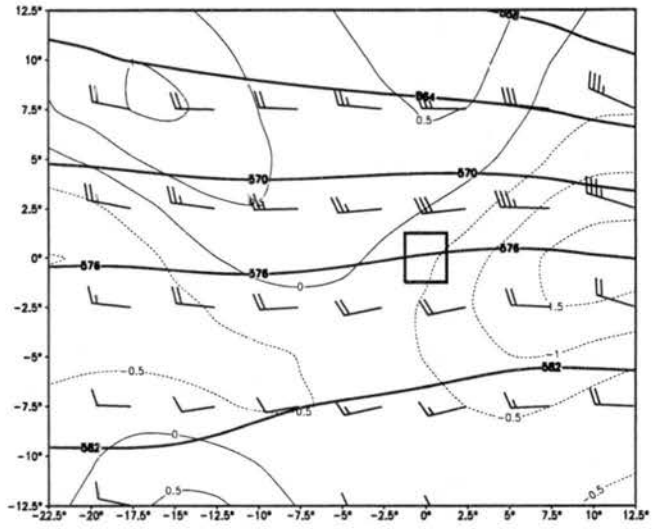

(a)

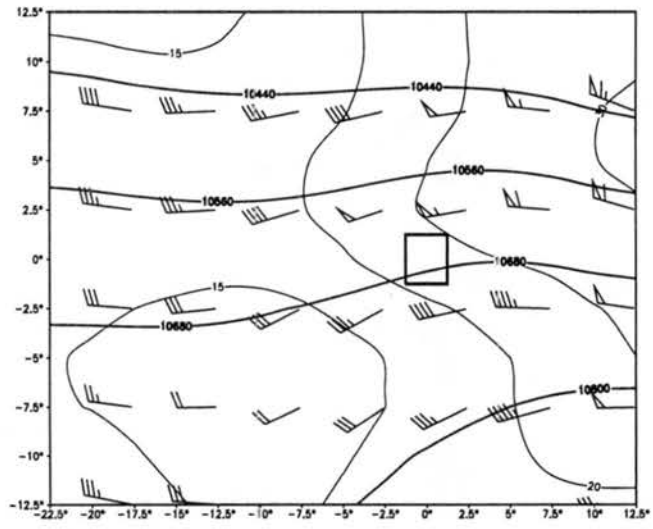

(b)

Figure 5.12: Same as Fig. 5.10 except for parallel stratiform (PS) archetype.

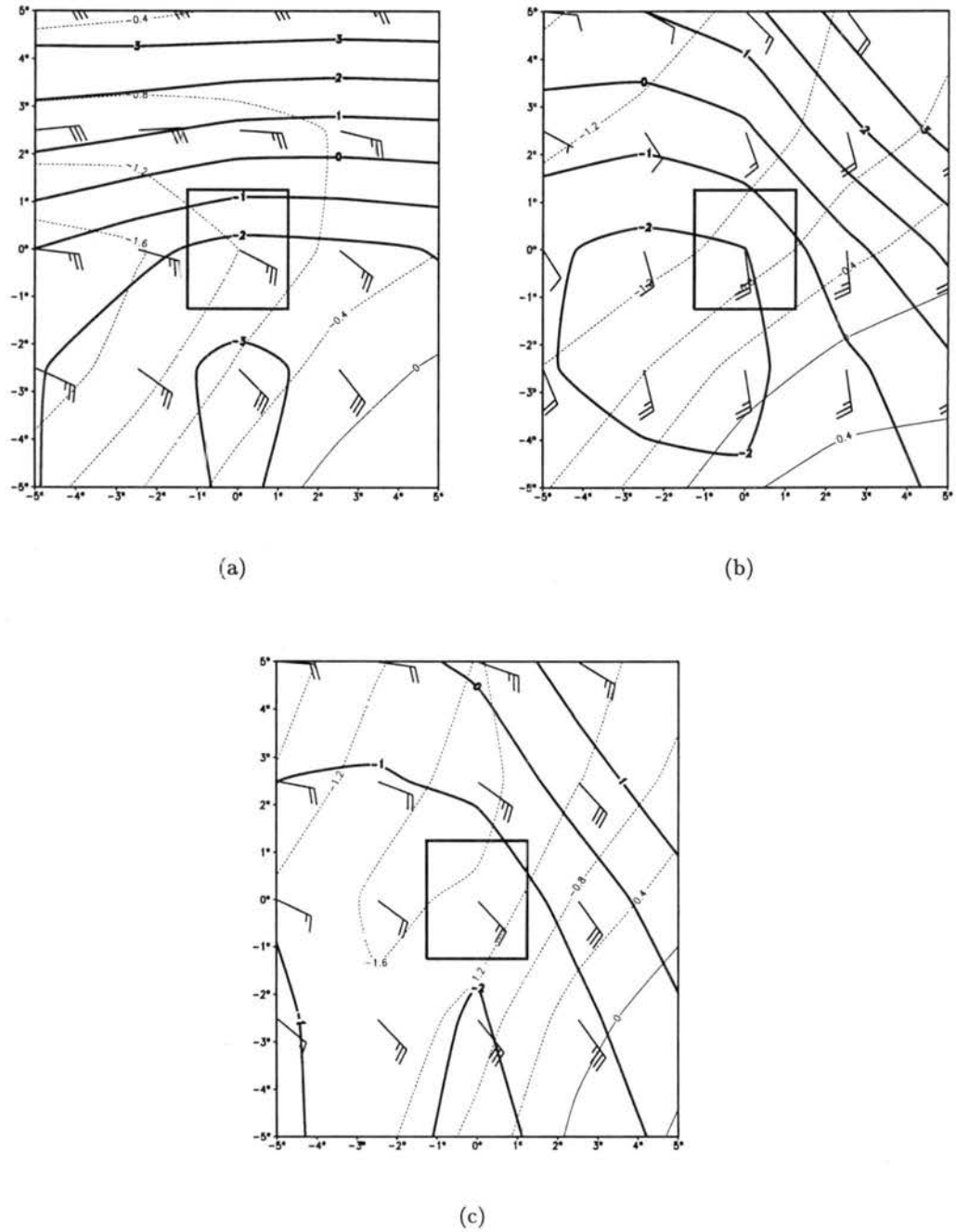

Figure 5.13: NCEP Reanalysis mean fields for (a) TS, (b) LS, and (c) PS classes. Plotted fields are: surface lifted index (K: heavy contours) and horizontal divergence ($\times 10^{-5}$ s^{-1}: light contours), and 925-850 hPa mean wind barbs. barb = 5 m s^{-1}, half barb = 2.5 m s^{-1}. Mean MCS location is denoted by heavy rectangle centered at 0°N, 0°W.

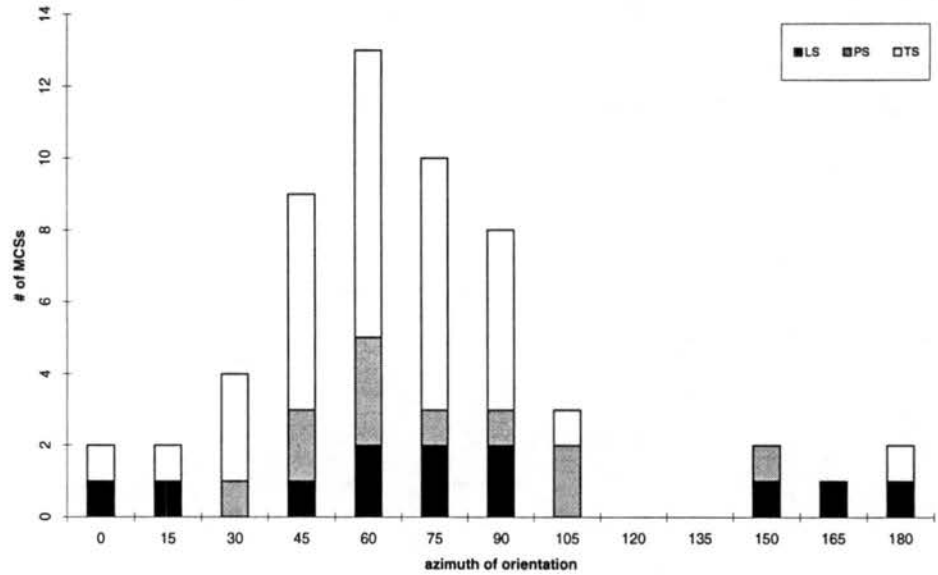

Figure 5.14: Histogram of linear MCS orientation by archetype. Abscissa values represent 15° bins centered at the given value. Orientations for each MCS are lifetime means. Black area: LS cases. Grey area: PS cases. White area: TS cases.

Table 5.3: Summary of relevant *statistically significant* rawinsonde variables. Units: for all vectors— m s^{-1}, for CAPE values— J kg^{-1}, for LCL and CCL— hPa, for all temperatures and LI— K, for RH_d— %, for HWBZ— m, for PW— $\times 2.54$ cm. Only mean values are shown: for additional statistical information, cf. Appendix C.

field	LS	PS	TS
$MLCAPE$	946	715	1554
pick $CAPE$	1366	1011	1821
LCL	806	759	834
CCL	727	685	780
LI	-3.4	-1.8	-5.3
$T_{v_{Tw}}$	292.6	291.5	294.9
$T_{v_{dd}} - T_v$	-0.6	-2.5	-4.8
$T_{v_{dd}} - T_{v_{Tw}}$	5.7	4.1	0.6
$HWBZ$	3210	2692	3131
PW	3.18	2.34	3.35
RH_d	63.4	54.7	67.0
$\overline{\mathbf{V}}_{5-8} : v$	-2.1	0.5	4.3
$\mathbf{V}_{z_{2-7}} : v$	-8.7	-4.4	-1.2
$\log_{10} BRN$	1.24	0.73	1.69

more stable airmasses (Fig. 5.13 b,c) and lack of strong post-line cold pools associated with LS and PS cases may have led to their shorter average durations. The hypothesized cold pool characteristics for the three linear MCS classes are further discussed in Section 5.2.4.

The region of expected stratiform rain was roughly opposite (with respect to the convective line) the region of lowest lifted indices for each MCS class (Fig. 5.13). This is not entirely surprising given the probable evaporative cooling of low-level air by stratiform rain regions. It raises the interesting question, however: from whence does the buoyant air in the LS updraft towers originate? While the most buoyant air existed to the west and southwest of the mean LS MCS, the low-level storm-relative flow suggested that inflow toward LS cases (in the mean) was from the south or south-southeast (Fig. 5.15b). Given their predominant orientation mode between 60° and 90° (cf. Fig. 5.14, discussed later), with a mean east-southeastward storm movement, the NCEP reanalysis mean implies that LS cases received updraft air from trajectories that passed *through* the stratiform rain region. This was not the case for either the PS or TS classes. Perhaps inflow air cooled to

its wet-bulb temperature was still positively buoyant and therefore fueled the LS updraft towers in some MCSs. Another possibility, illustrated by the case study in Section 6.1, is that buoyant air to the rear of the MCS arrived at the convective towers from farther *aloft*.

5.2.3 MCS motion

Merritt and Fritsch (1984) found that most *MCCs* propagated nearly parallel to the 1000–500 hPa thickness contours, which are a proxy for the lower and middle tropospheric temperature field (based upon near-hydrostaticity). As summarized in Table 5.4, the MCSs in this study also propagated nearly along the 1000-500 hPa thickness contours. As noted in Table 5.5, LS MCSs generally moved eastward most slowly ($\mathbf{c}_x = 6.7$ m s^{-1}), while PS and TS cases moved eastward (statistically) significantly more rapidly (10.3 and 12.9 m s^{-1} respectively). The average speed ($\overline{\mathbf{c}}$) of LS cases was only 7.3 m s^{-1}, as compared to 10.9 m s^{-1} for PS and 13.0 m s^{-1} for TS cases. These values imply two possible scenarios: *1)* a mean speed for convective lines, roughly represented by PS cases, may have been accelerated by the presence of a post-line cold pool (TS case) or retarded by the presence of a pre-line cold pool (LS case). Notably, however, the mean line-parallel and line-perpendicular motion components ($\overline{\mathbf{c}_{\parallel}}$ and $\overline{\mathbf{c}_{\perp}}$) for the PS class were very small (Table 5.5) with large standard deviations (cf. Table C.3 in Appendix C), suggesting a variability of sign not present for the LS and TS classes. Or, *2)* the distribution of stratiform rain may have resulted from line motion: given some mean middle and upper tropospheric flow, slower moving lines had a greater component of hydrometeors advected downwind than did faster moving cases. The former idea will be further discussed in the following section, while the latter will be taken up in Section 5.2.5.

5.2.4 Hypothesized MCS cold pools based upon rawinsonde data

As no direct measurements of cold pool depth and strength were available beyond surface temperature observations, the idealized cold pool calculations presented in Sec-

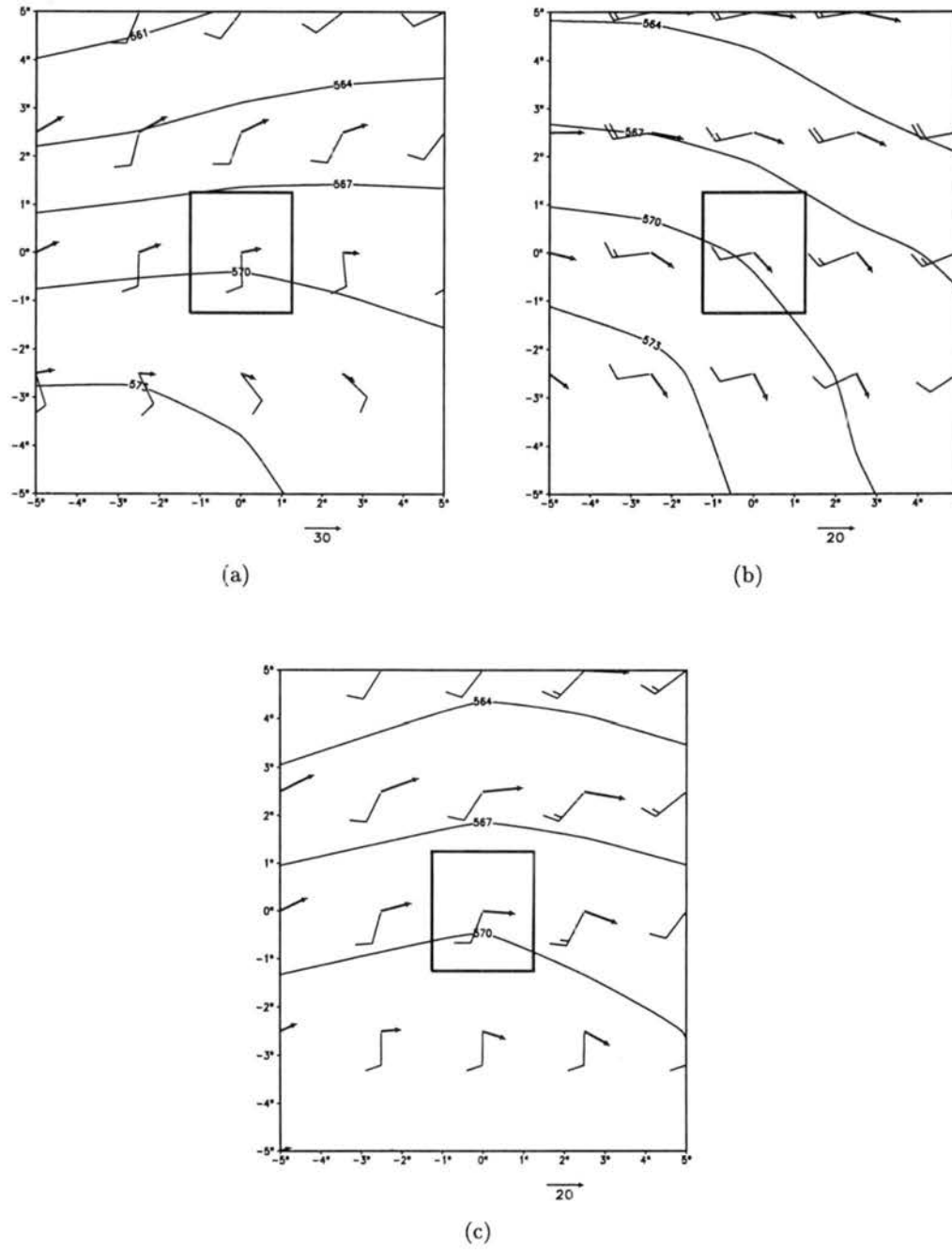

Figure 5.15: NCEP Reanalysis mean fields for (a) TS, (b) LS, and (c) PS classes. Plotted fields are: 1000 – 500 hPa thickness (m: contours), 500 hPa storm-relative wind barbs, and 700-300 hPa wind shear vectors (m s^{-1}). barb = 5 m s^{-1}, half barb = 2.5 m s^{-1}. Mean MCS location is denoted by heavy rectangle centered at 0°N, 0°W.

Table 5.4: LS, PS, and TS class average azimuth headings for vectors of interest: observed MCS motion and orientation of (a tangent to) 1000-500 hPa thickness contours.

archetype	**c**	$\perp$ *to* $\nabla(z_{500} - z_{1000})$
LS	114°	125°
PS	109°	96°
TS	96°	91°

Table 5.5: Summary of relevant *statistically significant* wind profiler variables. Units: for all vectors— m s^{-1}. Only mean values are shown: for additional statistical information, cf. Appendix C.

field	LS	PS	TS	field	LS	PS	TS
$\overline{\mathbf{V}}_{0-6} : v$	2.3	3.2	5.2	$\mathbf{c} : u$	6.7	10.3	12.9
$\overline{\mathbf{V}}_{3-10} : u$	11.2	15.7	12.8	$\mathbf{c} : line \parallel$	3.0	0.3	8.9
$\overline{\mathbf{V}}_{3-10} : v$	-1.8	0.3	3.2	$\mathbf{c} : line \perp$	6.0	3.9	8.6
$\overline{\mathbf{V}}_{5-8} : u$	11.3	16.1	12.2	$\overline{\mathbf{V}}_{0-1} - \mathbf{c} : line \parallel$	4.8	0.7	-2.1
$\overline{\mathbf{V}}_{5-8} : v$	-1.9	0.4	3.0	$\overline{\mathbf{V}}_{0-6} - \mathbf{c} : u$	0.8	-0.7	-4.0
$\overline{\mathbf{V}}_{9-10} : u$	14.2	20.0	17.0	$\overline{\mathbf{V}}_{0-6} - \mathbf{c} : line \parallel$	3.5	4.9	0.3
$\overline{\mathbf{V}}_{9-10} : v$	-3.4	-1.1	2.6	$\overline{\mathbf{V}}_{0-6} - \mathbf{c} : line \perp$	-3.4	-6.1	-7.7
$\mathbf{V}_{z_{0-3}} : u$	5.2	11.0	9.3	$\overline{\mathbf{V}}_{3-10} - \mathbf{c} : u$	4.5	5.0	-0.4
$\mathbf{V}_{z_{0-3}} : v$	-3.6	-3.1	1.8	$\overline{\mathbf{V}}_{3-10} - \mathbf{c} : line \perp$	1.5	0.2	-4.7
$\mathbf{V}_{z_{2-7}} : u$	4.0	9.4	5.3	$\overline{\mathbf{V}}_{5-8} - \mathbf{c} : u$	4.6	5.6	-1.0
$\mathbf{V}_{z_{0-10}} : u$	13.2	20.5	16.9	$\overline{\mathbf{V}}_{5-8} - \mathbf{c} : line \perp$	1.1	0.2	-4.9
$\mathbf{V}_{z_{0-10}} : v$	-7.2	-6.3	-1.1	$\overline{\mathbf{V}}_{9-10} - \mathbf{c} : u$	8.3	9.4	3.0
				$\overline{\mathbf{V}}_{9-10} - \mathbf{c} : line \perp$	4.9	4.1	-1.2

tion 3.5 are utilized for this discussion. These parameters were derived from pre-MCS rawinsonde data, making them viable forecast tools. The two *statistically significant* cold pool calculations were for a downdraft descending adiabatically below cloud base ($T_{v_{dd}}$) compared to both the surface T_v and the surface $T_{v_{Tw}}$ (i.e. $T_{v_{dd}} - T_v$ and $T_{v_{dd}} - T_{v_{Tw}}$). For both scenarios, it was clear (Table 5.3) that the mean TS environment could produce the strongest surface cold pool temperature perturbation. As given by Eq. 3.6, stronger temperature perturbations are associated with faster moving density currents. The TS mean case had higher PW and a lower LCL and CCL than did the other two classes (Table 5.3), implying a greater possible precipitation load and a lower cloud base. This might also have enhanced cold pool strength by both increasing the integrated cloud in an atmospheric column (more hydrometeors available for evaporation and melting) and decreasing the distance of adiabatic descent for downdraft parcels (the longer a downdraft parcel undergoes pseudo-adiabatic descent the lower its final temperature at the surface). Finally, the $T_{v_{Tw}}$ for TS cases was on average higher than for either the LS or PS cases. Therefore, should the mean surface airmasses be evaporatively cooled, a surface cold pool would represent a larger temperature perturbation for TS cases than for LS or PS cases (all other factors being equal). In addition, the mean PS environment, based upon $T_{v_{dd}} - T_v$ and $T_{v_{dd}} - T_{v_{Tw}}$, would apparently support stronger surface cold pool temperature perturbations than the LS mean environment (Table 5.3). Thus, should the linear MCSs in this study have moved *solely* as density currents, the relative ordering of classes' mean translational speeds (i.e. TS > PS > LS) would probably have been consistent with that observed.

5.2.5 Wind fields and their relationship to stratiform rain distribution

All three archetypes appeared to be most frequently oriented northeast–southwest, or roughly along 60° azimuth (Fig. 5.14), a result similar to that found by Geerts (1998) for southeastern United States MCSs. The TS class had the strongest northeast–southwest mode. This is attributed to TS MCSs' frequent relationship to synoptic cold fronts in this

study (not shown), which typically had a more consistent azimuthal orientation than did warm or stationary fronts and other linear boundaries. Based upon the predominant MCS orientation in this study, a v-wind represented flow largely perpendicular to most convective lines while a u-wind represented flow largely parallel to a mean convective line.

From the statistically significant wind profiler variables (Table 5.5), it is clear that the PS cases had, on average, the strongest u-wind component (3–10, 5–8, and 9–10 km), consistent with strong line-parallel advection of hydrometeors. As the v-wind was mainly perpendicular to the prominent linear MCS orientation mode, it was expected that differences would exist between LS and TS cases. Indeed, the mean v-wind (positive for front-to-rear flow) for TS cases was the strongest (for wind profiler layers 0–6, 3–10, 5–8, and 9–10 km as well as raob layer 5–8 km), implying the greatest rearward advective component, while that for the LS class was weakest. This discussion will be furthered below using *computed* line-parallel and line-perpendicular components of the storm-relative flow.

The vertical mixing of horizontal momentum was found to be an important feature of the midlatitude MCS studied by Gallus and Johnson (1992). Additionally, Smull and Augustine (1993) documented the relationship of hydrometeor distribution to momentum transports for a mid-latitude MCC. Therefore, it is worthwhile to consider the possible effects of vertically transported horizontal momentum upon the precipitation structures observed in this study. The magnitudes of the *storm-relative* low-level winds near the MCSs (as depicted by the 925-850 hPa NCEP reanalyses, Fig. 5.15) were relatively constant among archetypes. Notably, however, the wind vectors (which approximate an inflow layer) were increasingly backed from the LS to PS to TS archetypes. As a result, the TS MCSs (in the mean) mixed more easterly (storm-relative) momentum upward from the inflow layer than did LS or PS MCSs. Therefore, assuming no storm-relative wind in the middle and upper troposphere, it is consistent to expect hydrometeors to have moved west of the mean TS case, with increasingly northward parcel trajectories for PS and LS cases. However, the middle and upper-troposphere are not always at rest with respect to an MCS. The

magnitudes of the 500 hPa storm-relative winds (Fig. 5.15) were also relatively constant, with the vectors backing from LS to PS to TS. If the updraft parcels mixed no momentum upward, we might expect the distribution of stratiform rain to have been governed largely by advection due to the mean storm-relative flow aloft. Were this the case, it would be consistent for hydrometeors to have moved east of LS cases, and increasingly toward the north for the PS and TS archetypes.

Neither of the above simplified models is very likely in the atmosphere; upper tropospheric advection, mixing of momentum, and production of horizontal momentum by storm-generated pressure fields (LeMone 1988) are normally ongoing for convective clouds. As a first approximation, consider the mean movement of a parcel, entraining realistically from the low-level, inflow once it arrives at 500 hPa. In order to treat this situation ideally, storm-relative winds between the 925–850 hPa mean and 500 hPa were interpolated linearly at 1000 m intervals. Using an empirical equation for parcel entrainment from Bretherton (1997):

$$\lambda \equiv M^{-1}\frac{dM}{dz} = \frac{0.2}{R}, \tag{5.1}$$

wherein M is the mass of an entraining parcel, z is geopotential height, and R is the radius of an updraft parcel, and using $R = 2\ km$, an entrainment rate of $(10\ \text{km})^{-1}$ was obtained, a value appropriate for cumulonimbi according to Bretherton. The parcel's u and v-momentum were then computed at each 1000 m interval up to z(500 hPa) using the simple expression:

$$\mathbf{p}_{par}(z) = (1 - \lambda^*) \cdot \mathbf{p}_{par}(z - \Delta z) + \lambda^* \cdot \mathbf{p}_{env}(z), \tag{5.2}$$

wherein $\mathbf{p}$ is horizontal momentum, Δz is the evaluation interval (here 1000 m), λ^* is $\lambda \cdot \Delta z$, and all other terms are defined in Eq. 5.1. The net result was added to the horizontal storm-relative momentum of the environmental flow at 500 hPa. The resultant horizontal momentum, divided by mass, yielded an idealized movement vector for the MCS hydrometeors at 500 hPa, a level of interest near which Rutledge and Houze (1987) and Gallus and Johnson (1995) found the bulk transport of MCS hydrometeors to be focussed. It is

Table 5.6: Storm-relative velocity at 500 hPa for an entraining parcel from the low-levels, expressed as both the parcel's velocity and the sum of the parcel velocity and the 500 hPa storm-relative winds. All velocity units are m s^{-1}. Azimuth headings indicate direction from which parcel and storm relative winds blow.

MCS	parcel			net		
type	u	v	azimuth	u	v	azimuth
LS	-2.2	18.3	163°	7.7	20.0	201°
PS	-12.1	15.5	142°	-8.7	24.9	161°
TS	-16.7	10.4	122°	-16.7	20.4	141°

known that organized convection creates pressure fields that generate momentum (LeMone 1988), so that this idealized argument will not hold for mature MCSs. Nevertheless, this computation is believed to characterize the general movement of hydrometeors *early* in the lifetime of an MCS, *before* horizontally extensive circulations have been generated by the convection itself. The results of this calculation are summarized in Table 5.6. The idealized hydrometeor motion vector suggests a more eastward distribution for LS cases than PS and TS cases, with the greatest westward displacements for TS cases, a finding that is consistent with basic expectations for the archetypes, given what was observed from radar imagery.

Notably, the derived hydrometeor motion vectors were not 180° out of phase for the TS and LS cases (Table 5.6). This may be due, in part, to differences in orientation. As previously noted, however, the primary mode of orientation for the studied cases was nearly uniform. Therefore, some additional argument must be invoked to fully explain the displacement of stratiform rain perpendicular and/or parallel to a convective line. The additional line-normal component for TS and LS MCSs may be related to flow perturbations caused by strengthening cold pool circulations. Should hydrometeors depart an initial line of convection predominantly rearward (based upon the computed hydrometeor motion vectors above), most precipitation would presumably fall *behind* the deep convective cells. Once a pool of cold surface air begins to develop from evaporation and sublimation of falling hydrometeors, the solenoidal overturning at its edge may begin to reinforce the sense of updraft canting, rendering a *circulation* favorable for rearward distribution of hydrometeors.

This simple evolutionary model is similar to that described by RKW88. As well, the above cold pool process is consistent with the development of TS rain due to growth and decay of convective cells found by Fovell and Dailey (1995).

It is also illuminating to consider the storm-relative winds in line-parallel and line-perpendicular components (rather than to speculate based upon a mode in the orientation histogram), such as are illustrated in Fig. 5.16. The TS cases' line-perpendicular components, as anticipated, were significantly different from those of the LS and PS classes. The TS class mean exhibited negative line-perpendicular storm-relative winds in the 0–6, 3–10, 5–8, and 9–10 km layers, significantly lower values than those observed for the LS and PS classes. This is consistent with rearward advection of hydrometeors by the mean flow. In contrast, the LS and PS classes were nearly indistinguishable from one another in most of the line-perpendicular fields. The notable exception was the 0–6 km layer, in which the magnitude of line-perpendicular flow for the PS cases was, on average, almost twice that of the LS cases and nearly equal to that of the TS cases. At first, this appears to be inconsistent with the model presented above. The strength of the 0–6 km rearward flow for the PS mean is probably an artifact of strong lower tropospheric inflow perpendicular to the convective line, a feature captured by the 0–1 km mean (Fig. 5.16). As the case study in Section 6.2 will demostrate, the lower tropospheric line-perpendicular winds near PS cases may be quite strong but *shallow*, with flow nearly parallel to the convective line through the remainder of the troposphere. Indeed, farther aloft the mean line-perpendicular 3–10 km and 5–8 km storm-relative flows ($\overline{\mathbf{V}}_{3-10} - \mathbf{c}$: *line* $\perp$ and $\overline{\mathbf{V}}_{5-8} - \mathbf{c}$: *line* $\perp$) for PS cases were nearly zero (Table 5.5). As well, the only statistically significant variable to capture the strong line-*parallel* flow in PS cases was the 0–6 km mean wind ($\overline{\mathbf{V}}_{0-6} - \mathbf{c}$: *line* $\parallel$ in Table 5.5; the signal was also present in the 3–10, 5–8, and 9–10 km winds, but was not statistically significant at the 5% level). In conjunction with the case study, this lends credence to the hypothesis that PS MCSs have a very deep layer of line-parallel storm-relative flow, with strong line-perpendicular inflow confined to the lowest levels. In such a case, the

middle tropospheric advection of hydrometeors would probably still be largely along the line. The line-perpendicular storm-relative winds attending LS cases were not remarkably distinct from those in PS cases, although the line-parallel winds were much weaker. It may be that for the depicted line-perpendicular storm-relative wind field, the line-parallel component is the determining factor between LS and PS organization. The upper-tropospheric shear for LS cases was not dramatically different from that observed in PS and TS MCSs, suggesting that the hypothesis of Grady and Verlinde (1997) may not universally explain pre-line rain. As well, the lack of statistical significance in most of the parameters used to predict supercellular convection suggests that the quasi-supercellular characteristics observed by Fankhauser et al. (1992) are not applicable to many LS cases. Finally, the case study in Section 6.1 was apparently maintained by lower tropospheric inflow of buoyant air into the rear of the convective line. This scenario is not, however, depicted in the mean vertical profiles, and may therefore also be somewhat anomalous.

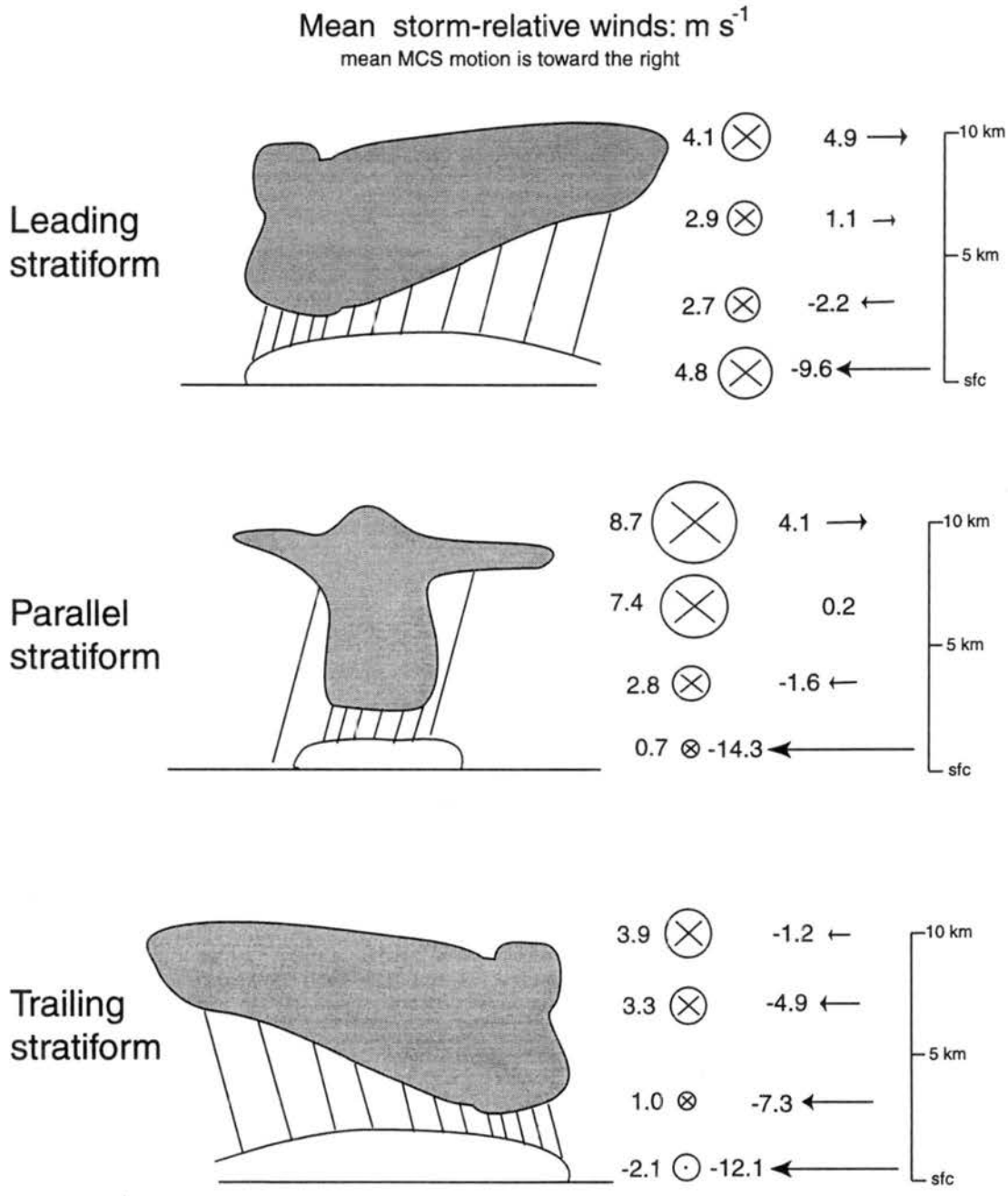

Figure 5.16: Vertical profiles of layer-mean *storm-relative* winds for linear MCS classes. Wind vectors depicted as line-parallel and line-perpendicular components in m s^{-1}. Layers depicted are 0–1 km, 2–4 km, 5–8 km, and 9–10 km.

Chapter 6

MCS CASE STUDIES

To better illustrate the distinctions made in Chapter 5, as well as to further document the genesis and evolution of the relatively less studied MCS classes of LS and PS, two case studies are presented here. By using actual sounding and wind profiler data, these case studies provide more insight into the less-well-documented LS and PS archetypes than afforded by NCEP reanalysis mean fields. These cases were chosen for study based upon *1)* their similarity to the reflectivity archetypes presented earlier, *2)* the availability of data near the MCSs, and *3)* their inclusion among the warm-sector MCSs in this study (i.e. they were not elevated or otherwise omitted based on the criteria in Chapter 3). While the vertical structure of and three-dimensional wind fields within the MCSs are not presented, their synoptic, meso-α, and meso-β scale environments are described to the degree enabled by NCEP reanalyses, NWS surface observations and rawinsondes, and NOAA wind profilers. In addition, the evolution of the reflectivity field is described. Finally, the similarities and inconsistencies of each case with the archetypes and general conditions presented in Chapter 5 are discussed.

6.1 May 18 1997: Leading stratiform

During the morning hours of 18 May 1997, a strong LS MCS travelled eastward along the Iowa/Missouri border (Fig. 6.1). Throughout its lifetime of approximately 7 hours, the MCS exhibited rapid east-northeastward motion (at 8–14 m s^{-1}), while producing a region of stratiform rain entirely forward of its convective line. It will be shown that the presence of

strong winds and a lobe of high θ_e in the lower troposphere, interacting with a surface cold pool, contributed to the genesis and maintenance of the MCS. Its leading stratiform rain may have resulted not only from the strong, adiabatically ascending low-level winds, but also from the slantwise motions induced by a density-driven solenoid *west* of a pre-existent cold pool.

6.1.1 Synoptic environment and initiation

At 0000 UTC, near the time of convective initiation, a broad longwave ridge in the 250 hPa geopotential height field was positioned over the central United States (Fig. 6.2a). The upper tropospheric flow over the upper Mississippi and Missouri Valleys was west-northwesterly, with jet streaks ≥ 40 m s^{-1} situated over North Dakota and Michigan. The incipient 18 May MCS was located in a region of anticyclonic curvature, roughly within the right entrance region of the eastern 250 hPa jet streak. The middle tropospheric height field was similarly ridged over the central United States. At 0000 UTC, negative relative vorticity prevailed over most of the central U.S. at 500 hPa (Fig. 6.2b). A region of strong cyclonic vorticity advection existed over and northwest of North Dakota, associated with a surface low pressure center (Fig. 6.3).

Further, at 0000 UTC on 18 May 1997, a surface pressure trough lay across the Great Plains, from the North Dakota surface cyclone roughly toward central New Mexico (Fig. 6.3). While cloudiness prevailed to the west of the surface trough, the warm sector to its east was clear with the exception of an MCS over eastern Kansas, which was located approximately 200 km east of the trough axis (Fig. 6.4). A warm front extended from the surface low pressure center through southern Minnesota, beyond which a stationary front lay east–west across the Great Lakes region (roughly from Iowa to Pennsylvania). To the north of the warm/stationary frontal boundary were clear skies with the exception of a narrow cloud band over northeast Missouri and central Illinois that roughly delineated the synoptic frontal position as well as a meso-α scale surface pressure trough associated with a weak low

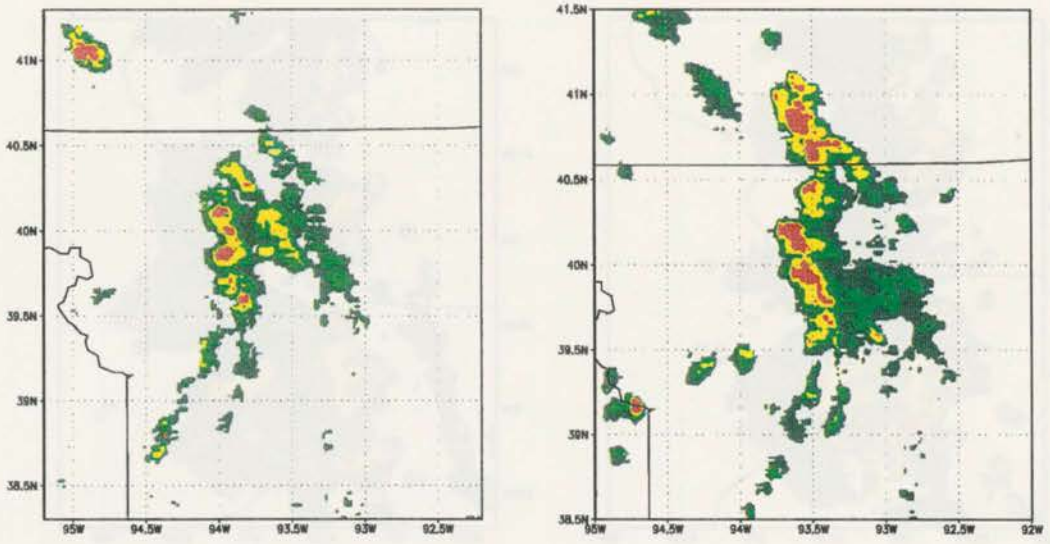

(a) 0800 UTC

(b) 0900 UTC

(c) 1000 UTC

(d) 1100 UTC

Figure 6.1: Hourly 2 km radar reflectivity composite images for 18 May 1997 LS MCS.

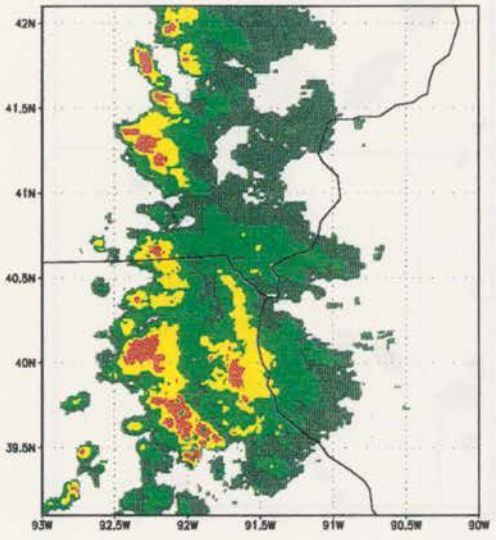

(e) 1200 UTC

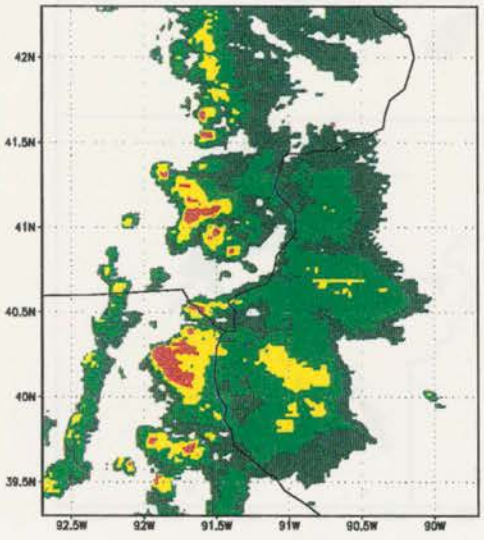

(f) 1300 UTC

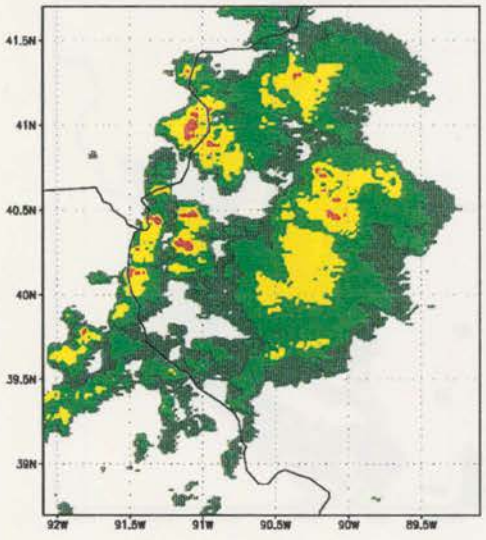

(g) 1400 UTC

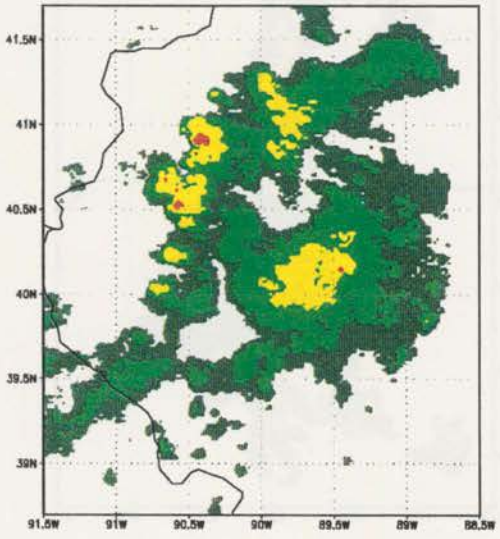

(h) 1500 UTC

Figure 6.1: *Continued*

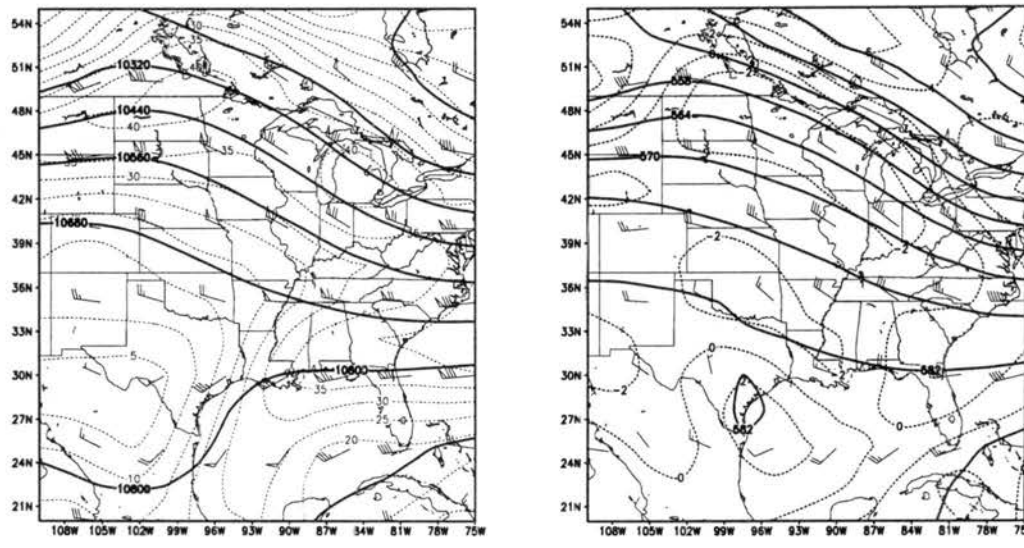

(a) (b)

Figure 6.2: NCEP reanalysis data for 0000 UTC on 18 May 1997: (a) 250 hPa geopotential heights (m: heavy contours), wind speeds (m s^{-1}: light dashed contours), and wind barbs. (b) 500 hPa geopotential heights (dam: heavy contours), relative vorticity (10^{-5} s^{-1}: light contours), and wind barbs. flag = 25 m s^{-1}, barb = 5 m s^{-1}, half barb = 2.5 m s^{-1}. Position of incipient MCS is approximately 40°N 94°W.

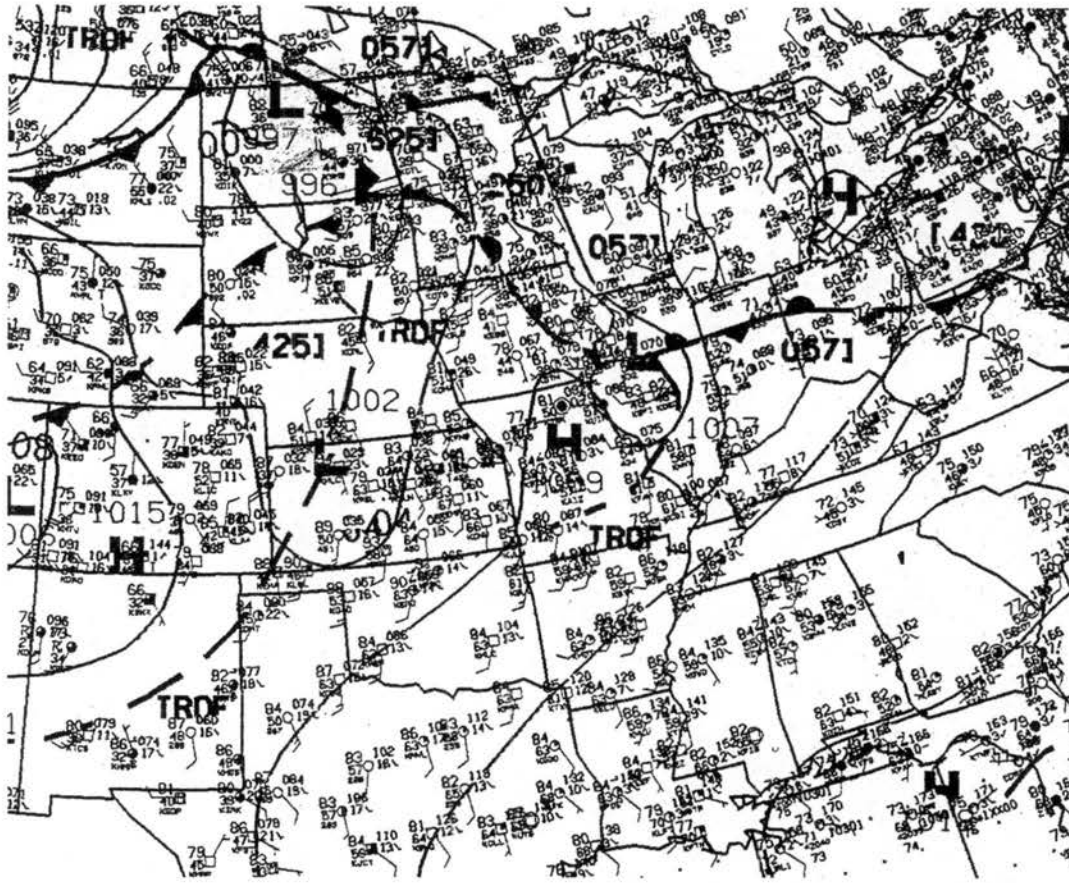

Figure 6.3: NCEP surface analysis for 0000 UTC on 18 May 1997: temperatures and dew-point temperatures in °F, pressures in hPa (contoured), and wind barbs. barb = 5 m s^{-1}, half barb = 2.5 m s^{-1}. Fronts, pressure troughs and extrema, and outflow boundaries analyzed by NCEP.

in western Illinois. The main surface cyclone was beginning to move east-southeastward in the region of middle and upper tropospheric PVA over the northern Plains.

At 850 hPa, an axis of warm, dry air extended from the Texas Panhandle to central Nebraska at 0000 UTC (Fig. 6.5). Its location was well-delineated by a chain of stations (MAF, AMA, DDC, and LBF: cf. Fig. 3.1 for positions) reporting temperatures *and* dewpoint *depressions* ($T-T_d$) ≥ 20 ° C. An axis of potentially warm air aloft implies hydrostatically lower surface pressures, which may in part explain the existence of the aforementioned surface trough (and its colocation with the axis of the High Plains cloud field). As well, the band of warm dry air was colocated with an instensifying lower tropospheric southerly jet. This juxtaposition of surface and lower tropospheric flows is similar to that depicted by Hobbs et al. (1996) for *drytroughs*, although the *surface* moisture gradient on 18 May 1997 was not particularly intense. Interestingly, the location of the 17 May and 18 May MCSs roughly corresponds with the probable placement of the "pre-drytrough rainband" discussed by Hobbs et al. (1996). The location and orientation of the lower tropospheric jet were consistent with the 850 hPa geopotential height gradient over the Plains: the strong southerly flow over western Texas, Oklahoma, and Kansas gave way to nearly 20 m s^{-1} west-southwesterly winds over western Nebraska (nearer the 850 hPa closed low). In advance of the 850 hPa dryline/drytrough, over east-central Kansas at 0000 UTC, was an axis of relatively moister air with higher θ_e (Fig. 6.6).

As the pre-existent 17 May Kansas MCS moved eastward and decayed between 0300 and 0600 UTC, an outflow boundary demarking evaporatively-cooled air became evident over Missouri (Fig. 6.7). Due to radiative cooling of the surface beneath clear skies, the temperature gradient was relatively weak north, south, and east of the diminishing MCS. However, to its west strong southerly winds ahead of the surface pressure trough were advecting relatively warmer air northward into central Kansas (note the axis of temperatures $\geq 70°$ F, or 21° C, extending from central Texas into eastern Nebraska in Fig. 6.7). Therefore, even though NCEP did not extend the outflow boundary to the west of the 17 May

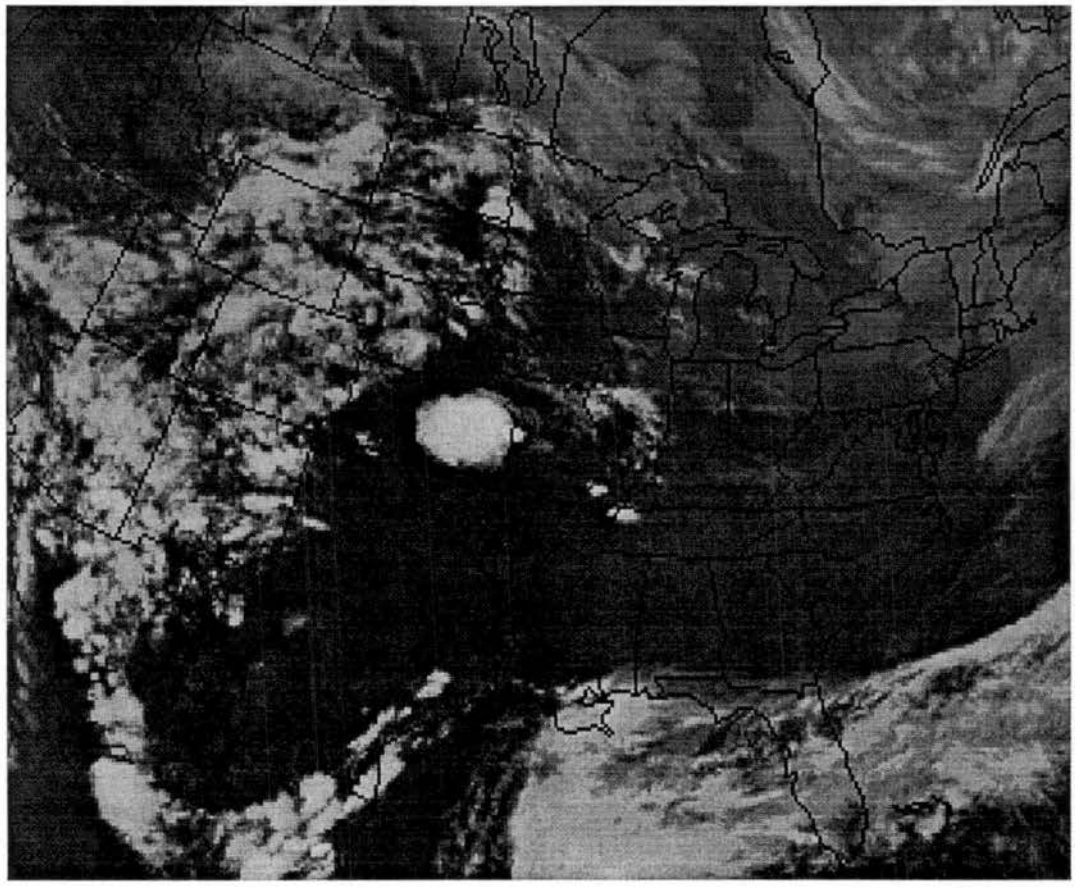

Figure 6.4: Infrared satellite image of the United States for 0000 UTC on 18 May 1997.

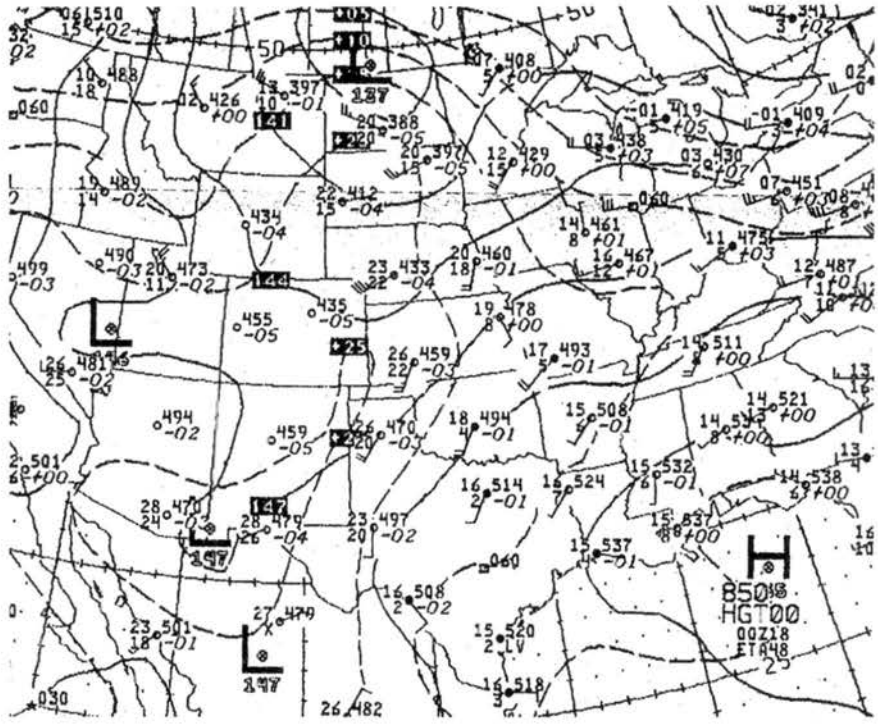

Figure 6.5: NCEP 850 hPa analysis chart for 0000 UTC on 18 May 1997: geopotential heights (dam: solid contours), temperatures (°C: dashed contours), dewpoint *depressions* (°C, not contoured), and wind barbs. barb = 5 m s^{-1}, half barb = 2.5 m s^{-1}.

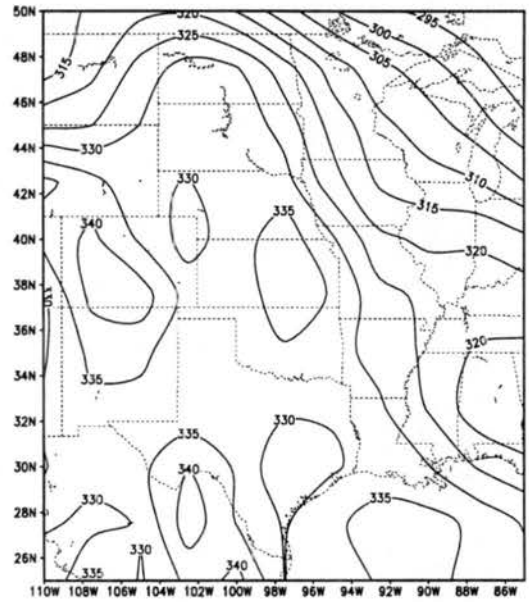

Figure 6.6: NCEP Reanalysis for 0000 UTC on 18 May 1997: 850 hPa equivalent potential temperature (K). Note that the 850 hPa surface is underground along the Rocky Mountain chain (maximum over New Mexico and Colorado is suspect).

MCS, a significant temperature gradient existed between the surface air processed by the earlier deep convection over Missouri and that transported northward over central and eastern Kansas. Indeed, while SZL (Whiteman A.F.B., Missouri) reported a temperature of 66° F (19° C) during a thunderstorm at 0600 UTC, MCI (Kansas City, Missouri) reported 73° F (23° C) and MHK (Manhatten, Kansas) reported 77° F (25° C), demonstrating the degree to which the surface airmass had recovered due to the southerly flow west of the passing MCS.

By the time that early convection (associated with the 18 May 1997 MCS) developed, the pocket of enhanced θ_e had moved northeast and, according to the NCEP reanalysis data, was colocated with the pre-existent surface outflow boundary at 0600 UTC (Fig. 6.8). At that time, the wind profiler at LTH had begun to exhibit the presence of the lower tropospheric wind maximum very near the surface (Fig. 6.9); constant-height regional wind profiler data suggested that the southerly jet was located over east-central Kansas (Fig. 6.10). The movement of the 850 hPa height minimum toward the upper Mississippi Valley gradually created a south-southeastward height gradient across the central Plains, in response to which the lower tropospheric winds became increasingly westerly. The low-level jet was well-established at LTH by 0900 UTC (Fig. 6.9). The increasing eastward component of the lower tropospheric winds probably accounted for a large part of the θ_e-pocket's northeastward displacement, and therefore its superposition with the surface outflow boundary.

The first convective echoes associated with the 18 May 1997 MCS were observed over northwestern Missouri at 0700 UTC (not shown). The MCS's initial and subsequent orientation was nearly north–south, perpendicular to the temperature gradient (near the Kansas/Missouri border) set up between previous thunderstorm outflow and differentially advected warm air to its west. The associated density gradient implied a solenoidal circulation with its ascending branch in the warmer, more buoyant surface air due west of the outflow air. Such mesoscale ascent along the *rear* edge of an outflow boundary is a bit

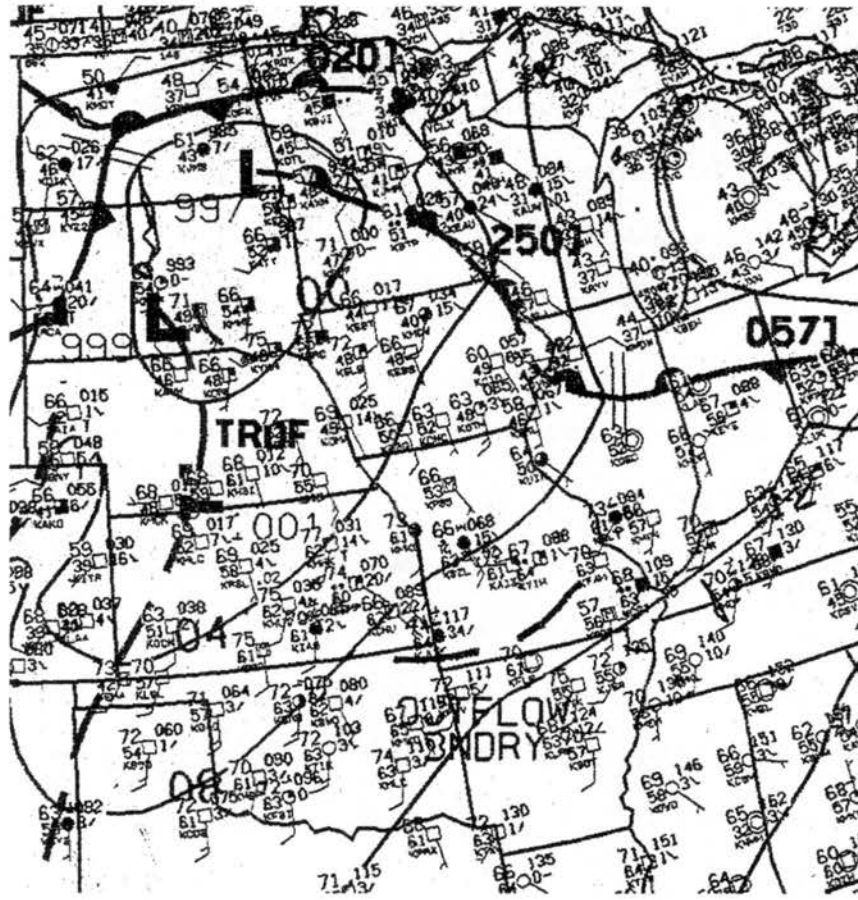

Figure 6.7: Same as Fig. 6.3 but for 0600 UTC on 18 May 1997.

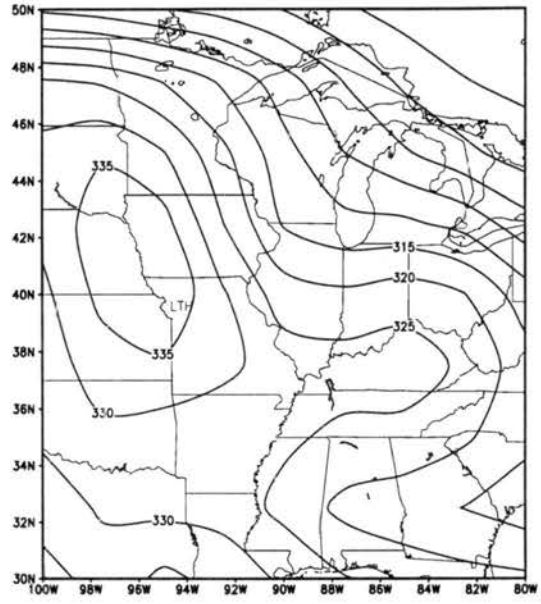

Figure 6.8: Same as Fig. 6.6 but for 0600 UTC on 18 May 1997.

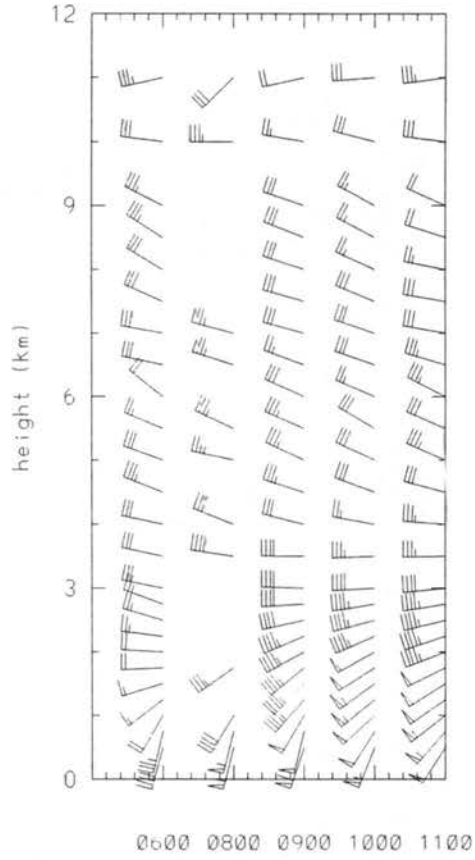

Figure 6.9: Time series of hourly wind profiles from Lathrop, Missouri (LTH) on 18 May 1997. All times are UTC. Altitudes are above ground level: station elevation is 297 m MSL. Missing barbs indicate data failing quality control checks. At 0700 UTC, all data failed quality control. flag = 25 m s^{-1}, barb = 5 m s^{-1}, half barb = 2.5 m s^{-1}.

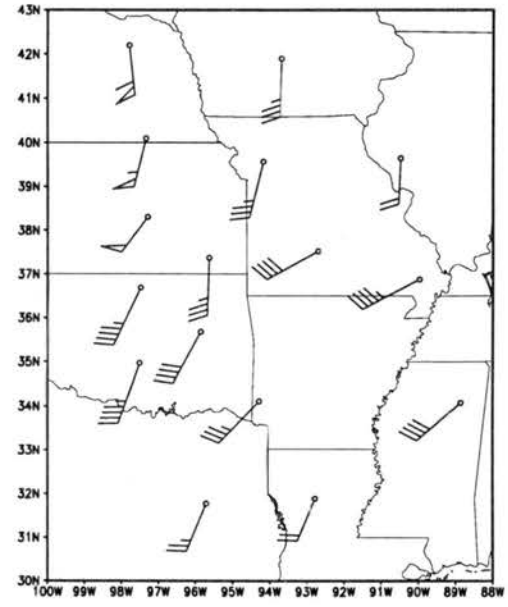

Figure 6.10: Regional plot of NOAA profiler network winds at 1250 m MSL at 0600 UTC on 18 May 1997. flag = 25 m s^{-1}, barb = 5 m s^{-1}, half barb = 2.5 m s^{-1}.

anomalous; in typical regimes the *leading* edge of a cold pool triggers new convection (as *it* is encountering buoyant air unmodified by deep convection). A mechanism similar to that described here, with ascent along an MCS's rear flank, was suggested in a potential vorticity framework by Fritsch et al. (1994).

As it passed by, the lobe of enhanced buoyancy at 850 hPa (Fig. 6.8) may have provided fuel for convective towers *aloft* when it encountered the ascending branch of the above solenoid. In such a case, the stable, cooled surface air due east of the circulation would not have severely inhibited the developing MCS. By 0800 UTC, the line of convective cells met the 100-km length criterion for MCSs in this study (Fig. 6.1a). Even at this earliest stage, the stratiform rainfall was observed to extend eastward of the convective line, whose motion was consistently toward the east-southeast. It is believed that the enhanced buoyancy of the high θ_e air and lower tropospheric convergence associated with the low-level jet nosing eastward (and probably adiabatically ascending the surface cold dome) combined with the outflow boundary's solenoidal circulation to provide deep and widespread lifting, which further organized and extended the convective line.

6.1.2 Evolution and maintenance of the MCS

What was initially a line of 5 convective cores with a small plume of pre-line rain lengthened and "filled in" between 0800 and 1000 UTC (Fig. 6.1 a–c). The development and organization of the line was probably via backbuilding, as defined by BJ85. The convective cells (evident by their reflectivity factors $\geq$ 50 dBZ) elongated toward the east, perhaps indicating an eastward (storm-relative) movement of decaying precipitation cores. Meanwhile, the leading stratiform rain region continued to extend farther to the east of the convective line, preceding its entire north–south extent. A weak line of echoes extended southwest from the southern end of the line (at about 39.0°N, 93.7°W in Fig. 6.1b), which may have been related to a meso-β scale outflow boundary generated by the thunderstorm reported at 0600 UTC over SZL (mentioned previously).

By 1100 UTC, the MCS had taken on the distinct appearance of a *reversed* TS MCS (Fig. 6.1d), as described in Section 5.1.2. Along the entire extent of the line, the region of stratiform rain was separated from the deep convective cells by a *transition zone.* A discussion of this arrangement of precipitation was given by Smull and Houze (1985), although their description was for a TS system. It is presumed that to a first approximation the model can be reversed in order to explain the transition zone observed in the 18 May 1997 MCS. It was at 1100 UTC that the MCS's convective line reached its maximum horizontal extent and (in my opinion) attained its most archetypal reflectivity signature. At this time, therefore, analysis of the meso-β and meso-α scale features associated with the maintenance of the LS MCS was undertaken.

The regional surface observations indicated the persistent synoptic scale warm front across northeastern Iowa and northern Illinois (Fig. 6.11). The surface pressure trough described above remained to the west of the MCS, as implied by the southerly winds and eastward pressure gradient across the plotted domain. Also apparent in Fig. 6.11 is the existence of yet another MCS to the north of the studied system. This "sister" MCS was also LS, but was shorter lived (it initiated later *and* decayed sooner, suggesting that the union of ingredients for the studied case was relatively unique in the region). Interestingly, winds both ahead of and behind the 18 May 1997 MCS were southerly, with remarkably consistent temperatures and dewpoints. It is therefore unclear from whence surface air arrived at the updraft towers and to what degree it represented positive buoyancy.

To better quantify the flow of surface air toward the convective line, advection of θ_e was considered in a storm-relative framework. Apart from the synoptic front over central Illinois, only relatively weak gradients in surface θ_e existed near the MCS (Fig. 6.12). Surface storm-relative flow toward the convective line apparently passed through the pre-line rain region. Additionally, relatively little or no surface wind convergence was evident near the location of the convective line (Fig. 6.12). This case may therefore resemble the MCCs studied by Maddox (1983), which were frequently decoupled from the surface layer. To help

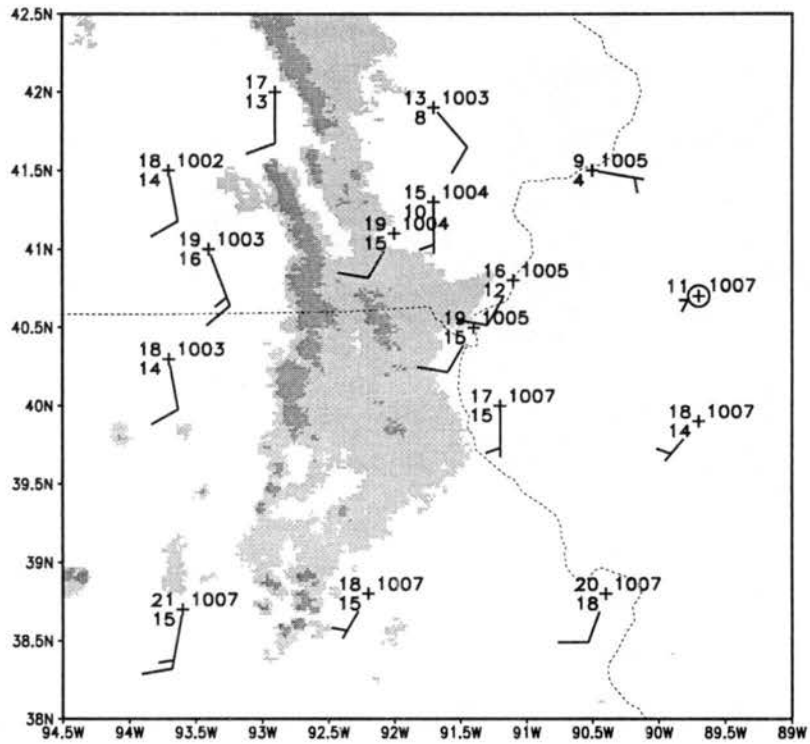

Figure 6.11: Surface observations and 2 km radar reflectivity at 1100 UTC on 18 May 1997. Temperatures and dewpoint temperatures in ° C. Pressures in hPa. Wind barb = 5 m s^{-1}, half barb = 2.5 m s^{-1}. Light shading: reflectivities 20-40 dBZ. Dark shading: reflectivities $\geq$ 40 dBZ. Sky cover not plotted.

explain the source of high θ_e air feeding the updrafts, data from aloft were analyzed.

While the lower tropospheric wind maximum discussed above was evident in the LTH wind profiler data at 1100 UTC (Fig. 6.9), the horizontal breadth of the jet was less than 300 km based upon the wind observations at three other regional sites (cf. Fig. 6.13), and was confined below 3.5 km based upon investigation of regional constant height plots. At 1200 UTC (a time at which NCEP reanalysis data were available), the highest 850 hPa θ_e near the MCS was to its rear (Fig. 6.14). The storm-relative winds at LTH alone displayed a substantial westerly component, indicating *localized* lower-tropospheric convergence of high-θ_e air at the trailing edge of the convective line. Notably, the values for θ_e at 850 hPa were higher than those found at the surface (compare Figs. 6.12 and 6.15). Therefore, parcels from 850 hPa would produce stronger updrafts. The elevated rear inflow both avoided contamination from the leading stratiform rain region *and* eliminated the need for less-buoyant surface air that had already been processed by previous deep convection.

The convective system decayed after 1200 UTC, and after 1400 UTC was no longer considered to meet the length criterion for MCSs in this study (cf. Fig. 6.1 e–h). While the convective line diminished, the associated regions of stratiform rain persisted through 1500 UTC and some time thereafter. The lysis of the 18 May 1997 LS MCS occurred shortly after local sunrise, a time at which the lower troposphere begins to again respond to surface heat fluxes with mixed-layer turbulence. The lower tropospheric southerly wind maximum over Missouri was still evident in the NOAA profiler network (not shown), but the pocket of high θ_e values at 850 hPa had decreased significantly (Fig. 6.15). Between 0000 and 1200 UTC on 18 May 1997, the 850 hPa observation at TOP (cf. Figs. 6.5 and 6.16) had changed from T=19° C, T_d=11° C to T=23° C, T_d=5° C (a decrease in θ_e of $\approx$ 1.5 K), thus the 850 hPa dryline/drytrough had moved eastward. Had the dry air moved sufficiently far eastward to interact with the MCS (a speculation not addressed by the coarse raob network), the buoyancy of updrafts would have been decreased while evaporation of the cloud would have increased. In either case, while storm-relative flow still arrived at the rear

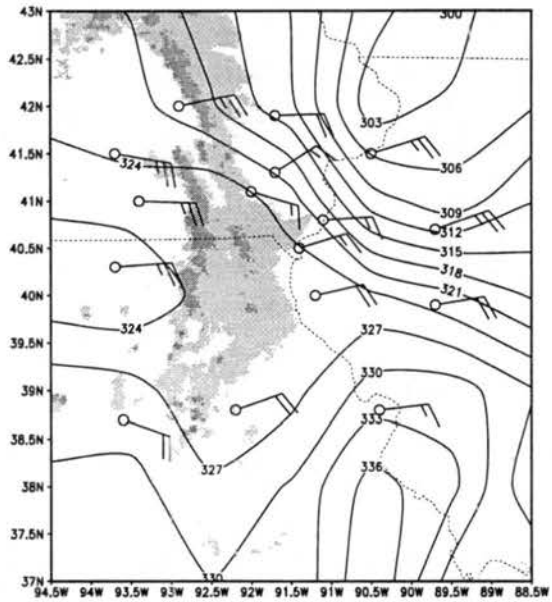

Figure 6.12: Surface equivalent potential temperature (K: contours), storm-relative winds, and 2-km radar reflectivity at 1100 UTC on 18 May 1997, using storm motion of 14 m s^{-1} from 270°. barb = 5 m s^{-1}, half barb = 2.5 m s^{-1}. Light shading: reflectivities 20-40 dBZ. Dark shading: reflectivities $\geq$ 40 dBZ.

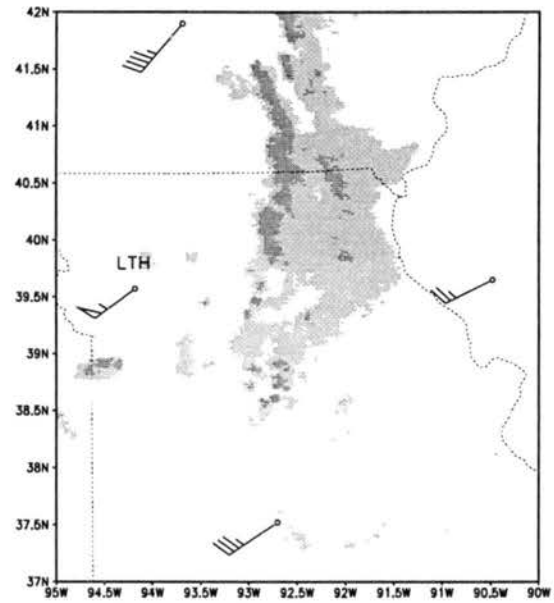

Figure 6.13: Regional NOAA profiler network winds at 1250 m MSL and 2 km radar reflectivity at 1100 UTC for 18 May 1997. flag = 25 m s^{-1}, barb = 5 m s^{-1}, half barb = 2.5 m s^{-1}. Light shading: reflectivities 20-40 dBZ. Dark shading: reflectivities $\geq$ 40 dBZ. Position of Lathrop, Missouri (LTH) wind profiler is indicated.

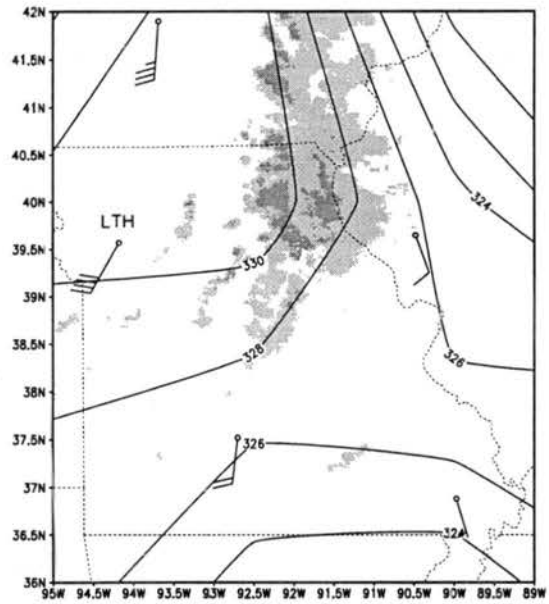

Figure 6.14: Regional NOAA wind profiler network storm-relative winds from 1250 m MSL (using an MCS motion of 14 m s^{-1} from 270°), NCEP Reanalysis 850 hPa equivalent potential temperature (K: contours), and 2 km radar reflectivity at 1200 UTC for 18 May 1997. barb = 5 m s^{-1}, half barb = 2.5 m s^{-1}. Light shading: reflectivites 20–40 dBZ. Dark shading: reflectivites $\geq$ 40 dBZ. Position of Lathrop, Missouri (LTH) wind profiler is indicated.

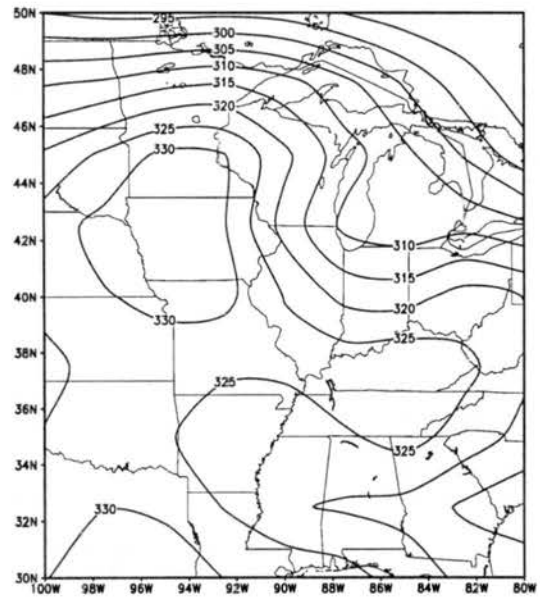

Figure 6.15: Same as Fig. 6.6 but for 1200 UTC on 18 May 1997.

of the convective line late in its lifetime, the buoyancy of the air advected toward the MCS had decreased. In addition to the possible presence of drier air, the decrease of θ_e in the 850 hPa lobe of buoyancy may have been due to turbulent mixing with less buoyant air at lower levels (due to an early morning increase in surface heat flux) as well as radiative cooling throughout the night. With diminished (or possibly negative) inflow buoyancy, the deep convective clouds weakened and decreased in areal coverage until the MCS definition was no longer met. The lifetime of the MCS was therefore governed by the juxtaposition of a linear boundary provided by outflow from previous convection, a pocket of buoyant air aloft in the lower troposphere, and convergence and enhanced ascent provided by a low-level wind maximum. The period in which these factors favorably encountered one another was approximately the lifetime of the MCS itself.

As the LS archetype represents a departure from the oft-studied TS class of MCSs, it is worthwhile to comment on the physical reasons for pre-line rain in the 18 May 1997 MCS. First, strong lower-tropospheric winds from the west impinged upon a convergence line where the deep convective motions occurred. As presented in Chapter 5, some component of the mean hydrometeor motion vector may be related to the vertical mixing of horizontal inflow momentum. This explanation is not definitive, however, as the role of mesoscale pressure gradients associated with thunderstorm outflows and circulations is not well resolved by conventional operational data platforms. More importantly, the forward movement of precipitation from the convective line was probably due to the establishment of a deep *slantwise* solenoidal circulation at the outflow edge's density gradient, a concept familiar for *TS* MCSs: Houze et al. (1989) related the ascending front-to-rear flow in a mature TS line to such a circulation. As the positions of cold outflow and warm lower-tropospheric air for the 18 May 1997 MCS were roughly reversed from the Houze et al. (1989) example, it is believed that the aformentioned solenoid played a major role in determining the precipitation archetype in a sense opposite that of the typical TS MCS.

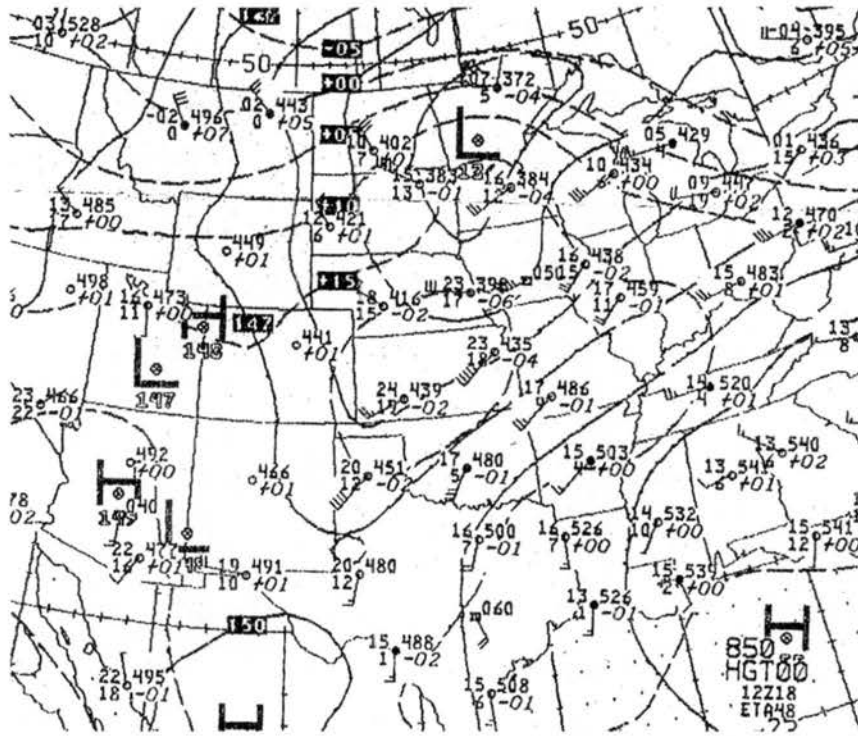

Figure 6.16: Same as Fig. 6.5 but for 1200 UTC on 18 May 1997.

6.1.3 Compatibility with leading stratiform archetype

The 18 May 1997 case study agreed fairly well with the mean fields observed for LS cases in Chapter 5, such that a certain degree of information about the *entire species* may be inferred. The axis of instability *was* to the west of the 18 May 1997 line, with southerly flow predominant across the region, both in advance and trailing the MCS. As well, the surface trough axis located approximately 200 km due west of the studied MCS seems well-correlated to the linear region of convergence observed for the class mean. The similarity of the location and orientation of the example's lower tropospheric θ_e maximum (to the west and southwest), along with southerly storm-relative winds (even the LTH profiler revealed a strong southerly component), to those of the mean are noteworthy as well. In this case study, the upper tropospheric winds (as observed at LTH) were nearly identical to the MCS motion vector, yielding no storm-relative flow above roughly 4 km AGL. It therefore seems doubtful that upper tropospheric advection of hydrometeors played a large role in the leading stratiform distribution of the 18 May 1997 MCS. This finding was inconsistent with the NCEP mean storm-relative winds for LS cases found in Section 5.2.5. As well, the upper-tropospheric vertical *shear* at LTH was fairly weak; the winds were nearly constant in speed and direction above 5 km. Therefore, the explanation given by Grady and Verlinde (1997) for a squall line with LS rain does not appear to be applicable to the 18 May 1997 MCS. It was suggested in Section 5.2.5 that the motion of hydrometeors is to some degree related to both the lower and middle tropospheric winds. Notably, the lower tropospheric westerly storm-relative flow was markedly stronger for this case than the LS mean, which may have accounted for a larger-than-average component of the forward rain distribution.

It is concluded, therefore, that the synoptic environment of the 18 May 1997 MCS resembles that found for the class mean. This suggests that the results of the above case study may have some relevance to LS MCSs in general. The following points merit emphasis: *1)* An unusual superposition of environmental factors (Fig. 6.17) was apparently necessary for the genesis and maintenance of the studied LS MCS. Perhaps this can explain the lesser

frequency of LS cases than TS cases, as well as their shorter duration (TS MCSs may provide their *own* forcing via retriggering on the *leading* edge of cold outflow). *2)* While the treatment of the LS archetype as a reversal of the TS archetype is probably excessively simple, it may be a fairly good "first guess" at an LS MCS's environment (Fig. 6.18). In such a case, the theoretical discussion of RKW88 may still be applicable to LS cases, which could represent a long-lived but less than optimal state in which the cold pool circulation is stronger than the low-level wind shear (aft of the cold pool). Alternately, the findings of Fritsch et al. (1994), who found that storm-relative flow toward the rear of an MCS could produce strong isentropic ascent near a middle tropospheric potential vorticity maximum, might apply. *3)* If the case studied here is representative, it may be that LS environments are somewhat anomalous, that is to say that their synoptic and mesoscale conditions are not those typically identified by forecasters using a decision tree–based analysis method. In order to predict similar LS cases, one must be aware of *all* temperature gradients associated with cold surface air, as well as the presence of narrow pools of high θ_e air aloft.

6.2 May 26 1996: Parallel stratiform

Early on 26 May 1996, a PS MCS formed along the Texas/New Mexico border and slowly traversed the southern Texas Panhandle (cf. Fig. 6.19). While no reports of severe weather accompanied the MCS, Andrews County in the southwestern Panhandle reported flash flooding associated with the convective line around 0400 UTC, during the MCS's early stage. During its lifetime of approximately 9 hours, the MCS was oriented from southwest to northeast, with its stratiform rain moving parallel to the line toward the northeast. It will be shown that the orientation and movement of the MCS were largely related to a meso-β scale outflow boundary (from previous convection over the Texas Panhandle) that encountered a topographic escarpment, while strong winds aloft probably accounted for the PS distribution of rain with respect to the line.

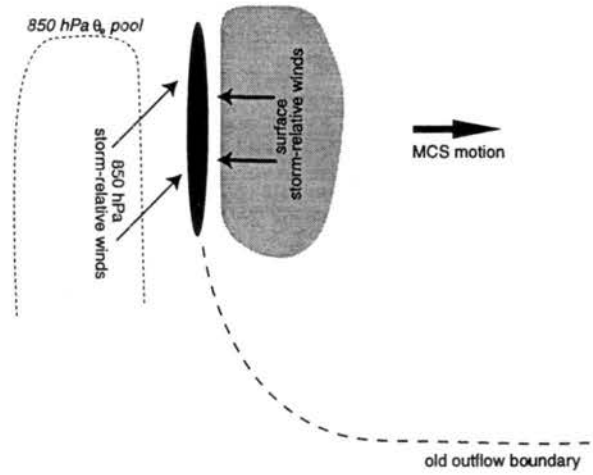

Figure 6.17: Schematic of 18 May 1997 LS MCS: plan view. Surface and 850 hPa features are depicted. Convective line shaded black, stratiform rain region shaded gray. Winds depicted by arrows are storm-relative.

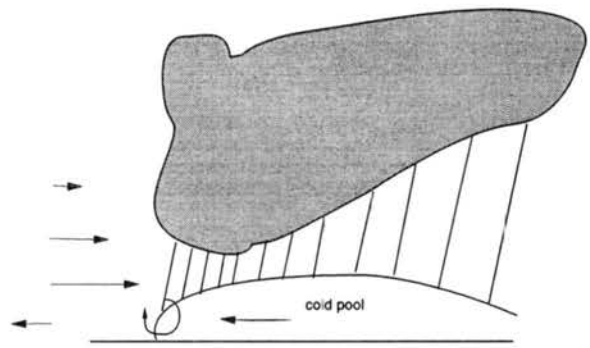

Figure 6.18: Schematic of 18 May 1997 LS MCS: through-line cross section. Winds depicted by arrows are storm-relative. Spacing of rain shaft lines indicates precipitation intensity. Sense of solenoidal circulation at outflow boundary indicated by clockwise arrow.

6.2.1 Synoptic environment and initiation

A strong, cut-off upper tropospheric low was positioned over northern Arizona by 0000 UTC on 26 May 1996 (Fig. 6.20a). A 250 hPa jet streak was rounding the associated high-amplitude trough, crossing southern New Mexico, and beginning to enter the High Plains. The position of the incipient MCS was within the left exit region of this upper level wind maximum, a region commonly associated with upward vertical motion (Uccellini and Johnson 1979). The closed wave was also evident at 500 hPa over northwest Arizona, with a wind maximum over western Texas and eastern New Mexico (Fig. 6.20b). While a large maximum in relative vorticity was colocated with the minimum in geopotential height at 500 hPa, relatively little vorticity advection was evident over the Texas Panhandle.

At 0000 UTC on 26 May 1996, a surface low pressure center was located over eastern New Mexico (Fig. 6.21). An occluded front extended northwest into Utah from the low, a stationary front east-northeast across the central Plains into the Ohio Valley, and a cold front south into (old) Mexico. A large band of frontal cloudiness covered the High Plains to the north of the stationary front (Fig. 6.22). The warm sector in advance of the synoptic cold front was relatively clear across southern and eastern Texas and regions farther east. Deep convective clouds had broken out over the Texas Panhandle by 0000 UTC, approximately 100 km in advance of the cold front location. While several intense quasi-linear thunderstorms existed in proximity to one another at this time (not shown), none met (individually or as an ensemble) the horizontal extent criterion for long enough to be considered an MCS.

Associated with the thunderstorms over the Panhandle was a broad surface cold pool, demarked by an outflow boundary which extended roughly from HOB (Hobbs, New Mexico) to LBB (Lubbock, Texas) to GAG (Gage, Oklahoma) to DDC (Dodge City, Kansas); the boundary was not analyzed by NCEP, but was clearly present in the surface data (Fig. 6.21). As an aside, Sanders and Doswell (1995) pointed out that NCEP analyses are frequently unsatisfactory in their recognition and placement of boundaries. The out-

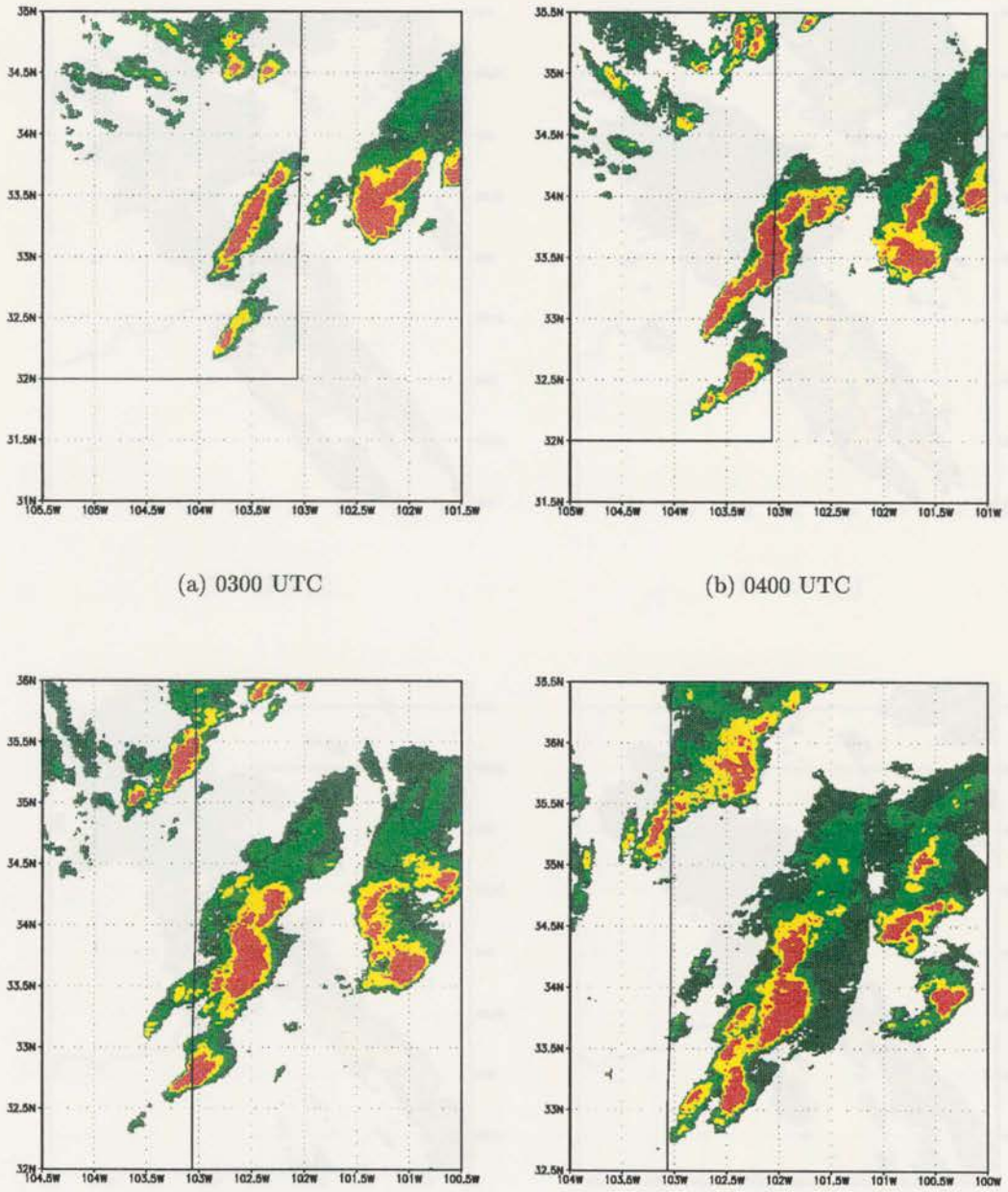

(a) 0300 UTC

(b) 0400 UTC

(c) 0500 UTC

(d) 0600 UTC

Figure 6.19: Hourly 2 km radar reflectivity composite images for 26 May 1996 PS MCS.

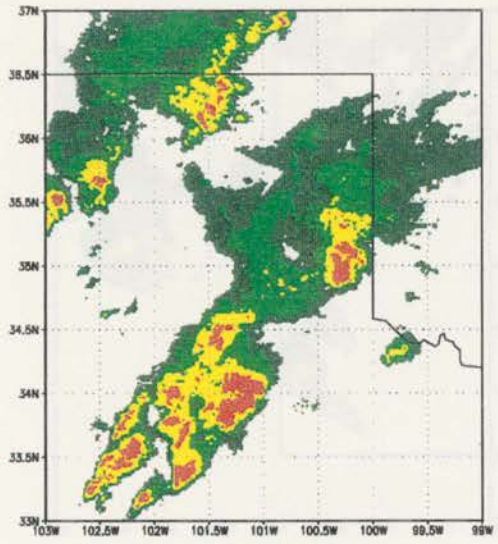

(e) 0700 UTC

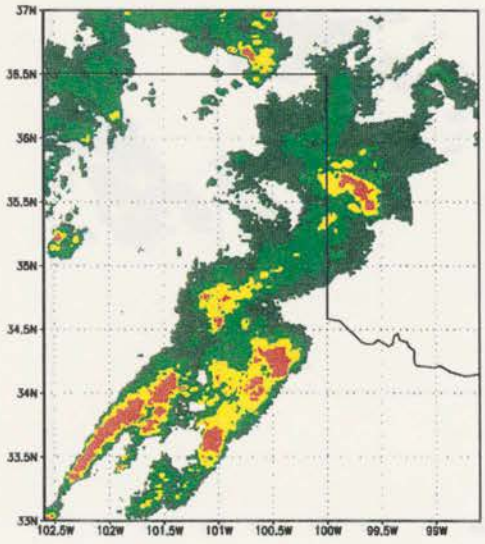

(f) 0800 UTC

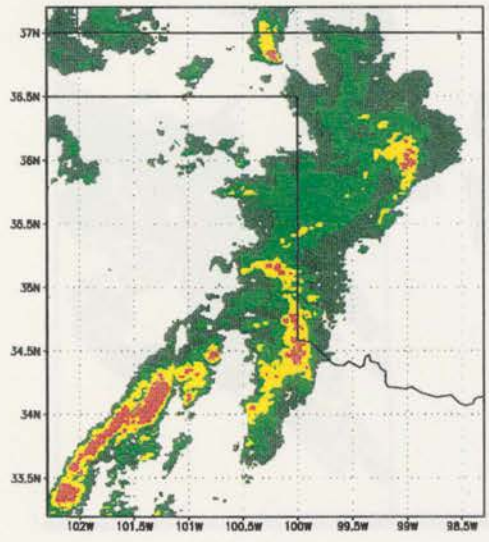

(g) 0900 UTC

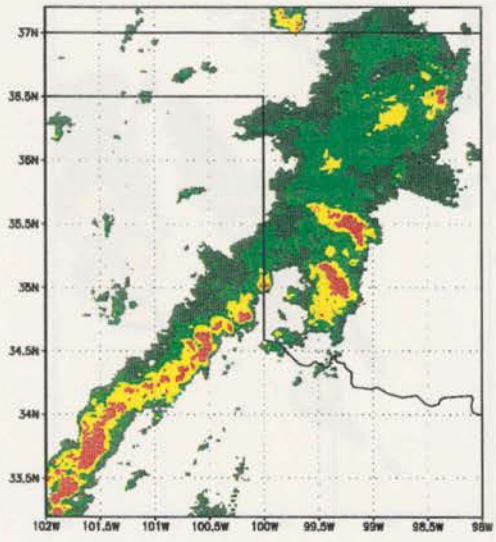

(h) 1000 UTC

Figure 6.19: *Continued*

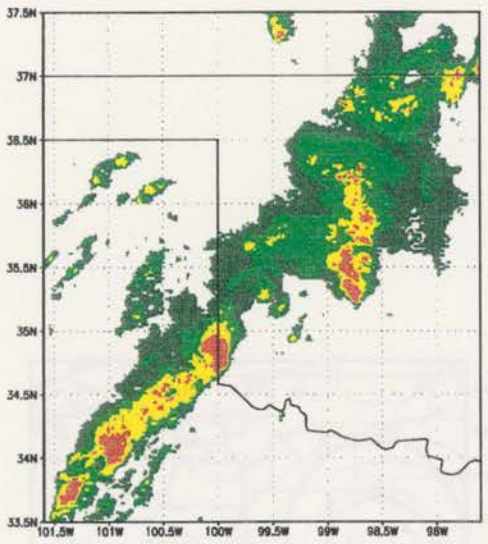

(i) 1100 UTC

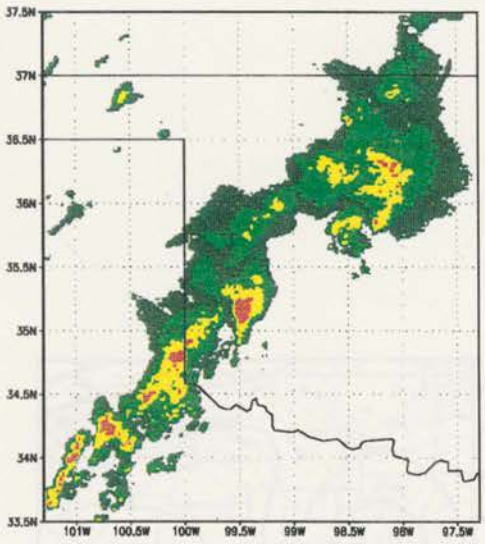

(j) 1200 UTC

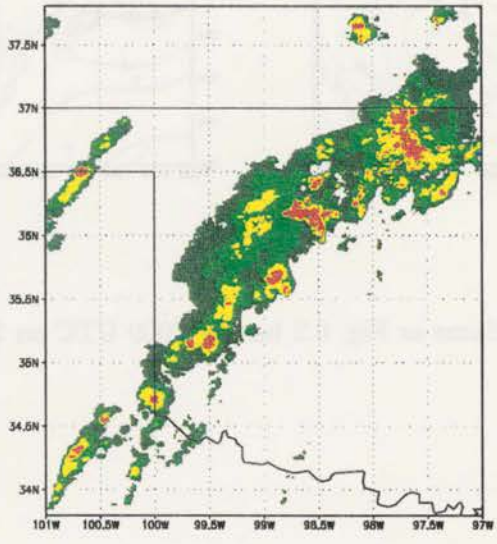

(k) 1300 UTC

Figure 6.19: *Continued*

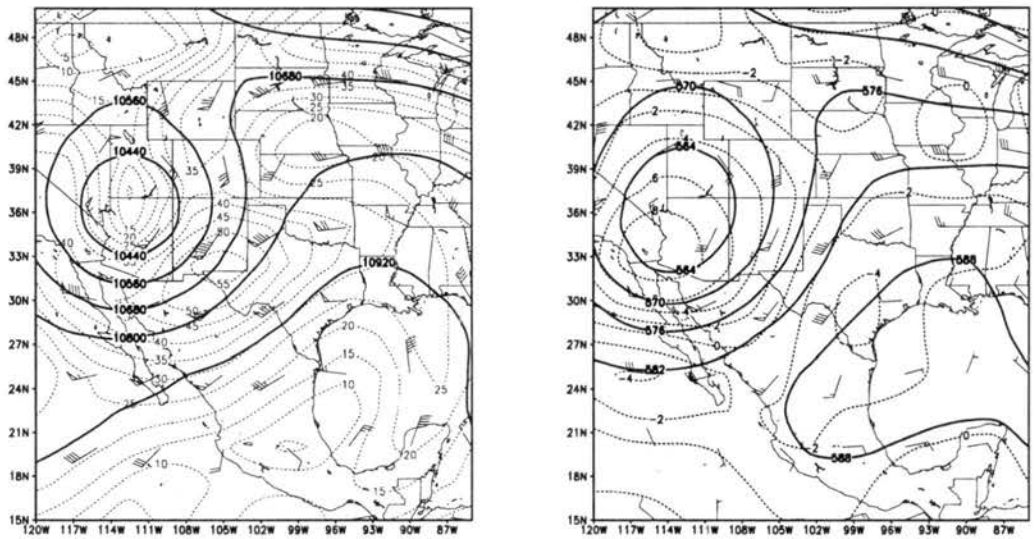

(a) (b)

Figure 6.20: Same as Fig. 6.2 but for 0000 UTC on 26 May 1996.

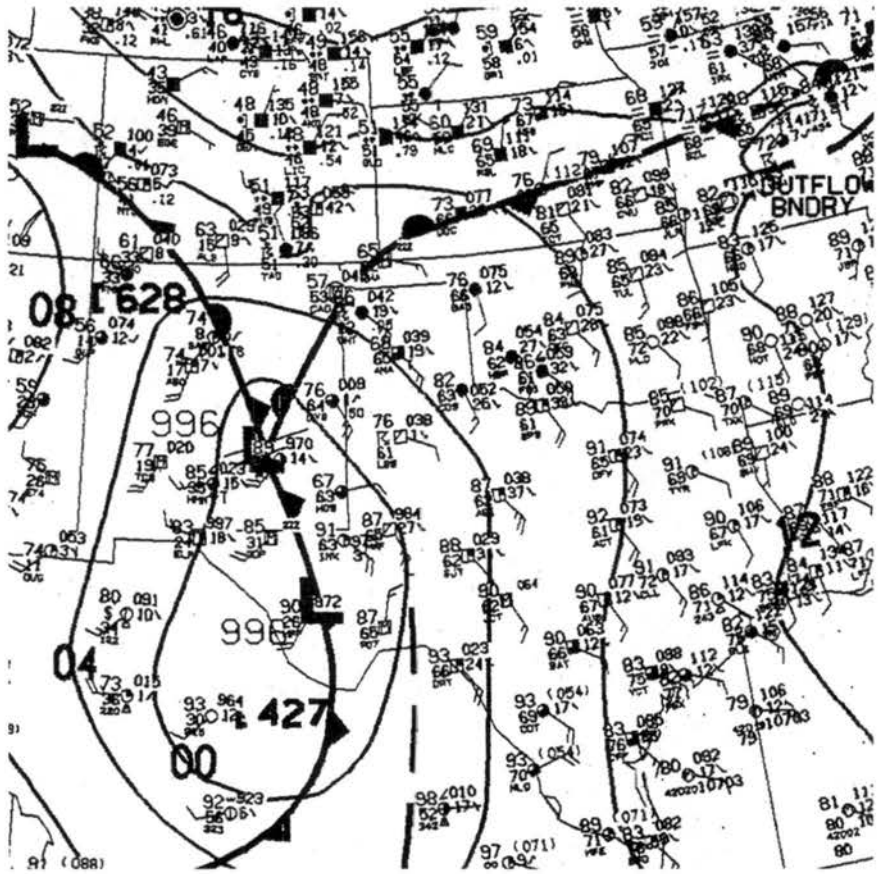

Figure 6.21: Same as Fig. 6.3 but for 0000 UTC on 26 May 1996.

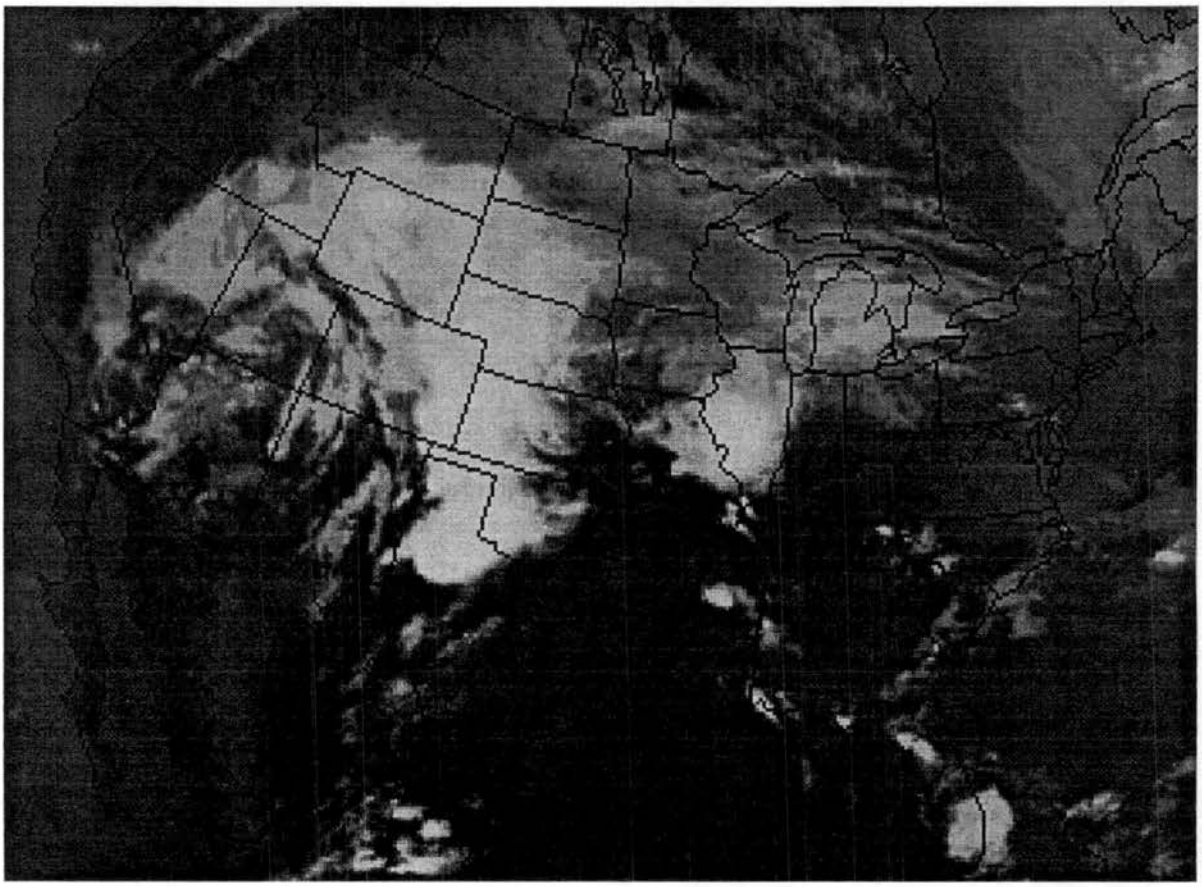

Figure 6.22: Infrared satellite image of the United States for 0000 UTC on 26 May 1996.

flow boundary's position roughly coincided with the thunderstorms' cloud shield axis. By 0300 UTC, the surface cold front had pivoted slightly eastward toward the Texas/New Mexico border (Fig. 6.23). Even though the surface low was apparently centered over the Texas/(old) Mexico border, the surface wind field in New Mexico was consistent with this frontal movement. Stations across eastern New Mexico and the Texas Pandhandle continued to exhibit signs of previous convection: HOB, LBB, CVS (Clovis, New Mexico), and GAG reported cloudy skies, cooler surface temperatures (than southern and central Texas), and variable winds, while CDS (Childress, Texas), DHT (Dalhart, Texas), and HBR (Hobart, Oklahoma) reported thunderstorms and/or rain showers. Thus, although NCEP had not yet analyzed an outflow boundary across the southern Texas Panhandle, its existence was evident from surface observations and supported by the continued existence of heavy precipitation across the Panhandle.

At 0300 UTC, a new elongated reflectivity core developed near HOB (Fig. 6.19a), approximately at the intersection of the aforementioned outflow boundary and the synoptic cold front, and almost immediately met the MCS length criterion for this study. The initial orientation of the reflectivity core was from southwest to northeast, or roughly parallel to the outflow boundary (which still passed through HOB, LBB, and GAG). In addition to convergence of the strong southerly flow evident at MAF (Midland, Texas) at 0300 (Fig. 6.23) with the cold pool, rapid intensification and elongation of the new convection was probably related to the colocation/collision of the outflow and cold frontal boundaries. Purdom (1986) found that the intersection of thunderstorm outflows with other boundaries was a favored location for initiation of new deep convection. The superposition of a density-driven solenoidal circulation from the outflow boundary upon a circulation associated with the cold front (which can also be considered a density-driven solenoid, as described by Parsons 1992) could produce locally deep and intense vertical motion. Additionally, the airmass near the boundary intersection was very unstable. The nearby 0000 UTC sounding from MAF (Fig. 6.24) had 2144 J kg^{-1} of CAPE and a surface lifted index of -5.2 K. The

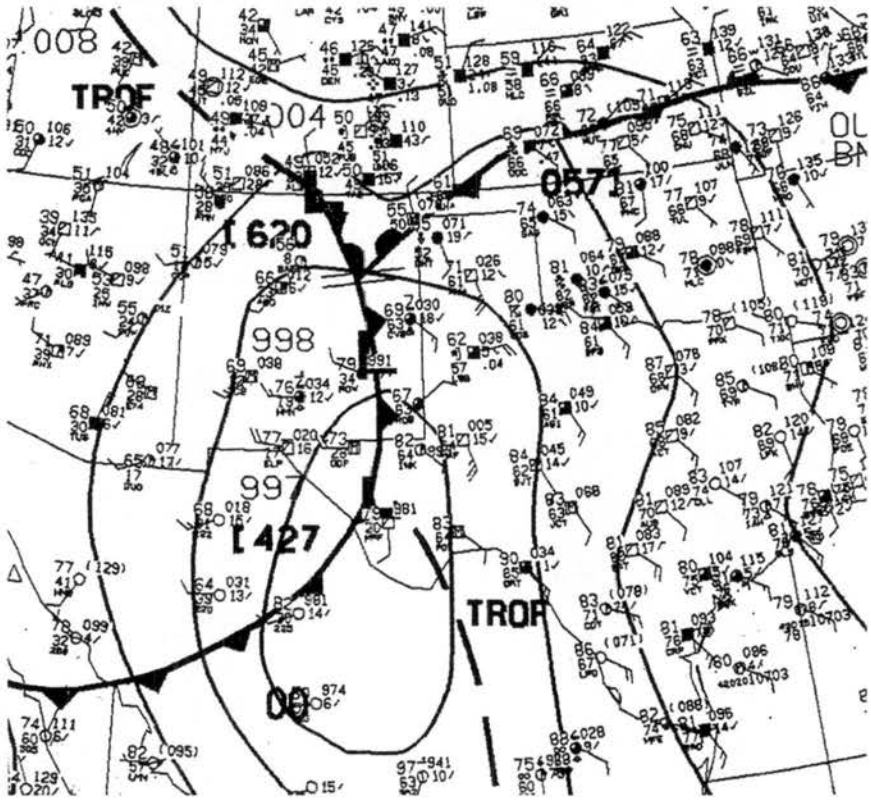

Figure 6.23: Same as Fig. 6.3 but for 0300 UTC on 26 May 1996.

solenoidal circulations were probably needed to overcome the -280 J kg^{-1} of CIN exhibited by the MAF raob.

Additionally, the MAF sounding revealed a great deal about the general environment within which the MCS developed and evolved. While the lower tropospheric winds veered approximately 60° below 750 hPa, there was relatively little middle and upper tropospheric directional shear. Since the convective line was oriented roughly southwest to northeast this wind profile implied strong lower tropospheric convergence along the eastern edge of the line, with very deep and fairly strong (25 m s^{-1} near 500 hPa, > 40 m s^{-1} above 300 hPa) middle and upper tropospheric flow parallel to the line. From the standpoint of pure advection of hydrometeors (previously discussed in Section 5.2.5), this scenario would appear to be ideal for the PS class. As well, the relatively dry air aloft at MAF suggested that deep downdrafts might produce strong surface temperature perturbations (the ρ-weighted DCAPE was 920 J kg^{-1}, a relatively large value in comparison to those given by Gilmore and Wicker 1998). Therefore, a mechanism for continued maintenance of the cold surface outflow air was in place. This was significant, as the outflow boundary played a continuing role in the orientation of the MCS.

6.2.2 Evolution and maintenance of the MCS

The elongated convective line, oriented along the Panhandle outflow boundary, had crossed into Texas by 0500 UTC and begun to merge with a smaller, slightly elongated reflectivity core to its south (Fig. 6.19c). The development and organization of the line was probably via a backbuilding and/or broken-line pathway, as defined by BJ85. The isolated storm with which the main line merged had many supercellular reflectivity characteristics (as judged from the 2-km data), even though no severe weather was reported near it. Notably, as the reflectivity cores amalgamated between 0500 and 0700 UTC (Fig. 6.19 c–e), the stratiform rain associated with *each* echo entity, *and* with the *entire region* of convection, was moving northeast, parallel to the elongated linear elements. By 0800 the mergers had

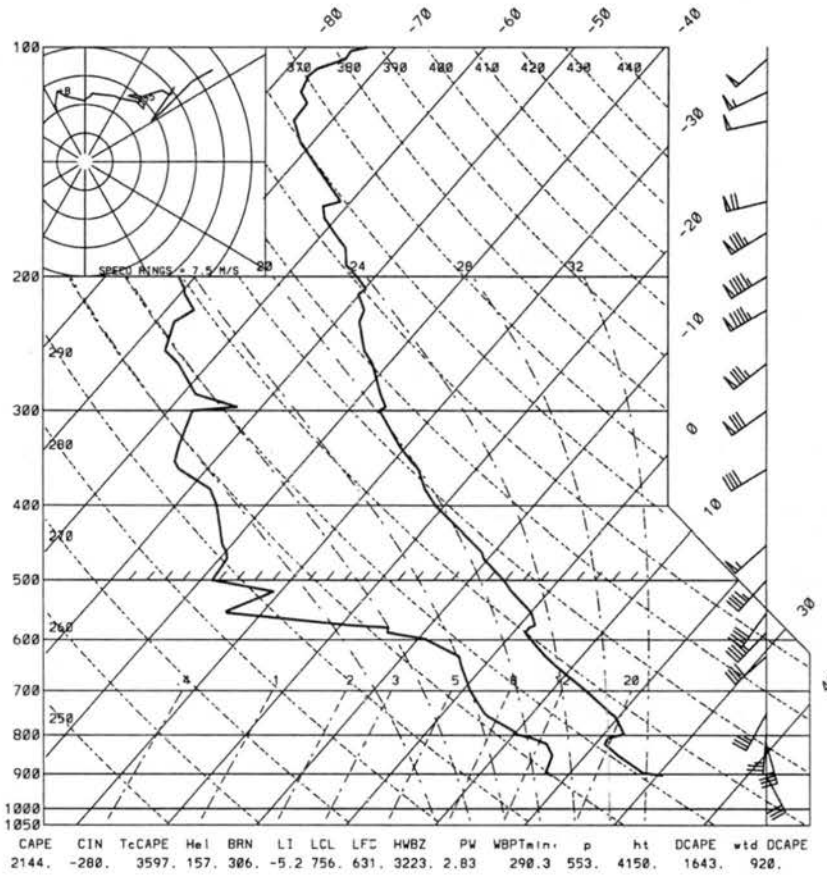

Figure 6.24: Skew-T ln-p plot of the NWS rawinsonde observation from Midland, Texas (MAF) at 0000 UTC on 26 May 1996. flag = 25 m s^{-1}, barb = 5 m s^{-1}, half barb = 2.5 m s^{-1}.

rendered a predominant convective line centered at 33.5° N, 102° W and a thin band of stratiform rain extending northeast (Fig. 6.19f). By 1000 UTC, the convective line had reached its greatest extent and the MCS had its most archetypal appearance (Fig. 6.19g). Accordingly, an investigation of the MCS's near-storm environment was undertaken for that time.

The existence of the aforementioned boundaries across the region was still evident at 1000 UTC (Fig. 6.25). The stationary front was located between Amarillo and Dalhart, Texas and between Medicine Lodge and Dodge City, Kansas, while the cold front extended south through Clovis, New Mexico (positions consistent with the 0900 UTC NCEP surface analysis, not shown). The outflow boundary was positioned roughly along the eastern edge of the 26 May 1996 MCS, extending northeastward from just south of Lubbock to near Childress, Texas and meeting the stationary front slightly west of Medicine Lodge, Kansas. At this time, the surface low pressure center was located just northwest of Midland, Texas. Associated with its position and attendant pressure gradient, strong southerly and south-southeasterly winds prevailed in the warm sector, advecting warm, moist air northward. In contrast to the LS case of 18 May 1997, there was little doubt that *1)* a strong density gradient existed at the leading edge of the outflow air (more treatment of this later), and *2)* the most buoyant surface air arrived at the convective line from *in advance* of its leading edge.

Easterly storm-relative inflow was occurring ahead of the MCS in the warm sector air (Fig. 6.26). A region of convergence was evident near the convective line's location, as storm-relative winds in its wake were more northwesterly. As expected (based upon the regional temperature and dewpoint observations), the highest θ_e air was located ahead (east) of the convective line. At 1000 UTC, a slight axis of enhanced θ_e extended west-northwestward from Wichita Falls, Texas (approx. 34° N, 98.5° W). The strong easterly storm-relative wind there ensured that the northern end of the convective line received buoyant surface air.

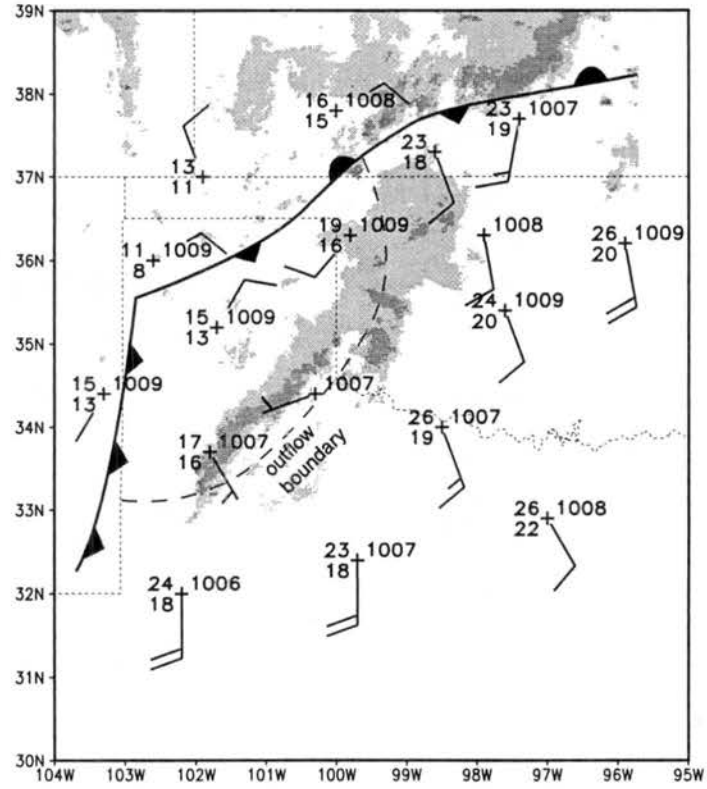

Figure 6.25: Same as Fig. 6.11 but for 1000 UTC on 26 May 1996.

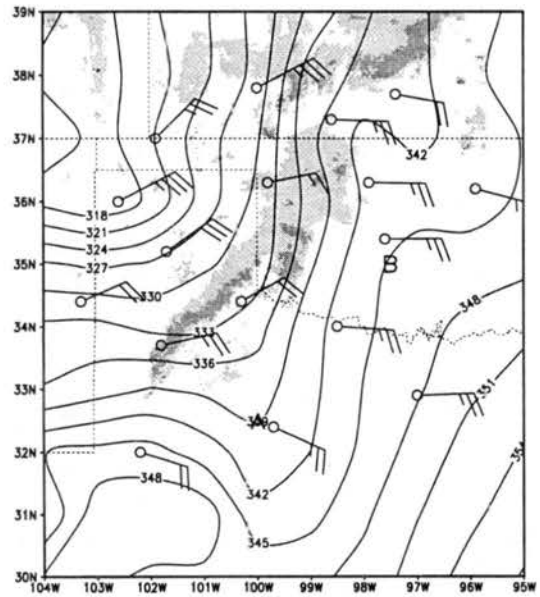

Figure 6.26: Same as Fig. 6.12 but for 1000 UTC on 26 May 1996, using storm motion of 10 m s^{-1} from 240°. A and B are locations for profiles in Fig. 6.27.

After 1000 UTC, the MCS began to lose strength, with a declining area of coverage by high reflectivity cores (Fig. 6.19 i–k). The lysis of the 25 May 1996 PS MCS was largely related to a decrease in instability of the convective airmass. Between 0600 and 1200 UTC, the CAPE due east of the convective line decreased, with warming aloft and cooling nearer the surface (Fig. 6.27). Several factors help to explain this stabilization. Firstly, the warm-sector over most of Texas remained clear throughout the night (local time), as confirmed by the infrared satellite image from 1200 UTC (Fig. 6.28) as well as sky cover observations from NWS stations between 0000 and 1200 UTC. Therefore, a relatively large amount of diurnal cooling could occur (due to the absence of downward longwave radiation from clouds). Between 0300 UTC (the time of onset) and 1200 UTC (just prior to lysis) the temperature at ABI (Abilene, Texas) decreased from 84° to 73° F (29 to 23° C) without the passage of a thermal boundary. This was important, as vertical NCEP reanalysis profiles confirmed that the source of convection was near the surface (the highest θ_e values were located there; not shown). Secondly, as was discussed by Bretherton and Smolarkiewicz (1989), deep convective clouds alter the environmental lapse rate beyond the cloud by compensating subsidence (which they found in a numerical model to be related to gravity waves). Prolonged deep convective clouds, due to their latent heat release, are buoyancy maxima in the troposphere. Resultant gravity waves commute the excess heat to the environment by perturbing the flow in a way that tends to lessen the buoyancy gradient aloft. Therefore, the available potential energy for the 26 May 1996 MCS was probably diminshed over a region *broader* than the convective storm, even though the intense overturning was localized. Mapes (1993) showed that in addition to the effects of the deep convection, a second gravity wave mode is produced by *stratiform* rain regions that *destabilizes* the troposphere. Perhaps the lack of stratiform rain immediately preceding or following the convective line in PS cases such as the 26 May 1996 MCS places a relative limit on their duration; they will probably not exhibit the positive feedback that Mapes (1993) suggested. Finally, weak warm advection was occurring aloft in advance of the

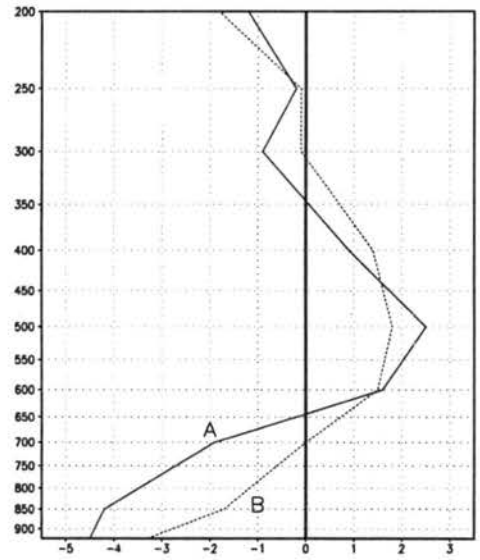

Figure 6.27: NCEP Reanalysis data: vertical profile of temperature change (K: abscissa) between 0600 and 1200 UTC on 26 May 1996. Profiles constructed at 32.5°N 100°W (solid curve: A) and 35°N 97.5°W (dashed curve: B). Ordinate values are pressures in hPa. Positions of A and B are indicated in Fig. 6.26.

middle tropospheric trough, particularly near 500 hPa (not shown). The combined effects of nocturnal cooling, convective stabilization, and middle tropospheric warm air advection therefore decreased the relative buoyancy of low-level parcels, contributing to the ultimate decline of the deep convection.

In addition, as the MCS moved to the northeast along the boundary, it moved into an environment of less favorable vertical motion. The deep synoptic cold frontal circulation mentioned above could contribute less to the late-term sustenance of the convective line due to its farther proximity from the intense reflectivity cores. As well, in moving northeast the MCS gradually entered the right exit region of the upper level jet streak (a region typified by descent) as the 250 hPa wind maximum rounded the base of the trough and moved northward across eastern New Mexico. Although synoptic scale lifting was probably not of first order importance to the 26 May 1996 MCS, the changes to the large scale vertical motion profile certainly were not beneficial to the maintenenace of deep convection.

The orientation of the MCS— parallel to the winds between approximately 700 hPa

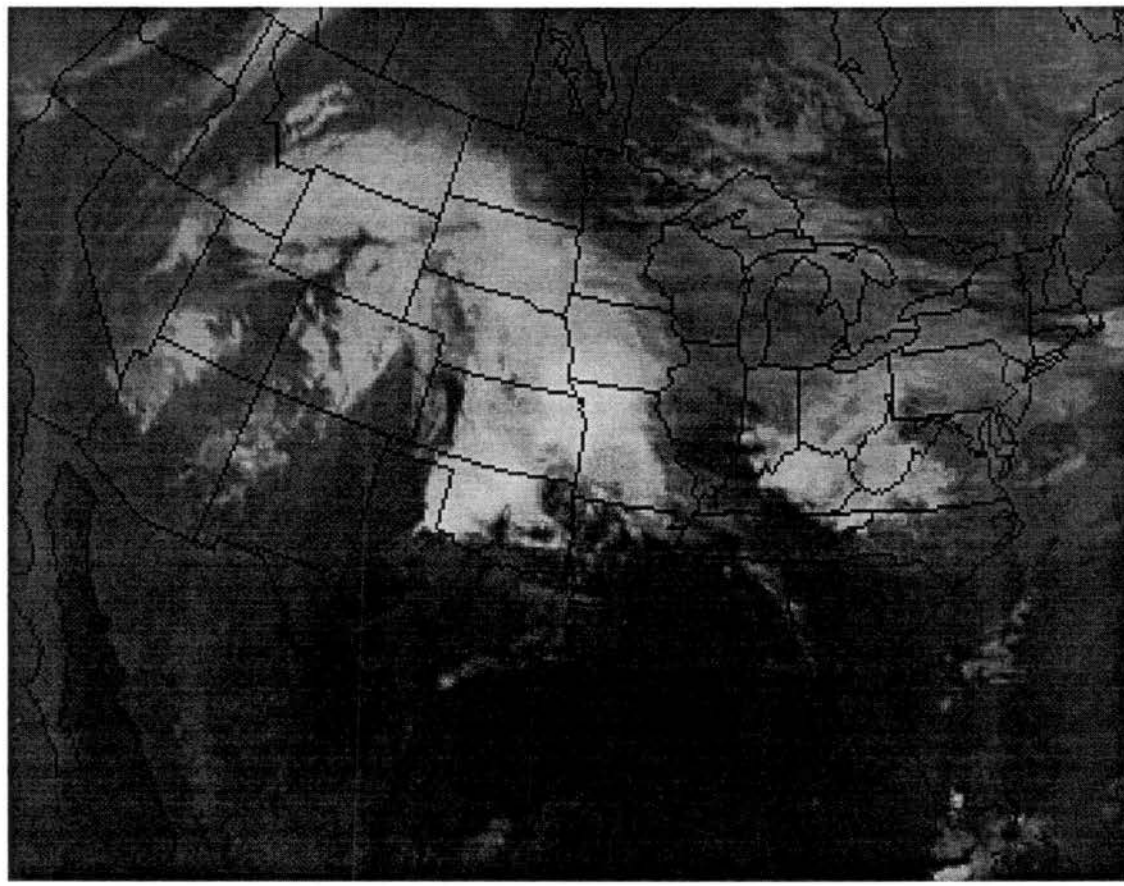

Figure 6.28: Infrared satellite image of the United States for 1200 UTC on 26 May 1996.

and the tropopause, as mentioned above— probably favored advection of hydrometeors (downwind) in a direction parallel to the line itself. It is relevant, therefore, to consider reasons for the convective line's orientation. Primarily, as was emphasized above, the MCS was aligned with the leading edge of the pre-existent outflow boundary. Because this boundary was *quasi-stationary* during the lifetime of the PS MCS, there was little or no impetus for the convective line to propagate away from its initial locale. Instead, echoes trained along the boundary's persistent lifting, moving with the middle and upper tropospheric flow.

It is therefore important to investigate the outflow boundary's apparent lack of motion. The density perturbation represented by the outflow air was strong throughout the MCS's lifetime. Thus, the boundary did not stall due to lack of a hydrostatic pressure gradient. Instead, topography played an important role in the location of the boundary *and* the location of the convective line. Running roughly north–south through the center of the Texas Panhandle, the *Caprock Escarpment* represents a discontinuity in elevation and terrain. On the high plain above the escarpment, the elevation of Amarillo, Texas is approximately 1100 m. Due east-southeast of Amarillo, below the escarpment, sits Wheeler, Texas at approximately 680 m elevation. Nearby Childress, Texas has an elevation of 595 m, while to the southwest Lubbock sits atop the escarpment at 988 m above sea level. It is proposed that the interaction of a surface cold pool with this feature was relevant to the location and maintenance of the PS MCS on 26 May 1996.

Expanding outward as a gravity current, the cold air descended the terrain along the escarpment by virtue of its greater weight than surrounding air. However, as the surface outflow descended, it warmed according to the adiabtic lapse rate, $\approx 10\ \mathrm{K\ km^{-1}}$. An air parcel descending from Amarillo to Childress would warm adiabatically by approximately 4.9 K (or, with reference to the NCEP chart, 8.8° F). Therefore, once descending the Caprock Escarpment, surface outflows should represent a smaller density perturbation with respect to nearby surface air. As an aside, the reader can be assured of the actual existence of a cold pool, rather than a terrain-related ∇T, by returning to the 2100 UTC surface observations

in Fig. 6.29: less than half of the temperature differences between CDS and SPS— Wichita Falls, Texas— and between HOB and INK— Wink, Texas— can be explained by isentropic temperature changes with altitude. As given by Eq. 3.6, weakened cold pools expand outward at slower speeds should their depths remain constant (an assumption made here for want of observational verification). Hence, once the outflow air "traversed" the escarpment, its eastward motion was probably greatly diminished. Even at 1200 UTC on 26 May 1996, the NCEP analyzed outflow boundary was not far east of Childress, Texas (Fig. 6.30).

The importance of cold air near the escarpment is two-fold, however. Solenoidal circulations are forced by density gradients *along pressure surfaces*, following the circulation theorem:

$$\frac{DC_a}{Dt} = -\oint \rho^{-1}\, dp, \tag{6.1}$$

wherein C_a is the absolute circulation (for a closed path, this is twice the rotation rate multiplied by the area enclosed), ρ is density, and dp is an incremental change in pressure along the closed integral path. When considering density-driven solenoids previously, it was implicitly assumed that along the earth's surface, the *local* environment for the circulation was nearly isobaric such that surface density gradients corresponded to the intersection of pressure and density surfaces. Near sharp gradients in terrain elevation, however, this assumption is invalid. Rather, the character of the solenoidal circulation will be similar to the idealized model in Fig. 6.31. In order to evaluate such a scenario, Eq. 6.1 is rewritten (using the equation of state) as:

$$\frac{DC_a}{Dt} = -R \oint T\, d\ln p, \tag{6.2}$$

wherein R is the gas constant for dry air and T is temperature. For the idealized flow of cold air over an escarpment in Fig. 6.31, we then find (integrating counterclockwise and noting that only sections b and d of the integration loop contribute to the integral: a and c are isobaric):

$$\frac{DC_a}{Dt} = -R\,[(\overline{T_d} - \overline{T_b}) \cdot (\ln p_1 - \ln p_2)], \tag{6.3}$$

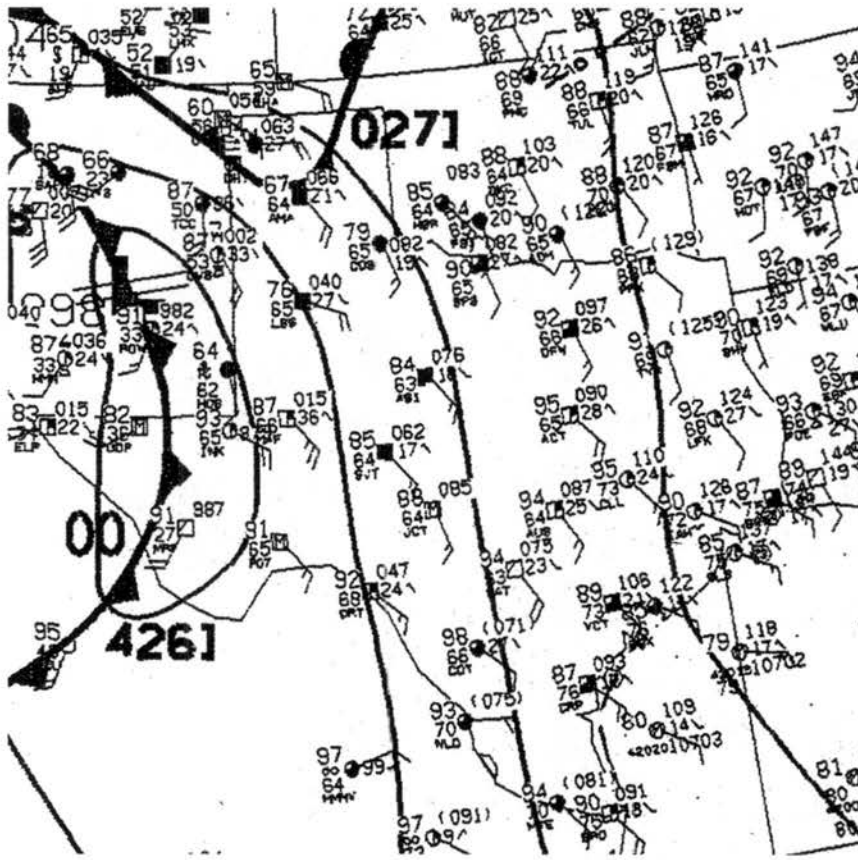

Figure 6.29: Same as Fig. 6.3 but for 2100 UTC on 25 May 1996.

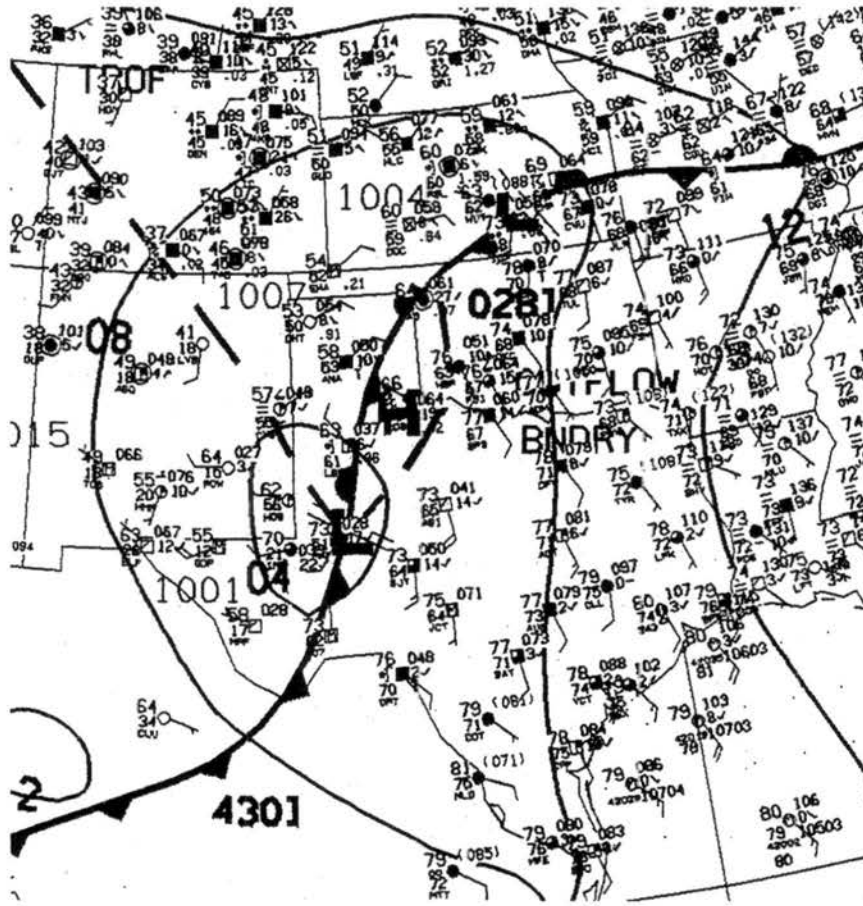

Figure 6.30: Same as Fig. 6.3 but for 1200 UTC on 26 May 1996.

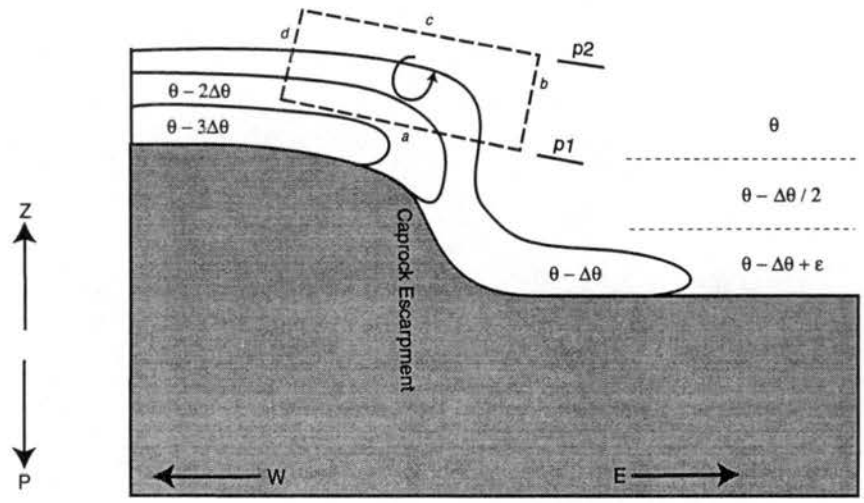

Figure 6.31: Idealized schematic for the density-driven solenoid occurring as cold air spills down the Caprock Escarpment. The dashed box represents a path of integration for Eq. 6.3, with a through d segments of the closed circuit. The cold outflow and environment have been idealized as stratified fluids for ease of illustration. Water vapor content was also neglected. Potential temperature (θ) is used to designate layers of fluid as it is both conservative and easily comparable along a pressure surface. ϵ represents some small additional increment in the potential temperature of the airmass as compared to the cold pool. Pressure surfaces are sloped to reflect hydrostatic pressure gradient. Sense of circulation indicated by arrow within integration circuit.

wherein overbars refer to mean values along sections of the loop, temperature subscripts represent sections of the loop, and pressure subscripts represent pressure levels as labeled in Fig. 6.31. Because $p_1 > p_2$ and $\overline{T_b} > \overline{T_d}$, the material derivative is positive; a cyclonic circulation (as the reader looks at the page) is produced by the density gradient. Therefore, as dense air spills down the escarpment, an interface between dense and less dense fluids remains at the top edge of the topography and a solenoidal circulation is implied for as long as the cold pool exists above the escarpment. Buoyant lower-tropospheric air approaching the escarpment would ascend upon encountering the solenoid and could further fuel deep convective cells there.

If the potential temperature structure of the scenario depicted in Fig. 6.31 is to be accepted, it is necessary to establish that the environmental stratification was indeed stable. As moisture was neglected for the simplified derivation, the quantity of interest along pressure surfaces is the temperature. Since potential temperature is conserved for adiabatic flows, θ facilitates easy comparison of the environment to the density current on *all* pressure surfaces. To support the model in Fig. 6.31, therefore, NCEP reanalysis vertical profiles during the MCS's lifetime are presented in Fig. 6.32. As in the idealized model, the potential temperature increases throughout the sounding (indeed, this must nearly always be the case in a fluid). An important concern would be the existence of the deep nearly-adiabatic layer which is often observed during diurnal turbulent growth of the mixed layer. The nocturnal life span of the 26 May 1996 MCS and its cold pool, however, would not have encountered such a layer. Rather, as the earth's surface cooled radiatively under clear night skies, downward sensible heat flux would continue to lower the near-surface air temperature more rapidly than that of the air aloft in the lower troposphere, yielding a stably stratified nocturnal profile. Notably, a θ–profile similar to that depicted by Fig. 6.32 was also observed at Fort Worth, Texas at 1200 UTC (Fig. 6.33). With such an evolution, the inflow to the MCS was probably increasingly elevated during its lifespan. Such elevated inflow is consistent with the topographically fixed solenoidal circulation depicted above.

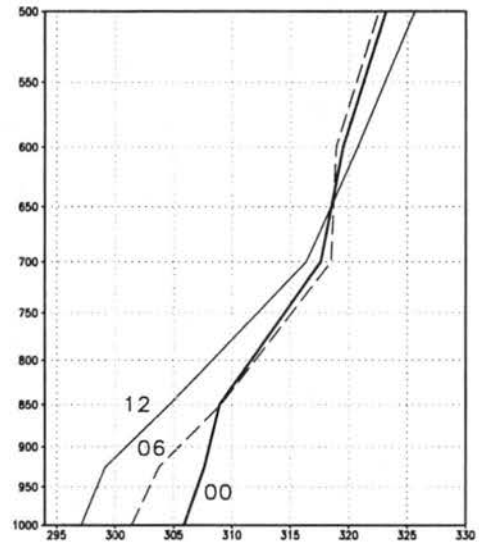

Figure 6.32: NCEP Reanalysis data: vertical profiles of potential temperature (K: abscissa) for 32.5°N, 100°W at 0000 UTC (thick curve), 0600 UTC (medium dashed curve), and 1200 UTC (light curve). Ordinate values are pressures in hPa. Position for these soundings is given by letter A in Fig. 6.26.

Given the applicability of the idealized model, not only would the forward progress of the outflow boundary have apparently stalled on 26 May 1996, but the deep lifting at its edge would have persisted above the Caprock Escarpment throughout the episode. This circulation may have played an important role in the organization of the MCS. Indeed, between 0700 and 0800 UTC, cells which moved east of the main line centered near 34° N, 102° W appeared to dissipate while the intense reflectivity cores remained near the southern extent of the escarpment. Therefore, it is also speculated that in addition to the previously mentioned contributors to lysis, another factor in the demise of the 26 May 1996 PS MCS may have been the disruption of this persistent circulation, perhaps due to the deepening of the surface cold pool *below* the escarpment or the exhaustion of buoyant air arriving at the solenoidal circulation from the east.

The dynamical scenario described above would dicatate a fairly consistent orientation for the convective line throughout. Because this orientation was parallel to the strong upper level winds, hydrometeors were advected along the line rather than perpendicular to it. The

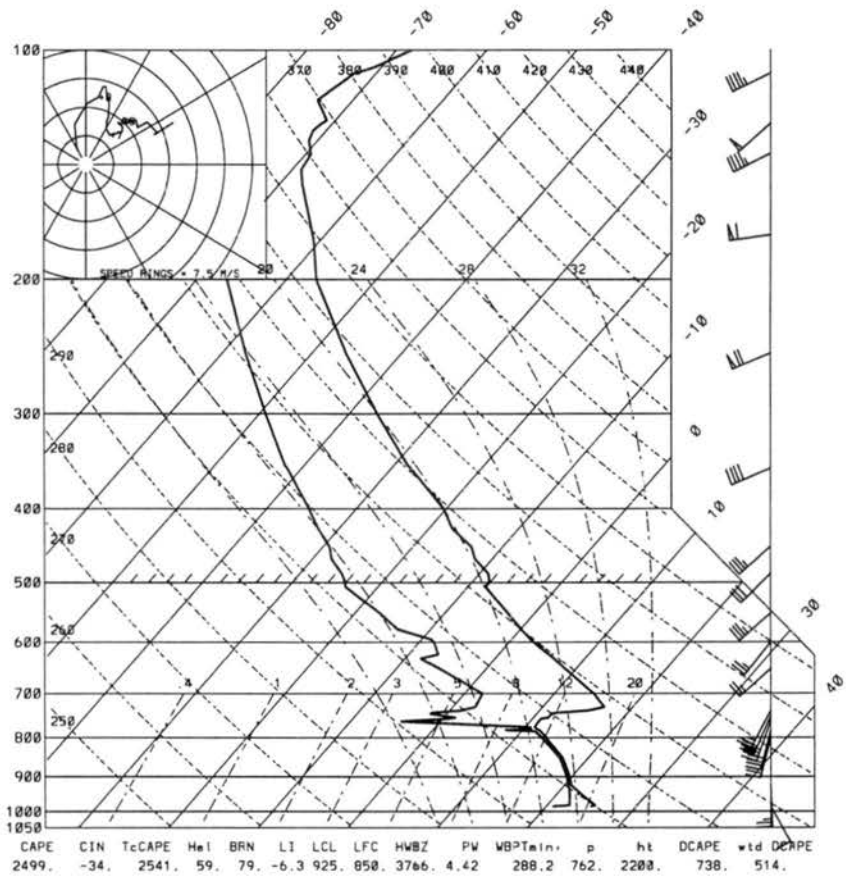

Figure 6.33: Same as Fig. 6.24 but for Forth Worth, Texas at 1200 UTC on 26 May 1996.

26 May 1996 MCS was relatively stationary; however, should a PS MCS move more rapidly, the same arguments can be applied to the *storm-relative* flow (therefore, PS MCSs can and do occur apart from the 26 May 1996 topographic scenario). Apparently, low-level horizontal momentum was not a significant contributor to the stratiform rain location, whether due to the deceleration of inflow parcels by the non-hydrostatic pressure gradient (which theoretically should have accompanied the pre-existent outflow boundary) or due to the relatively shallow layer in which winds were not parallel to the line. Skamarock et al. (1994) argued that hydrometeors aloft usually have some northwward displacement (to the left of the storm's motion vector) due to Coriolis effects, which may also have played a role in the observed stratiform rain distribution.

6.2.3 Compatibility with parallel stratiform archetype

Much as for the PS class mean, the case exhibited lower tropospheric flow from the southeast. The storm-relative winds near 500 hPa for the studied PS case were southwesterly, parallel to the northeastward-oriented line, just as exhibited for the PS mean. The west-southwesterly mean 250 hPa winds for the PS class were also fairly well captured by the 26 May MCS's environment. The orientation of the studied MCS was remarkably close to the mode for PS cases: therefore, it is not surprising that the wind field aloft was similar to that of the archetype's mean.

Several points about the PS class in general are inferred from the 26 May 1996 MCS and its similarity to the class means: *1)* The orientation of the boundary was apparently crucial to the *prolonged* orientation of the convective line parallel to the middle and upper tropospheric winds. For the 26 May 1996 MCS, a fortuitous colocation of previous thunderstorm outflows and the Caprock Escarpment provided a linear trigger roughly parallel to the upper level flow. If the orientation of the triggering boundary *is* a constraint upon whether a case becomes PS, then it is not surprising that they are less frequent than TS cases. The appropriate alignment of a boundary with the upper-level winds may be some-

what unusual (recall that PS cases accounted for 21% of all MCSs in this study). *2)* For this case, the line-parallel winds were quite deep (extending down to near the surface). The strong signal in the 0-6 km PS mean wind fields, as discussed in Chapter 5, may be related to the added importance of lower tropospheric winds in PS cases (as compared to the other classes of MCS, in which lower to middle tropospheric winds might play a less significant role). *3)* Finally, the convective echoes were observed to move *along* the outflow boundary in the 26 May 1996 MCS, to the left of its leading edge, an example of "training" reflectivity cores. As discussed in Chapter 5, however, many PS cases were observed to "backbuild" to the right of their leading edges. A relatively weak *mean* signal was observed for $\mathbf{c}_{\|}$ in PS cases, with a fairly high standard deviation. In fact, PS MCSs were approximately evenly distributed between "backbuilders" and "echo-trainers", yielding a near-zero mean line-parallel storm motion component.

6.3 General insight into predictability of MCS archetypes

It seems worthwhile to note that, to the degree of representativeness afforded by the case studies in this chapter, the orientation and sense of circulation associated with thermal boundaries is important to the eventual MCS precipitation distribution. In a sense, therefore, the forecasting of MCS archetypes requires the accurate prognostication of boundary locations and alignments, as well as an accurate depiction of low-level buoyancy transport. The lead time with which such a forecast can be accurately made may seem quite short based upon the two case studies presented here, which occurred along mesoscale outflow boundaries that were oriented, with respect to the wind profile, in a particular way. Note, however, in Table 4.2 that outflow boundaries were not among the most common triggers for MCSs. The possible reasons for this are beyond the scope of the present discussion, although the failure of NCEP to analyze the boundary for the 26 May 1996 MCS suggests that they may be underestimated in the present study. Nevertheless, the observed frequency of MCSs near persistent linear boundaries provides a glimmer of hope for the forecaster (given

the possibilities of boundary detection by Doppler radars operating in "clear-air mode", for example). While not explicitly investigated here, it is believed that LS and PS cases along synoptic boundaries (e.g. cold fronts and warm fronts) instead of outflow boundaries probably have similar relationships to the upper-level wind field. This would allow for a broader generalization of the results presented here, suggesting that the forecaster may be able to predict linear MCS archetypes when obvious triggers are present. More cases studies will help to evaluate this hypothesis.

Chapter 7

CONCLUDING REMARKS

7.1 Summary

Using national 2-km base scan reflectivity data, 88 linear mesoscale convective systems (MCSs) were identified over the central Plains during May 1996 and May 1997. Within this manuscript, *linear mesoscale convective systems* were defined as convective lines, with their attendant stratiform rain, that exceeded 100 km in horizontal extent for longer than 3 hours. The mean synoptic environment attending the MCSs in this investigation corresponded well with those discovered in previous studies. In general, convective systems were located in a region of lower tropospheric warm air advection in advance of an approaching upper tropospheric short wave trough, similar to the MCC environments reported by Maddox (1983). It was found that 31% of the studied cases occurred above frontal inversions (i.e. were *elevated*). The remaining linear *warm sector* MCSs occurred predominantly near linear surface boundaries, most frequently near cold fronts. Related to this result, linear MCS frequency was maximized when surface cyclones traversed the region. Periods of MCS activity were found to have, on average, weaker westerly wind shear than inactive periods, a result that supports modeling results obtained by Thorpe et al. (1982). A nocturnal maximum in linear MCSs, similar to those noted by Maddox (1980) and Houze et al (1990, or HSD90), was noted during the study period. Additionally, a less well-documented secondary maximum occurred near local sunrise, a phenomenon similar to that observed by Geerts (1998) for the southeastern United States.

Observation of the radar data revealed three prominent modes of linear MCS precip-

itation distribution: those with trailing stratiform rain (TS), leading stratiform rain (LS), and parallel stratiform rain (PS). A taxonomy using these three archetypes was therefore proposed. Among the 88 cases during May 1996 and May 1997, 51 fit the TS archetype and 17 each fit the LS and PS archetypes (3 were unclassifiable). The prominence of the TS mode confirmed previous findings by HSD90 for Oklahoma. Warm sector TS MCSs were found to persist the longest of the three classes by nearly a factor of two (12.1 hours, versus 6.8 and 6.4 hours for LS and PS cases respectively). TS MCSs also moved the fastest of the linear MCS groups, while LS cases on average moved the slowest.

For warm sector cases rawinsonde, wind profiler, and NCEP reanalysis data were utilized to characterize the mean environment near each linear MCS mode. TS MCSs existed, on average, in more unstable airmasses than did LS or PS cases, a finding consistent with their longer durations. All three archetypes were observed to move roughly along the 1000-500 hPa thickness contours, a finding that agrees with results reported by Merritt and Fritsch (1984). Based upon pre-storm raobs, it was found that TS MCSs generally occurred in environments conducive to stronger cold pools than those of PS cases, which in turn occurred in environments conducive to stronger cold pools than those of LS MCSs. In general, transport of lower tropospheric momentum and advection by middle and upper tropospheric winds were both consistent with the direction of stratiform rain displacement from the observed convective lines. Rearward storm-relative advection of hydrometeors was indicated for TS cases, while the reverse was implied for LS MCSs. Deep tropospheric winds blew *along* the convective line, on average, for PS cases.

Two case studies were performed in order to investigate in greater detail the local conditions associated with an LS and a PS MCS. The 18 May 1997 LS MCS was apparently related to the juxtaposition of a surface cold pool, a lower-tropospheric axis of high θ_e at its back edge, and a low-level jet. Notably, inflow of bouyant air to the storm appeared to be aloft at the trailing edge of the MCS, near the level of a lower tropospheric wind maximum. The case had very weak upper-level wind shear, such that the mechanism observed by Grady

and Verlinde (1997) for an LS squall line (strong upper tropospheric shear contributing to the leading anvil) was probably not relevant to the 18 May 1997 MCS. The 26 May 1996 PS MCS occurred along a quasi-stationary outflow boundary that encountered an escarpment and apparently produced a persistent solenoidal circulation there. Throughout most of the troposphere, winds were strong and parallel to the convective line, suggesting that advection of hydrometeors played a significant role in the PS rain distribution. Decay of the MCS may have been related to convective stabilization of the environment; it was noted that the positive feedback due to gravity waves from stratiform rain regions, as discussed by Mapes (1993), would not contribute to the longevity of PS MCSs due to the lateral displacement of the stratiform rain region from the convective line.

In summation, statistically significant variations in many environmental parameters between the linear MCS classes were noted, supporting the hypothesis that dynamical differences exist between the three archetypes. This study was able to address those differences in only a cursory way due to relatively coarse data. The present results should, nevertheless, call meteorologists' attention to the spectrum of linear convective modes over the central United States and inspire further research into the 3-dimensional structure and dynamics of each class. Suggestions for such future investigations are presented in Section 7.3.

7.2 Thoughts on relevance

In commenting on a previous effort to classify MCSs (by Blanchard 1990), Doswell (1990) opined that: "...a radar based echo classification scheme for mesoscale convective systems... is a laudable effort and... can become a valuable contribution to our understanding of such storm systems and their recognition by field forecasters," a belief that I share and that has motivated the present study. As has been emphasized, the taxonomy presented here is founded solely on the characteristics of MCSs as observed from 2-km base scan radar data. An ideal taxonomy of MCSs would be based largely upon the physics of its member archetypes, a goal that this study could not fully achieve with the datasets

used (beyond the somewhat speculative interpretation of nearby wind fields). However, I take comfort in Doswell's reflection: "it may be a *long* time before we have a taxonomy for mesoscale convective systems that is *truly* physical rather than keyed to one or another set of observations" (emphasis mine).

Doswell insisted that, "a proper taxonomy must depend on *readily identifiable* characteristics" (emphasis mine), a requirement that I feel is met by the classification scheme presented in Chapter 5. While the archetypes I suggest *were* evaluated *subjectively*, I am convinced that others would concur with my assessment of each case's reflectivity pattern. Even so, Doswell (1990) pointed out that, "...the development of a taxonomy almost invariably means that the author's view will be disputed." While the MCS organization *mechanisms* that I've inferred are open to reinterpretation, the radar-based taxonomy itself seems to have some basis. Indeed, Schiesser et al. (1995) produced a figure depicting quite similar modes of linear convection for a study of Swiss MCSs. Nevertheless, more work is needed to ascertain the degree to which the populations in this limited study correspond to more spatially and temporally extensive samples.

7.3 Indications for future work

This paper is but an initial survey of linear MCSs for a relatively short period and confined geographic region. The findings herein require testing and verification with cases collected from a longer sample time. Particularly, the present results are probably dependent upon the chosen time of year: as upper tropospheric winds and frequency and speed of surface boundaries change throughout the seasons, the observed linear MCS distributions may also change. In addition, information about the prominence of the identified convective modes in other regions of the United States and the world is desirable in order to further qualify the representativeness of this and numerous other Great Plains MCS studies. While the results of this investigation are promising, conclusions can *only* be definitively made about the linear MCSs I've documented and studied. Broad inferences about the general

population of convective systems are tenuous based upon such a limited number of cases. Notably, however, the LS and PS archetypes were also observed during a survey of May 1996 MCSs over the *entire* United States. The reader will also recall that non-warm sector MCSs were omitted from this study, a void that could be remedied by future work. Hopefully, meteorologists will take up the gauntlet and attend to the existence of these archetypes in *other* MCS populations.

In addition to further testing of the taxonomy, greater insight into the vertical structure and internal flow features of the LS and PS archetypes is needed. My view of storms was restricted to the composited radar base scans, which gave a decidedly 2-dimensional view of reflectivity. Future case studies should include multiple radar elevation scans, as well as range-height indicator (RHI) imagery, to depict the depth and movement of convective and stratiform hydrometeors. Further, the addition of dual-Doppler radar data (such as used by Grady and Verlinde 1997), when available, would help to demonstrate recurrent flow features for LS and PS MCSs, much as has been done for many TS cases. The incorporation of lightning data could also enhance the knowledge of cloud microphysics in non-TS MCSs. Only with full knowledge of these three-dimensional structures can robust conceptual models for the less-studied archetypes be developed.

Future investigation of the possible sub-divisions within the three major classes of linear MCS are also recommended. In particular, the 18 May 1997 LS case study suggested a tantalizing possibility: that the LS structure may arise from several unique scenarios. Fankhauser et al. (1992) found that an MCS with a leading anvil had many quasi-supercellular characteristics. Grady and Verlinde (1997) attributed the forward distribution of rainfall in a High Plains squall line to strong upper tropospheric wind shear. The 18 May 1997 case study suggested yet another mechanism: initiation and sustenance by inflow *behind* the convective line (eliminating the possibly detrimental effects of the pre-line rain region on inflow air). More detailed and frequent observations of LS MCSs may provide insight into a dominant mode of formation, or may reveal a broad spectrum

of environmental scenarios and convective structures.

Finally, sensitivity studies within numerical models are indicated. Several hypotheses relating the distribution of stratiform rain to lower, middle, and upper tropospheric winds were suggested and evaluated with the observational data from this study, none of which were disproved. Can the PS archetype arise when tropospheric line-parallel winds are not particularly deep? To what degree can the initial tilting of convective towers and positive cold pool feedback suggested in Section 5.2.5 determine the final MCS precipitation structure of TS and LS cases? Are particular environmental scenarios (among the several suggested above) exceptionally favorable for LS MCSs? Only in the controlled environment of a numerical model will these questions receive a detailed treatment.

The desired end of the above recommendations is a rigorous conceptual model for *each* of the three linear MCS archetypes (only the TS is currently well known). From such a conceptual model, improved recognition and forecasting of linear MCS modes may be possible, the implications of which were discussed in Chapter 1. As well, numerical models may better parameterize the effects of mesoscale organized convection if different modes and their attendent effects can be diagnosed. Fankhauser et al. (1992) noted that early studies of line convection (e.g. Newton and Newton 1959) emphasized *leading anvils*. The current work will, hopefully, (re)turn meteorologists' attention to the LS and PS archetypes in the future.

REFERENCES

Alexander, G.D. and G.S. Young, 1992: The relationship between EMEX mesoscale precipitation feature properties and their environmental characteristics. *Mon. Wea. Rev.*, **120**, 554-564.

Arritt, R.W., T.D. Rink, M. Segal, D.P. Todey, C.A. Clark, M.J. Mitchell, and K.M. Labas, 1997: The Great Plains low-level jet during the warm season of 1993. *Mon. Wea. Rev.*, **125**, 2176-2192.

Atlas, D., R. Tatehira, R.C. Srivastava, W. Marker, and R.E. Carbone, 1969: Precipitation-induced mesoscale wind perturbations in the melting layer. *Quart. J. R. Met. Soc.*, **95**, 544-560.

Augustine, J.A., and F. Caracena, 1994: Lower-tropospheric precursors to nocturnal MCS development over the central United States. *Wea. Forecasting*, **9**, 116-135.

Augustine, J.A. and K.W. Howard, 1988: Mesoscale Convective Complexes over the United States during 1985. *Mon. Wea. Rev.*, **116**, 685-701.

Augustine, J.A. and K.W. Howard, 1991: Mesoscale Convective Complexes over the United States during 1986 and 1987. *Mon. Wea. Rev.*, **119**, 1575-1589.

Barnes, G.M. and Sieckman, 1984: The Environment of Fast- and Slow-Moving Tropical Mesoscale Convective Cloud Lines. *Mon. Wea. Rev.*, **112**, 1782-1794.

Barth, M.F., R.B. Chadwick, and D.W. van de Kamp, 1994: Data processing algorithms used by NOAA's wind profiler demonstration network. *Ann. Geophysicae*, **12**, 518-528.

Bjerknes, J., and H. Solberg, 1922: Life cycle of cyclones and the polar front theory of atmospheric circulation. *Geofys. Publ.*, **3**, No. 1, 1-18.

Blanchard, D.O., 1990: Mesoscale Convective Patterns of the Southern High Plains. *Bull. Amer. Meteor. Soc.*, **71**, 994-1005.

Bluestein, H.B. and M.H. Jain, 1985: Formation of mesoscale lines of precipitation: Severe squall lines in Oklahoma during the spring. *J. Atmos. Sci.*, **42**, 1711-1732.

Bluestein, H.B., G.T. Marx and M.H. Jain, 1987: Formation of Mesoscale Lines of Precipitation: Nonsevere Squall Lines in Oklahoma during the Spring. *Mon. Wea. Rev.*, **115**, 2719-2727.

Bluestein, H.B., and C.R. Parks, 1983: Synoptic and photographic climatology of low-precipitation severe thunderstorms in the Southern Plains. *Mon. Wea. Rev.*, **111**, 2034-2046.

Bolton, D., 1980: The computation of equivalent potential temperature. *Mon. Wea. Rev.*, **108**, 1046-1053.

Bretherton, C.S., 1997: Entrainment, detrainment and mixing in atmospheric convection. In *The physics and parameterization of moist atmospheric convection*, R.K. Smith (ed.). Kluwer Academic Publishers, The Netherlands. 211-230.

Bretherton, C.S. and P.K. Smolarkiewicz, 1989: Gravity waves, compensating subsidence and detrainment around cumulus clouds. *J. Atmos. Sci.*, **46**, 740-759.

Brooks, H.E., Doswell, C.A. III, and J. Cooper, 1994: On the Environments of Tornadic and Nontornadic Mesocyclones. *Wea. Forecasting*, **9**, 606-618.

Browning, K.A., 1964: Airflow and precipitation trajectories within severe local storms which travel to the right of the mean wind. *J. Atmos. Sci.*, **21**, 634-639.

Carbone, R.E., 1982: Severe frontal rainband, Pt. 1, Stormwide hydrodynamic structure. *J. Atmos. Sci.*, **39**, 258-279.

Colman, B.R., 1990: Thunderstorms above frontal surfaces in environments without positive CAPE. Part I: A climatology. *Mon. Wea. Rev.*, **118**, 1103-1121.

Corfidi, S.F., 1997: Forecasting MCS mode and motion. Preprints, 28th Conf. on Radar Meteor., Austin, TX, Amer. Meteor. Soc., 626-629.

Cotton, W.R., M.-S. Lin, R.L. McAnelly and C.J. Trenback, 1989: A Composite Model of Mesoscale Convective Complexes. *Mon. Wea. Rev.*, **117**, 765-783.

Dallal, G.E., and L. Wilkinson, 1986: An Analytic Approximation to the Distribution of Lilliefors's Test Statistics for Normality. *Amer. Statistician*, **40**, 294-296.

Davies, J.M., and R.H. Johns, 1993: Some wind and instability parameters associated with strong and violent tornadoes. 1. Wind shear and helicity. *The tornado: its structure, dynamics, prediction, and hazards,* C.R. Chruch, Ed., Amer. Gephys. Union, 573-582.

Davies-Jones, R.P., D.W. Burgess, and M. Foster, 1990: Test of helicity as a forecast parameter. *Preprints, 16th Conf. on Severe Local Storms,* Kananaskis Park, Alberta, Amer. Meteor. Soc., 588-592.

Doswell, C.A. III, 1990: Comments, *Bull. Amer. Meteor. Soc.*, **72**, 389-390.

Droegemeier, K.K., S.M. Lazarus, and R. Davies-Jones, 1993: The influence of helicity on numerically simulated convective storms. *Mon. Wea. Rev.*, **121**, 2005-2029.

Elliott, W.P., and D.J. Gaffen, 1991: The utility of radiosonde humidity archives for climate studies. *Bull. Amer. Meteor. Soc.*, **72**, 1507-1520.

Emanuel, K.A., 1986: Overview and Definition of Mesoscale Meteorology. In *Mesoscale Meteorology and Forecasting*, P.S. Ray (Ed.), Amer. Meteor. Soc., Boston, 1-17.

Emanuel, K.A., 1994: *Atmospheric Convection.* Oxford Univ. Press, New York, 580 pp.

Fankhauser, J.C., G.M. Barnes, and M.A. LeMone, 1992: Strcture of a Midlatitude Squall Line Formed in Strong Unidirectional Shear. *Mon. Wea. Rev.*, **120**, 237-260.

Foster, D.S., 1958: Thunderstorm gusts compared with computed downdraft speeds. *Mon. Wea. Rev.*, **86**, 91-94.

Fovell, R.G., and P.S. Dailey, 1995: The temporal behavior of numerically simulated mulitcell-type storms. Part I: Modes of behavior. *J. Atmos. Sci.*, **52**, 2073-2095.

Fovell, R.G., and Y. Ogura, 1988: Numerical simulation of a midlatitude squall line of two dimensions. *J. Atmos. Sci.*, **45**, 3846-3879.

Fritsch, J.M., J.D. Murphy, and J.S. Kain, 1994: Warm core vortex amplication over land. *J. Atmos, Sci.*, **51**, 1780-1807.

Gallus, W.A. and R.H. Johnson, 1992: The momentum budget of an intense midlatitude squall line. *J. Atmos. Sci.*, **49**, 422-450.

Gallus, W.A. and R.H. Johnson, 1995: The Dynamics of Circulations within the Trailing Stratiform Regions of Squall Lines. Part II: Influence of the Convective Line and Ambient Environment. *J. Atmos. Sci.*, **52**, 2188-2211.

Geerts, B., 1998: Mesoscale convective systems in the Southeast United States during 1994-95: A survey. *Wea. Forecasting*, **13**, 860-869.

Gilmore, M.S., and L.J. Wicker, 1998: The influence of midtropospheric dryness on supercell morphology and evolution. *Mon. Wea. Rev.*, **126**, 943-958.

Golden, J.H., R. Serafin, V. Lally, and J. Facundo, 1986: Atmospheric Sounding Systems. In *Mesoscale Meteorlology and Forecasting*, P.S. Ray (Ed.), Amer. Meteor. Soc., Boston, 50-70.

Gould, S.J., 1989: *Wonderful Life.* W.W. Norton and Co., Inc., 347 pp.

Grady, R.L., and J. Verlinde, 1997: Triple-Doppler analysis of a discretely propagating, long-lived, High Plains squall line. *J. Atmos. Sci.*, **54**, 2729-2748.

Gray, W.M., and R.W. Jacobson Jr., 1977: Diurnal variation of deep cumulus convection. *Mon. Wea. Rev.*, **105**, 1171-1188.

Hashem, M.S., and M.I. Biggerstaff, 1997: Organization of convection in mesoscale systems. Preprints, 28th Conf. on Radar Meteor., Austin, TX, Amer. Meteor. Soc., 483-484.

Hilgendorf, E.R., 1996: Evolution of precipitation structures within mesoscale convective systems. Colorado State Univ., Dept. of Atmos. Sci., Bluebook #624.

Hilgendorf, E.R., and R.H. Johnson, 1997: A study of the evolution of mesoscale convective systems using WSR-88D data. *Wea. Forecasting*, **13**, 437-452.

Hobbs, P.V., J.D. Locatelli, and J.E. Martin, 1996: A new conceptual model for cyclones generated in the lee of the Rocky Mountains. *Bull. Amer. Meteor. Soc.*, **77**, 1169-1178.

Houghton, H.G., 1968: On precipitation mechanisms and their artificial modification. *J. Appl. Meteor.*, **7**, 851-859.

Houze, R.A., Jr., 1993: *Cloud Dynamics.* Academic Press, Inc., San Diego, 573 pp.

Houze, R.A., Jr., and E.N. Rappaport, 1984: Air motions and precipitation structure of an early summer squall line over the eastern tropical Atlantic. *J. Atmos. Sci.*, **41**, 553-574.

Houze, R.A., Jr., S.A. Rutledge, M.I. Biggerstaff, and B.F. Smull, 1989: Interpretation of Doppler weather radar displays of midlatitude mesoscale convective systems. *Bull. Amer. Meteor. Soc.*, **70**, 608-619.

Houze, R.A., Jr., B.F. Smull, and P. Dodge, 1990: Mesoscale organization of springtime rainstorms in Oklahoma. *Mon. Wea. Rev.*, **118**, 613-654.

Huschke, R.E., 1959: *Glossary of Meteorology.* Amer. Meteor. Soc., 638 pp.

Kalnay, E., and Coauthors, 1996: The NCEP/NCAR 40-year Reanalysis Project. *Bull. Amer. Meteor. Soc.*, **77**, 437-471.

Kane, R.J. Jr., C.R. Chelius, and J.M. Fritsch, 1987: Precipitation characteristics of mesoscale convective weather systems. *J. Climate Appl. Meteor.*, **25**, 1345-1357.

Kessinger, C.J., P.S. Ray, and C.E. Hane, 1987: The Oklahoma squall line of 19 May 1977. Part I: A multiple Doppler analysis of convective and stratiform structure. *J. Atmos. Sci.*, **44**, 2840-2864.

Lafore, J.-P., and M.W. Moncrieff, 1989: A Numerical Investigation of the Organization and Interaction of the Convective and Stratiform Regions of Tropical Squall Lines. *J. Atmos. Sci.*, **46**, 521-544.

Laing, A.G., and J.M. Fritsch, 1993a: Mesoscale convective complexes over the Indian monsoon region. *J. Climate*, **6**, 911-919.

Laing, A.G., and J.M. Fritsch, 1993b: Mesoscale convective complexes in Africa. *Mon. Wea. Rev.*, **121**, 2254-2263.

Laing, A.G., and J.M. Fritsch, 1997: The global population of mesoscale convective complexes. *Quart. J. R. Meteor. Soc.*, **123**, 389-405.

Laing, A.G., and J.M. Fritsch, 1998: The large-scale environments of different organizational modes of mesoscale convective overturning. *Mon. Wea. Rev.*, accepted.

LeMone, M.A., 1988: Perturbation pressure fields measured by aircraft around the cloud base updraft of deep convective clouds. *Mon. Wea. Rev.*, **116**, 313-327.

LeMone, M.A., and M.W. Moncrieff, 1994: Momentum and mass transport by convective bands: comparisons of highly idealized dynamical models to observations. *J. Atmos. Sci.*, **51**, 281-305.

LeMone, M.A., E.J. Zipser, and S.B. Trier, 1998: The Role of Environmental Shear and Thermodynamic Conditions in Determining the Structure and Evolution of Mesoscale Convective Systems during TOGA COARE. *J. Atmos. Sci.*, **55**, 3493-3518.

Loehrer, S.M. and R.H. Johnson, 1995: Surface Pressure and Precipitation Life Cycle Characteristics of PRE-STORM Mesoscale Convective Systems. *Mon. Wea. Rev.*, **123**, 600-621.

Ludlam, F.H., 1963: Severe local storms: a review. *Meteor. Monogr.*, **5**, Amer. Meteor. Soc., 1-30.

McAnelly, R.L., and W.R. Cotton, 1986: Meso-β-scale characteristics of an episode of meso-α-scale convective complexes. *Mon. Wea. Rev.*, **114**, 1740-1770.

Maddox, R.A., 1980: Mesoscale convective complexes. *Bull. Amer. Meteor. Soc.*, **61**, 1374-1387.

Maddox, R.A., 1981: Satellite depiction of the life cycle of a mesoscale convective complex. *Mon. Wea. Rev.*, **109**, 1583-1586.

Maddox, R.A., D.M. Rodgers, and K.W. Howard, 1982: Mesoscale convective complexes over the United States during 1981, annual summary. *Mon. Wea. Rev.*, **110**, 1501-1514.

Maddox, R.A., 1983: Large-Scale Meteorological Conditions Associated with Midlatitude Mesoscale Convective Complexes. *Mon. Wea. Rev.*, **111**, 1475-1493.

Maddox, R.A. and C.A. Doswell III, 1982: An Examination of Jet Stream Configurations, 500-mb Vorticity Advection and Low-Level Thermal Advection Patterns During Extended Periods of Intense Convection. *Mon. Wea. Rev.*, **110**, 184-197.

Mapes, B.E., 1993: Gregarious tropical convection. *J. Atmos. Sci.*, **50**, 2026-2037.

Merritt, J.H., and J.M. Fritsch, 1984: On the movement of the heavy precipitation areas of mid-latitude mesoscale convective complexes. Preprints, 10th Conference on Weather Forecasting and Analysis, Tampa, FL, Amer. Meteor. Soc., 520-536.

Miller, P.A., M.F. Barth, J.R. Smart, and L.A. Benjamin, 1997: The extent of bird contamination in the hourly winds measured by the NOAA profiler network: Results before and after implementation of the new bird contamination quality control check. Preprints, First Symp. on Integrated Observing Systems, Long Beach, CA, Amer. Meteor. Soc., 138-144.

Moncrieff, M.W., 1992: Organized convective systems: Archetypal dynamical models, mass and momentum flux theory, and parameterization. *Q. J. R. Meteor. Soc.*, **118**, 819-850.

Nachamkin, J.E., 1998: Observational and Numerical Analysis of the Genesis of a Mesoscale Convective System. Colorado State Univ., Dept. of Atmos. Sci., Bluebook #643.

Newton, C.W., 1950: Structure and Mechanism of the Prefrontal Squall Line. *J. Meteor.*, **7**, 210-222.

Newton, C.W., 1963: Dynamics of severe convective storms. *Meteor. Monogr.*, **5**, Amer. Meteor. Soc., 33-58.

Newton, C.W., 1966: Circulations in large sheared cumulonimbus. *Tellus*, **18**, 699-712.

Newton, C.W. and J.C. Fankhauser, 1964: On the movements of convective storms, with emphasis on size discrimination in relation to water-budget requirements. *J. Appl. Meteor.*, **3**, 651-668.

Newton, C.W., and H.R. Newton, 1959: Dynamical interactions between large convective clouds and environment with vertical shear. *J. Meteor.*, **16**, 483-496.

Orlanksi, I., 1975: A rational subdivision of scales for atmospheric processes. *Bull. Amer. Meteor. Soc.*, **56**, 527-530.

Orville, H.D., 1968: Ambient wind effects on the initiation and development of cumulus cloud over mountains. *J. Atmos. Sci.*, **25**, 385-403.

Parsons, D.B., 1992: An explanation for intense frontal updrafts and narrow cold-frontal rainbands. *J. Atmos. Sci.*, **49**, 1810-1825.

Pedgley, D.E., 1962: A meso-synoptic analysis of the thunderstorms on 28 August 1958. Brit. Meteor. Off. Geophys. Mem. No. 106, 74 pp.

Purdom, J.F.W., 1986: Convective-scale interaction: arc cloud lines and the development and evolution of deep convection. Colorado. State Univ., Ft. Collins, Dept. of Atmospheric Sciences Paper No. 408, 1986. 197 p.

Rasmussen, E. N., and J. M. Straka, 1998: Supercell morphology variations. Part I. Observations of upper-level storm-relative flow. *Mon. Wea. Rev.*; accepted for publication.

Rasmuseen, E.N., and R.B. Wilhelmson, 1983: Relationships between storm characteristics and 1200 GMT hodographs, low-level shear, and stability. *Preprints*, 13th Conf on Severe Local Storms, Tulsa, Oklahoma, Amer. Meteor. Soc., J5-J8.

Rickenbach, T.M., and S.A. Rutledge, 1998: Convection in TOGA COARE: Horizontal scale, morphology, and rainfall production. *J. Atmos. Sci.*, **55**, 2715-2729.

Rodgers, D.M., K.W. Howard, and E.C. Johnston, 1983: Mesoscale convective complexes over the United States during 1982. *Mon. Wea. Rev.*, **111**, 2363-2369.

Rodgers, D.M., M.J. Magnano, and J.H. Arns, 1985: Mesoscale convective complexes over the United States during 1983. *Mon. Wea. Rev.*, **113**, 888-901.

Rutledge, S.A., and R.A. Houze Jr., 1987: Diagnostic modeling study of the trailing stratiform region of a midlatitude squall line. *J. Atmos. Sci.*, **44**, 2640-2656.

Rotunno, R., J.B. Klemp and M.L. Weisman, 1988: A theory for strong, long-lived squall lines. *J. Atmos. Sci.*, **45**, 463-485.

Sanders, F., and C.A. Doswell III, 1995: A Case for Detailed Surface Analysis. *Bull. Amer. Meteor. Soc.*, **76**, 505-521.

Schiesser, H.H., R.A. Houze Jr., and H. Huntrieser, 1995: The Mesoscale Structure of Severe Precipitation Systems in Switzerland. *Mon. Wea. Rev.*, **123**, 2070-2097.

Schwartz, B.E., and C.A. Doswell III, 1991: North American rawinsonde observations: Problems, concerns, and a call to action. *Bull. Amer. Meteor. Soc.*, **72**, 1885-1896.

Siegel, A.F., and C.J. Morgan, 1996: *Statistics and Data Analysis.* 2nd ed. Wiley and Sons, Inc., 635 pp.

Simpson, J.E., 1987: *Gravity currents in the environment and the laboratory.* John Wiley and Sons, New York, 244 pp.

Skamarock, W.C., M.L. Weisman and J.B. Klemp, 1994: Three dimensional evolution of simulated long-lived squall lines. *J. Atmos. Sci.*, **51**, 2563-2584.

Smull, B.F., and J.A. Augustine, 1993: Multiscale analysis of a mature mesoscale convective complex. *Mon. Wea. Rev.*, **121**, 103-132.

Smull, B.F. and R.A. Houze Jr., 1985: A Midlatitude Squall Line with a Trailing Region of Stratiform Rain: Radar and Satellite Observations. *Mon. Wea. Rev.*, **113**, 117-133.

Steiner, M., R.A. Houze Jr., and S.E. Yuter, 1995: Climatological characterization of three-dimensional storm structure from operational radar and rain gauge data. *J. Appl. Meteor.*, **34**, 1978-2007.

Thorpe, A.J., M.J. Miller, and M.W. Moncrieff, 1982: Two-dimensional convection in non-constant shear: A model of mid-latitude squall lines. *Q. J. R. Meteor. Soc.*, **108**, 739-762.

Trier, S.B., and D.B. Parsons, 1993: Evolution of environmental conditions preceding the development of a nocturnal Mesoscale Convective Complex. *Mon. Wea. Rev.*, **121**, 1078-1098.

Uccellini, L.W., and D.R. Johnson, 1979: The Coupling of Upper and Lower Tropospheric Jet Streaks and Implications for the Development of Severe Convective Storms. *Mon. Wea. Rev.*, **107**, 682-703.

Velasco, I. and J.M. Fritsch, 1987: Mesoscale convective complexes in the Americas. *J. Geophys. Res.*, **29**, 9591-9613.

Wallace, J.M., 1975: Diurnal variations in precipitation and thunderstorm frequency over the conterminous United States. *Mon. Wea. Rev.*, **103**, 406-419.

Walpole, R.E., and R.H. Myers, 1989: *Probability and Statistics for Engineers and Scientists*, 4th ed. Macmillan Publ. Co., New York, 765 pp.

Weber, B.L., D.B. Wuertz, D.C. Welsh, and R. McPeek, 1993: Quality control for profiler measurements of winds and RASS temperatures. *J. Atmos. Oceanic Technol.*, **10**, 452-464.

Weisman, M.L., and J.B. Klemp, 1982: The dependence of numerically simulated convective storms on vertical wind shear and buoyancy. *Mon. Wea. Rev.*, **110**, 504-520.

Weisman, M.L., J.B. Klemp and R. Rotunno, 1988: Structure and Evolution of Numerically Simulated Squall Lines. *J. Atmos. Sci.*, **45**, 1990-2013.

Wilczak, J.M., and Coauthors, 1995: Contamination of wind profiler data by migrating birds: Charactertistics of corrupted data and potential solutions. *J. Atmos. Oceanic Technol.*, **12**, 449-467.

Zipser, E.J., 1977: Mesoscale and convective-scale downdrafts as distinct components of squall-line structure. *Mon. Wea. Rev.*, **105**, 1568-1589

Zipser, E.J., 1982: Use of a conceptual model of the life cycle of mesoscale convective systems to improve very-short-range forecasts. *Nowcasting*, K. Browning, Ed., Academic Press, 191-204.

Appendix A

STATISTICS OF OMITTED CASES

Naturally, the omission of cases from a dataset produces suspicion. One particular species of MCS may have frequently occurred in warm advection above a frontal inversion, thus biasing the data once elevated cases were removed. Similarly, had a particular wind profiler often been contaminated during the study period (for whatever reason), fewer data would exist with which to evaluate an archetype whose members frequently passed near such a site. In order to quantify the effects of case omissions, several tables are here provided.

The effect of rawinsonde omissions on the number of cases was similar for all archetypes (Table A.1). There were more elevated cases during May 1996 than during May 1997 (despite fewer total cases for the period), suggesting some fundamental difference between the synoptic regimes for the two periods (a discrepancy discussed in Section 4.1). Even though a disproportionate amount of the 1996 cases were elevated, however, the distribution of elevated cases by archetype was fairly even (with a slightly smaller percentage of elevated PS cases). Thus, while the elimination of elevated and contaminated cases may have intro-

Table A.1: Information on omitted cases. "Other omissions" include the removal of cases due to contamination by precipitation or lack of a suitably representative observation.

MCS type	total cases	# elevated	% elevated	other omissions	# retained	% retained
unclass.	3	1	33%	0	2	67%
LS	17	5	29%	1	11	65%
PS	17	3	18%	3	11	65%
TS	51	18	35%	1	32	63%
1996	33	17	52%	0	16	48%
1997	55	10	18%	5	40	73%

Table A.2: Information on contaminated and omitted wind profiler observations. Column 3 represents data from omitted *cases* (cf. Table A.1). Column 4 represents data omitted due to failed quality control tests.

MCS type	total obs	discarded case obs	bad QC obs	retained obs	% retained
unclass.	7	1	4	2	33%
LS	49	13	14	22	45%
PS	51	13	13	25	49%
TS	136	35	50	51	38%
1996	87	32	32	23	26%
1997	156	30	49	77	49%

duced some bias into the data, no MCS archetype was especially depleted by the omission of cases.

As well, a similar percentage of profiler observations were retained for all three MCS archetypes (Table A.2). The omissions of profiler data were due to both general removal of cases (as given in Table A.1), and the removal of individual observations contaminated by migrating birds or failing NOAA quality control checks (as detailed in Section 3.4). A discrepancy between May 1996 and May 1997 omissions again appeared in the profiler omissions. While the percentage of "bad" data remained relatively constant from year to year (36% vs. 31%), the percentage of data omitted due to elevated cases and "other discards" is disproportionately higher in May 1996. This is not surprising given the case omission statistics presented in Table A.1. Altogether, 64% of the initial cases were retained, while 41% of the initial wind profiler observations were retained. The difference between these two percentages approximately represents the effects of bad or contaminated wind profiler data (as any profiler data associated with discarded cases were automatically removed).

Reassuringly, none of the three MCS archetypes lost a disproportionate number of observations due to the omission of elevated and contaminated cases (Table A.3). It appears that the omission of elevated cases and bad observations does not preferentially affect any one subset of MCSs in this study. This provides some confidence that no strong bias was introduced into the data from the case and data omissions.

Table A.3: Distribution of cases and observations by archetype.

MCS type	% of initial cases	% of retained cases	% of retained profiler obs
unclass.	3%	4%	2%
LS	19%	20%	22%
PS	19%	20%	25%
TS	58%	57%	51%

Appendix B

RADAR REFLECTIVITY SCALE FOR FIGURES IN THIS MANUSCRIPT

As detailed in Section 3.2, the radar data used in this study are binned in 5-dBZ increments. While investigating the data, this scale proved useful in the observation of MCS evolution and the determination of archetypal similarities. In the process of producing, printing, and copying manuscripts, however, choices must often be made. In presenting the radar data, image "size" (in bytes, not physical dimension) became critical. I therefore elected to produce images with a slightly degraded reflectivity scale in order that additional examples might be included. This degradation of reflectivity resolution does not, in my opinion, lessen the readability or import of the figures in this manuscript, although the reader may judge this for him/herself (cf. Figure B.1). The location, intensity, and conformity of MCSs to precipitation archetypes are still evident in the reduced images.

The reflectivity scale presented in this manuscript is largely motivated by reflectivity thresholds for convective and stratiform rain discussed in Section 3.2. As echoes with reflectivity factors less than 20 dBZ were not considered during my investigation, I have omitted them from the figures altogether. Between 20 and 50 dBZ, 10 dBZ resolution was chosen in order to characterize the local differences in stratiform rain intensity as well as to set off individual convective cores which were embedded within lines of convective rainfall. Reflectivity factors greater than 50 dBZ were not differentiated, as values in the 50–70 dBZ range were not treated significantly differently in this study. The scale presented in Figure B.1b has been used throughout this document without the unnecessary reproduction of a color bar adjacent to every radar image.

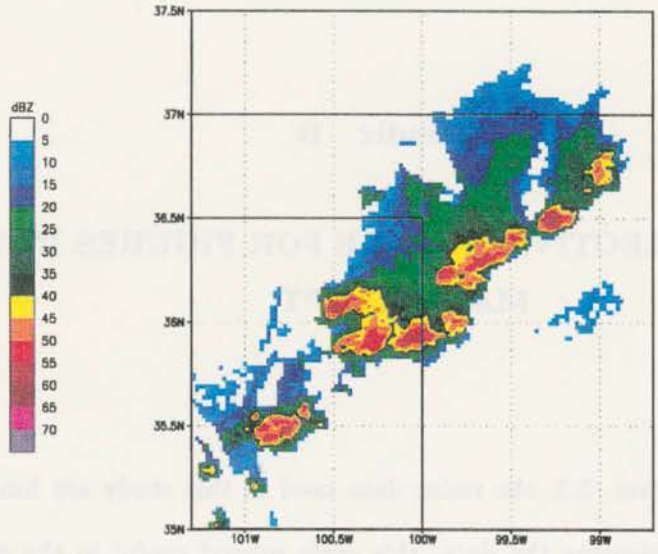

(a)

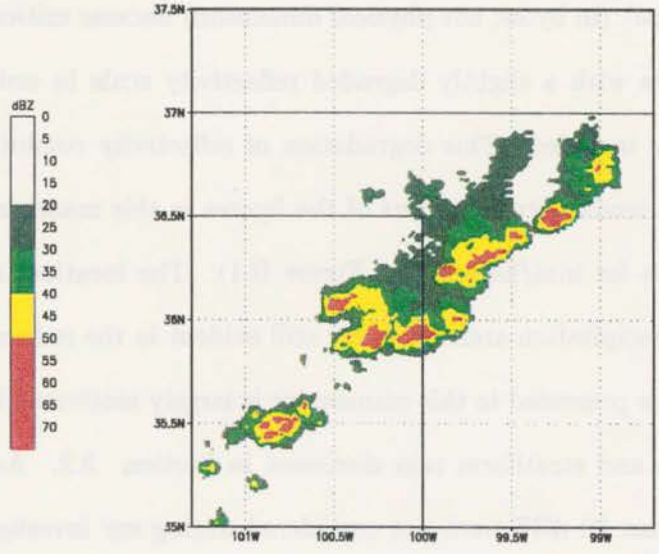

(b)

Figure B.1: Radar reflectivity scales: depiction of identical data with (a) original scale, and (b) degraded scale used within this manuscript.

Appendix C

RESULTS OF ANOVA FOR RAWINSONDE AND WIND PROFILER DATA

Table C.1: Summary of statistics for rawinsonde data. Units: J kg^{-1} for $MLCAPE$, $TCCAPE$, $pickCAPE$, CIN, $DCAPE$, $DCAPE_\rho$, and HEL. hPa for LCL, CCL, and $p(\theta_{w_{min}})$. K: LI, $\theta_{w_{min}}$, $\theta_{e_{sfc}}$, T_v, $T_{v_{Tw}}$, $T_{v_{sd}} - T_v$, $T_{v_{sd}} - T_{v_{Tc}}$, $T_{v_{sd}} - T_{v_{Tw}}$, $T_{v_{dd}} - T_v$, $T_{v_{dd}} - T_{v_{Tc}}$, and $T_{v_{dd}} - T_{v_{Tw}}$. m: $z(\theta_{w_{min}})$, and $HWBZ$. $(25.4)^{-1}$ mm: PW. %: RH_t, and RH_d. All velocity vectors: m s^{-1}. p-values are unitless.

field	LS mean	LS σ	PS mean	PS σ	TS mean	TS σ	p value	significant at 5%?
$MLCAPE$	946	757	715	859	1554	963	0.017	√
$TCCAPE$	1916	972	1416	1053	1979	991	0.274	
pick $CAPE$	1366	824	1011	736	1821	912	0.026	√
CIN	-222	105	-228	137	-152	116	0.110	
LCL	806	56	759	58	834	74	0.009	√
LFC	*no suitable transformation*							
CCL	727	67	685	68	780	78	0.002	√
LI	-3.4	2.8	-1.8	3.4	-5.3	2.4	0.001	√
$\theta_{w_{min}}$	289.0	1.5	288.5	1.7	289.0	1.0	0.511	

Table C.1: Summary of statistics for rawinsonde data. Units: J kg^{-1} for $MLCAPE$, $TCCAPE$, $pickCAPE$, CIN, $DCAPE$, $DCAPE_\rho$, and HEL. hPa for LCL, CCL, and $p(\theta_{w_{min}})$. K: LI, $\theta_{w_{min}}$, $\theta_{e_{sfc}}$, T_v, $T_{v_{Tw}}$, $T_{v_{sd}} - T_v$, $T_{v_{sd}} - T_{v_{Tc}}$, $T_{v_{sd}} - T_{v_{Tw}}$, $T_{v_{dd}} - T_v$, $T_{v_{dd}} - T_{v_{Tc}}$, and $T_{v_{dd}} - T_{v_{Tw}}$. m: $z(\theta_{w_{min}})$, and $HWBZ$. $(25.4)^{-1}$ mm: PW. %: RH_t, and RH_d. All velocity vectors: m s^{-1}. p-values are unitless.

field	LS mean	LS σ	PS mean	PS σ	TS mean	TS σ	p value	significant at 5%?
$z(\theta_{w_{min}})$	3442	2303	2774	1588	3993	1473	0.122	
$p(\theta_{w_{min}})$	654	176	673	147	603	126	0.294	
$\theta_{e_{sfc}}$	333.2	11.6	335.3	12.7	340.5	7.1	0.055	
T_v	298.8	6.8	298.1	7.9	300.3	5.1	0.540	
$T_{v_{Tw}}$	292.6	4.7	291.5	4.6	294.9	2.9	0.018	√
$T_{v_{sd}} - T_v$	-9.0	6.5	-11.1	7.2	-11.3	4.6	0.461	
$T_{v_{sd}} - T_{v_{Tc}}$	-17.7	4.7	-17.7	4.5	-16.0	4.0	0.359	
$(T_{v_{sd}} - T_{v_{Tw}})^3$	-99	75000	-233	59000	-279	54000	0.102	
$T_{v_{dd}} - T_v$	-0.6	5.8	-2.5	5.3	-4.8	3.1	0.016	√
$T_{v_{dd}} - T_{v_{Tc}}$	-9.4	3.1	-9.1	2.8	-9.5	3.1	0.924	
$T_{v_{dd}} - T_{v_{Tw}}$	5.7	5.3	4.1	3.7	0.6	3.4	0.0006	√
$HWBZ$	3210	397	2692	464	3131	388	0.005	√
$DCAPE$	924	539	822	529	1022	338	0.392	
$DCAPE_\rho$	537	185	589	253	576	163	0.776	
PW	3.18	0.59	2.34	0.52	3.35	0.70	0.0002	√
RH_t	50.4	12.5	44.2	12.9	50.4	8.3	0.217	

Table C.1: Summary of statistics for rawinsonde data. Units: J kg^{-1} for $MLCAPE$, $TCCAPE$, $pickCAPE$, CIN, $DCAPE$, $DCAPE_\rho$, and HEL. hPa for LCL, CCL, and $p(\theta_{w_{min}})$. K: LI, $\theta_{w_{min}}$, $\theta_{e_{sfc}}$, T_v, $T_{v_{Tw}}$, $T_{v_{sd}} - T_v$, $T_{v_{sd}} - T_{v_{Tc}}$, $T_{v_{sd}} - T_{v_{Tw}}$, $T_{v_{dd}} - T_v$, $T_{v_{dd}} - T_{v_{Tc}}$, and $T_{v_{dd}} - T_{v_{Tw}}$. m: $z(\theta_{w_{min}})$, and $HWBZ$. $(25.4)^{-1}$ mm: PW. %: RH_t, and RH_d. All velocity vectors: m s^{-1}. p-values are unitless.

field	LS mean	LS σ	PS mean	PS σ	TS mean	TS σ	p value	significant at 5%?
RH_d	63.4	14.7	54.7	16.2	67.0	11.4	0.034	√
$\overline{\mathbf{V}}_{0-6} : u$	10.0	3.5	10.2	5.2	9.6	4.0	0.885	
$\overline{\mathbf{V}}_{0-6} : v$	2.1	6.5	2.7	6.6	4.5	5.1	0.405	
$\overline{\mathbf{V}}_{3-10} : u$	12.5	4.7	16.1	7.3	13.8	5.8	0.344	
$\overline{\mathbf{V}}_{3-10} : v$	-1.9	8.7	1.7	9.3	5.5	5.5	0.060	
$\overline{\mathbf{V}}_{5-8} : u$	11.9	5.3	15.1	7.8	13.7	5.8	0.469	
$\overline{\mathbf{V}}_{5-8} : v$	-2.1	8.7	0.5	9.3	4.3	6.3	0.044	√
$\overline{\mathbf{V}}_{9-10} : u$	14.6	6.3	22.0	10.1	17.4	9.4	0.159	
$\overline{\mathbf{V}}_{9-10} : v$	-2.9	11.9	4.5	12.7	5.0	9.5	0.105	
$\mathbf{V}_{z_{0-1}} : u$	3.9	4.7	4.0	3.8	6.1	5.0	0.277	
$\mathbf{V}_{z_{0-1}} : v$	4.4	4.9	1.8	3.7	3.4	3.8	0.311	
$\mathbf{V}_{z_{0-3}} : u$	12.6	5.9	11.7	7.4	9.3	4.7	0.183	
$\mathbf{V}_{z_{0-3}} : v$	-1.0	8.2	-1.4	5.8	-1.1	5.5	0.987	
$\mathbf{V}_{z_{2-7}} : u$	3.7	7.3	8.9	8.1	6.6	7.6	0.286	
$\mathbf{V}_{z_{2-7}} : v$	-8.7	6.5	-4.4	10.6	-1.2	8.1	0.043	√
$\mathbf{V}_{z_{0-10}} : u$	17.2	9.0	25.8	15.1	18.8	11.9	0.187	

Table C.1: Summary of statistics for rawinsonde data. Units: J kg^{-1} for $MLCAPE$, $TCCAPE$, $pickCAPE$, CIN, $DCAPE$, $DCAPE_\rho$, and HEL. hPa for LCL, CCL, and $p(\theta_{w_{min}})$. K: LI, $\theta_{w_{min}}$, $\theta_{e_{sfc}}$, T_v, $T_{v_{Tw}}$, $T_{v_{sd}} - T_v$, $T_{v_{sd}} - T_{v_{Tc}}$, $T_{v_{sd}} - T_{v_{Tw}}$, $T_{v_{dd}} - T_v$, $T_{v_{dd}} - T_{v_{Tc}}$, and $T_{v_{dd}} - T_{v_{Tw}}$. m: $z(\theta_{w_{min}})$, and $HWBZ$. $(25.4)^{-1}$ mm: PW. %: RH_t, and RH_d. All velocity vectors: m s^{-1}. p-values are unitless.

field	LS mean	LS σ	PS mean	PS σ	TS mean	TS σ	p value	significant at 5%?
$\mathbf{V}_{z_{0-10}} : v$	-6.6	13.4	0.4	12.4	0.4	10.8	0.220	
HEL	180.7	143.0	156.7	151.9	161.4	99.0	0.869	
$\log_{10} BRN$	1.24	0.56	0.73	0.56	1.69	0.30	0.0002	√
$\log_{10} BRN(T_c)$	1.70	0.40	1.50	0.29	1.76	0.44	0.497	
$BRN(pick\ CAPE)$	*no suitable transformation*							
S_{BRN}	51.1	28.7	53.3	49.1	38.3	33.7	0.381	

Table C.2: Summary of statistics for wind profilers. All units m s^{-1} except for HEL: J kg^{-1} p-values are unitless.

field	LS mean	LS σ	PS mean	PS σ	TS mean	TS σ	p value	significant at 5%?
$\overline{\mathbf{V}}_{0-6} : u$	7.5	5.1	10.0	6.5	9.2	5.2	0.170	
$\overline{\mathbf{V}}_{0-6} : v$	2.3	4.9	3.2	5.9	5.2	4.3	0.006	√
$\overline{\mathbf{V}}_{3-10} : u$	11.2	5.8	15.7	6.6	12.8	7.2	0.031	√
$\overline{\mathbf{V}}_{3-10} : v$	-1.8	7.6	0.3	6.4	3.2	7.3	0.003	√
$\overline{\mathbf{V}}_{5-8} : u$	11.3	6.0	16.1	6.9	12.2	9.2	0.040	√

Table C.2: Summary of statistics for wind profilers. All units m s^{-1} except for HEL: J kg^{-1} p-values are unitless.

field	LS mean	LS σ	PS mean	PS σ	TS mean	TS σ	p value	significant at 5%?
$\overline{\mathbf{V}}_{5-8} : v$	-1.9	7.9	0.4	6.5	3.0	11.0	0.040	√
$\overline{\mathbf{V}}_{9-10} : u$	14.2	7.6	20.0	8.5	17.0	8.0	0.019	√
$\overline{\mathbf{V}}_{9-10} : v$	-3.4	9.8	-1.1	8.5	2.6	6.6	0.0006	√
$\mathbf{V}_{z_{0-1}} : u$	2.6	3.5	5.4	7.0	5.3	6.3	0.073	
$\mathbf{V}_{z_{0-1}} : v$	4.7	6.7	3.3	6.0	5.2	6.1	0.318	
$\mathbf{V}_{z_{0-3}} : u$	5.2	5.6	11.0	7.7	9.3	7.8	0.005	√
$\mathbf{V}_{z_{0-3}} : v$	-3.6	10.2	-3.1	5.5	1.8	7.3	0.0004	√
$\mathbf{V}_{z_{2-7}} : u$	4.0	6.1	9.4	7.6	5.3	9.4	0.027	√
$\mathbf{V}_{z_{2-7}} : v$	-6.6	8.3	-5.7	7.9	-3.2	12.0	0.221	
$\mathbf{V}_{z_{0-10}} : u$	13.2	8.4	20.5	10.2	16.9	11.3	0.026	√
$\mathbf{V}_{z_{0-10}} : v$	-7.2	12.7	-6.3	9.1	-1.1	9.8	0.005	√
HEL	243	223	245	121	214	209	0.659	

Table C.3: Summary of statistics for storm-relative wind profiler fields. All units m s^{-1} except for SRH: J kg^{-1}. p-values are unitless.

field	LS mean	LS σ	PS mean	PS σ	TS mean	TS σ	p value	significant at 5%?
$\mathbf{c} : u$	6.7	7.5	10.3	6.8	12.9	6.2	0.00002	√
$\mathbf{c} : v$	-3.0	7.5	-3.6	6.4	-1.4	8.0	0.267	
$\mathbf{c} : line \parallel$	3.0	7.4	0.3	11.1	8.9	9.2	0.00005	√

Table C.3: Summary of statistics for storm-relative wind profiler fields. All units m s^{-1} except for SRH: J kg^{-1}. p-values are unitless.

field	LS mean	LS σ	PS mean	PS σ	TS mean	TS σ	p value	significant at 5%?
$\mathbf{c}$: *line* $\perp$	6.0	7.0	3.9	9.0	8.6	6.2	0.009	$\surd$
$\overline{\mathbf{V}}_{0-1} - \mathbf{c}$: u	3.4	6.5	1.9	5.2	3.5	5.9	0.414	
$\overline{\mathbf{V}}_{0-1} - \mathbf{c}$: v	8.5	6.6	7.9	4.5	6.9	5.8	0.378	
$\overline{\mathbf{V}}_{0-1} - \mathbf{c}$: *line* $\parallel$	4.8	9.2	0.7	9.8	-2.1	8.8	0.003	$\surd$
$\overline{\mathbf{V}}_{0-1} - \mathbf{c}$: *line* $\perp$	*no suitable transformation*							
$\overline{\mathbf{V}}_{0-6} - \mathbf{c}$: u	0.8	8.4	-0.7	8.1	-4.0	6.7	0.004	$\surd$
$\overline{\mathbf{V}}_{0-6} - \mathbf{c}$: v	5.3	7.1	7.5	5.9	7.1	7.4	0.386	
$\overline{\mathbf{V}}_{0-6} - \mathbf{c}$: *line* $\parallel$	3.5	8.2	4.9	8.8	0.3	8.0	0.022	$\surd$
$\overline{\mathbf{V}}_{0-6} - \mathbf{c}$: *line* $\perp$	-3.4	6.3	-6.1	4.3	-7.7	5.3	0.001	$\surd$
$\overline{\mathbf{V}}_{3-10} - \mathbf{c}$: u	4.5	9.6	5.0	7.1	-0.4	9.7	0.004	$\surd$
$\overline{\mathbf{V}}_{3-10} - \mathbf{c}$: v	1.2	7.6	4.6	6.2	5.1	10.7	0.119	
$\overline{\mathbf{V}}_{3-10} - \mathbf{c}$: *line* $\parallel$	2.8	10.5	7.0	8.4	1.8	11.1	0.067	
$\overline{\mathbf{V}}_{3-10} - \mathbf{c}$: *line* $\perp$	1.5	5.9	0.2	4.1	-4.7	5.6	0.00000009	$\surd$
$\overline{\mathbf{V}}_{5-8} - \mathbf{c}$: u	4.6	9.8	5.6	7.3	-1.0	11.9	0.004	$\surd$
$\overline{\mathbf{V}}_{5-8} - \mathbf{c}$: v	1.1	8.0	4.7	6.6	4.9	14.2	0.273	
$\overline{\mathbf{V}}_{5-8} - \mathbf{c}$: *line* $\parallel$	2.9	10.8	7.4	8.5	3.3	8.7	0.083	
$\overline{\mathbf{V}}_{5-8} - \mathbf{c}$: *line* $\perp$	1.1	6.8	0.2	4.7	-4.9	5.6	0.0000006	$\surd$
$\overline{\mathbf{V}}_{9-10} - \mathbf{c}$: u	8.3	11.3	9.4	8.4	3.0	11.2	0.006	$\surd$
$\overline{\mathbf{V}}_{9-10} - \mathbf{c}$: v	-0.3	9.3	3.2	7.8	3.8	11.3	0.149	
$\overline{\mathbf{V}}_{9-10} - \mathbf{c}$: *line* $\parallel$	4.1	13.1	8.7	9.5	3.9	10.0	0.102	

Table C.3: Summary of statistics for storm-relative wind profiler fields. All units m s^{-1} except for SRH: J kg^{-1}. p-values are unitless.

field	LS mean	LS σ	PS mean	PS σ	TS mean	TS σ	p value	significant at 5%?
$\overline{\mathbf{V}}_{9-10} - \mathbf{c} : line \perp$	4.9	8.0	4.1	6.9	-1.2	6.9	0.00006	$\surd$
SRH	276	266	291	176	280	235	0.962	